Title: A hydro-climatological approach to predicting regional landslide probability using Landlab
Author(s): Ronda Strauch et al.
MS No.: esurf-2017-39

Response to Anonymous Referee #1

No.	Comment	Response
1	Main Problems: 1. Manuscript structure: the paper is long and a little bit convoluted. In my opinion the length of the paper could be reduced without any important loss of information and the structure could be improved. For example the sections related to the cyberinfra-structure Landlab (sect. 2.2 and figure 3 and the last part of the section 2.3) could be reduced or removed since it is less important for the reader of ESurf (see Aims and Scope of the ESurf Journal). Some parts are difficult to understand (see other comments) and there are some repetitions that can be removed.	We feel that the manuscript supports the aims and scope of eSurf, such as "numerical modelling of Earth surface processes." The model is also built to work with Landlab, which was described earlier this year in eSurf: Hobley, et al., Earth Surf. Dynam., 5(1): 21-46, 2017. We have reduced the length of the manuscript by deleting material described elsewhere in cited papers (e.g., soil evolution component) or the software User Manual. Reduced description of hydrologic data processing in Section 2.3. *Removed repetitions* and details about Landlab in Section 2.2. However, additional material was added to address referee comments. We choose to retain Fig. 3 because it provides visual context of the study area and mapped landslides for readers unfamiliar with the area.
2	Basic Assumptions: 2a. The authors fixed a soil density equal to 2000 kg/cubic meter constant over the entire domain; is this relative to the bulk density of the soil or to the wet soil density? Is this assumption realistic considering that you have different soil type in your domain?	Soil density represents saturated bulk density of soil (as stated in the paper), which is the same as wet bulk density. The study area has two similar soil types: sandy loam and loamy sand. A saturated bulk density of 2000 km/m^3 has been used in other similar models and studies as a constant (e.g., Shalstab by Montegomery and Dietrich 1994 and SINMAP by Pack et al. 1992). However, model flexibility allows users to provide varying values of soil density and associated uncertainty as a distributed field throughout a study domain as constrained by available data. In addition, the infinite slope stability model has been found to be insensitive to soil unit weight (density*g) (Hammond et al. (1992) and Lepore et al. 2013); *text added Page 16, lines 1-2.*

3	2b. The authors assume the soil as incoherent (C=0) assigning all the cohesion to the root? Again is this assumption realistic? Please consider that also a loamy sand could provide a cohesion greater than that given by the root system. Please try to justify this assumption using field data relative to the soil mechanics parameters.	The referee is correct that we considered soils cohesionless. Generally soil behaves much like cohesionless soil when the clay fraction is <15% (Kulhawy et al. EPRI – Manual on Estimating Soil Properties of for Foundation Design, EPRI EL-6800, 1990). Our soils have less than 10% clay and thus low in cohesion (DOA-NRCS, 2012). The aim of our model is for risk assessment; thus, we use total cohesion given the assumption that soil cohesion is a small fraction of the total cohesion. *Added clarification on page 14, lines 7-11.* Our aim was to develop a model for regional applications that can utilize existing spatial information; thus, no field data is collected.
4	2c. The authors assume that the recharge is given by the sum of the baseflow and the surface runoff (page 10) at each VIC grid cell. It is not clear the reason of such an assumption since usually the recharge is given only from the subsurface flow (i.e. part of the baseflow) as highlighted by the authors (page 6 – line 23-25). In similar modelistic approach (SINMAP) R is considered as a climatic factor (rainfall). Please clarify this apparent contradiction.	In our model application, we made the assumption that in steep forested mountainous landscapes runoff is generated by saturation excess mechanism due to relatively high soil infiltration capacities. A steady-state kinematic wave approach for subsurface flow is used with a depth-averaged hydraulic conductivity. This model technically requires recharge, defined as precipitation and snowmelt less of evapotranspiration and soil storage. In the VIC model this corresponds to the sum of surface and subsurface flow rates taken and averaged over a grid cell as input recharge rate. This approach is still less conservative than using rainfall directly as recharge input to the model. The use of the annual daily maximum sum of runoff and baseflow is designed to represent when the ground is likely to be the *most* saturated. *Additional clarifying text added on page 9, lines 11-16.*
5	2d. It is not clear how the soil depth evolution model and the stability model are coupled (if they are coupled). I thought that the outcome of soil depth evolution model is provided as soil depth map (in terms of mode) but there is a sentence (page 11 – line 26-27) which is in contrast with my previous thoughts	The soil evolution model is not coupled to the probabilistic stability model and the reviewer is correct that the outcome of the soil evolution model did produce a soil depth map used as the mode in running the stability model. This map is developed as an alternative to SSURGO to better capture the spatial granularity of soil depth due to topography. The model is also used to obtain uncertainties in soil depth due to

	("Eq (a) and Eq (2) are used to calculate FS within the soil evolution model". So please try to clarify the connection between these models. I think that a figure with a flow chart describing models and connections together with the setup of the experiment could be useful to the readers. How many simulations did they run?	temporal fluctuations as a result of episodic landslides such that this uncertainty can be used to parameterize a probability density function. The soil evolution model includes a infinite slope stability model within it, to represent the long-term effects of landslides on the temporal variability of soil thickness as the model iterates over many years to produce a long-term soil depth record. We now indicated this purpose clearly. *Sections 2.4. and 4.1.2. edited in detail* in response to referee's comments. Edits clarify the soil evolution model, how it was implemented and how the model results are used in the LandslideProbability component. The soil evolution model was run for *10,000 years (line 3 on page 20)*. Based on the statistics obtained from the soil evolution model, the infinite slope model Monte Carlo simulation was run for *3,000 iterations (line 8 on page 23).*
6	3. Choice of model parameters: the choice of geotechnical and soil parameters (mode and range of variability used for MonteCarlo simulation) is, at least, not convincing. a. The internal friction angles are fixed in Table 1 in terms of mode, min and max. I'm not convinced by these values; they seems to be very high especially for the loamy sand and sandy loam. Could you provide references or field data used to fix these values? b. The authors use different relationship to define minimum and maximum value of trasmissivity T and friction angle. How do they define these relationships? What is the impact of these values on the final results (sensitivity analysis).	Section 3.2.1 describes the parameterization of vegetation and soil properties. The source of internal friction angle mode values shown in Table 1 are *described in line 42 on page 15,* specifically Table 5.5 within Hammond et al., 1992 and Table 5.2 within Shelby, 1993. The values are corroborated by online sources such as: http://www.geotechdata.info/parameter/angle-of-friction.html. The minimum and maximum relationships to mode for friction angle were determined by the minimum and maximum values found in the literature and requisite right-skewed distribution. The mean, minimum, and maximum values for T shown in Table 1 are for the distributed T values over the study area and not based on the parameterized relationship for T derived as a function of mode (*see table footnote*). The parameterized relationship for T

		was kept consistent with soil depth (hs) because T is partially derived from hs, along with Ksat. At the regional scale, no specific field data is collected for this study and all model parameters are obtained from the existing literature and digital maps, as the intent was to develop a regional scale model applicable with existing information. A sensitivity analysis was not included in this research as these analyses have been included elsewhere (Hammond et al., 1992; Sidle 1984); *clarified on page 6, lines 26-27.*
7	4. Low performance of hazard maps: the authors affirm that the performance of pro- posed approach is modest. I agree with them and if the aim of this model is to create a map of landslide hazard, better results could be achieved using classical susceptibility approach based on statistical methods or data-driven methods. Moreover I think that they can remove the CD approach to test the performance of the proposed approach. The CD approach is aimed to highlight the existence of a statistically significant difference between the two P(F) cdfs (within and outside) for fixed soil depth scheme. The authors can only affirm that the two cdfs are different but this does not imply that the model performances are acceptable. I understand that this could be a first level check, but I think that can be removed without any problem for the paper.	The objective of this paper was stated in the second paragraph of Introduction, which did not include the use of a statistical model. Classical susceptibility using statistical methods may 'perform better' against observed landslides than a physical model. However, this is because statistical approaches are based on the observations while physical models are not, which are then compared to the model. Part of the purpose for the Landlab landslide component is to base landslide prediction on physical processes that allow for prediction (1) in areas *without* observed landslides and (2) under conditions (climate and vegetation) that may change in the future. Statistical susceptibility models suffer from the assumption that the statistically derived relationships between historical landslides and site conditions at the time of the inventory holding true in the future. Challenges in validating physical models with observations are described in lines 28-37 on page 33. *The CD comparison was removed* from the paper as suggested by the reviewer.
8	*Other comments:* Page 7, lines 9-10: The sentence is not clear. How does the use of maximum annual daily recharge help to define uncertainty in R?	*Clarified sentence Page 6, lines 13*. The dataset developed from maximum annual daily recharge was used to represent the uncertainty of R over time at each grid cell.

9	Page 7, equation (3a): Please define n and n(FS<1).	Equation 3a has been *clarified (page 6)* to $P(F) = P(FS \leq 1) = n(FS \leq 1)/N$ where n() is the number of conditions met in bracket and N is the number of iterations
10	Page 9, line 9-21: The difference between options 2 (lognormal) and 3 (lognormal spatial) is not enough clear. Also the option 4 is not clear. Please clarify this paragraph.	The difference between the lognormal and lognormal-spatial options is the first one applies a lognormal distribution uniformly over the model domain, while the second applies a different lognormal distribution to each grid cell. *Additional clarification provided on page 8, lines 33-40.*
11	Page 9, line 30: what is core node? Is it a computational element of spatial domain? I think that these details on the computational framework are not necessary since they create a little bit confusion in the main line of the paper.	Nodes are an architectural feature of Landlab and represent the central point of a grid cell. Core nodes are the nodes that the modeler chooses to evaluate or perform the calculations on. We *removed the word 'core'* because it wasn't necessary and creates confusion.
12	Page 10, lines 16-19: please check the sentence since it is not very clear.	*Improved clarity to sentence within Sect. 2.3*.
13	Page 15, line 11: define combined curvature (reference). Is it different from the total curvature used further?	Combined and total curvature are the same, also referred to standard curvatures, which combines plan and profile curvatures. To avoid confusion, *'combined' was changed to 'total' within the manuscript*.
14	Page 16, line 22-23: sentence not clear; lines 23-25: this sentence can be removed.	*Paragraph was deleted.*
15	Page 17, lines 7-8: what is the meaning of "spatially consistent". You can use consis- tent when map is compared with the field data. Did you carry out this task?	*Sentence (page 15, lines 10-11) was revised to clarify* that the evolved soil map is more spatially heterogeneous than the SSURGO soils map with map unit polygons
16	Page 17, lines 18-19: how can the authors "confirm" the ranges of soil depth used through a long term evolution model which needs to be calibrated on soil data as well?	The soil evolution model was used to confirm the soil skewed distribution used in the triangle distribution. *Sentenced revised accordingly on page 15, lines 20-22.*
17	Page 19, lines 15-17: how the authors calculate pore-water pressure starting from the maximum daily recharge? Do they use pore-	R is an input to calculate pore-water pressure in the model, which is intertwined in the formulation and cannot be immediately shown.

	water pressure in their stability model? I think they use directly the recharge (see equation 2).	
18	The section 4.1.2 is not clear especially the role of regression based equation which seems to provide the soil depth as a function of slope and curvature. If you run the soil evolution model, why do you need a regression to obtain soil depth? In the same section it is not clear the difference between M-SD and M-SD LT. I think that there is a lot of information but this is not well-organized.	*We improved the description and application* of the soil evolution model and how we used it. Section 2.4. describes broadly why we needed a soil evolution model, what we obtained from it, and how we used the modeled soil depth. It also provides a narrative of the soil production processes modeled. *Section 4.1.2. describes in more detail* how the model is implemented at select locations that represent the topography and vegetation of the domain and how this limited model information is used to make a map of mode of soil depth and set minimum and maximum parameters of the triangular distributions used in the Landlab Landslide Probability component. This section clarifies the differences between M-SD and M-SD LT.
19	Figures 10 and 11 highlight the same information (Probability or return period). Please consider removing one of the two figures.	We would like to *retain both these figures* because, while they highlight similar albeit transformed data, they communicate different information about landslide hazard. This may be meaningful for different readers, especially resource managers who may prefer return period information.
20	Page 32, line 13: The authors are not using "observations" in figure 13 but model results. Please change the sentence.	Correct, *changed* "observations" to 'model results' on *page 31, line 5*.
21	Figure 13c: in the legend line relative to M-SD LT is missing.	The mean soil depth line for M-SD LT was *purposely left out* because it is relatively similar to M-SD and we desired minimizing the lines shown in the figure.
22	Page 34, line 16: since the authors use 10% of highest elevation cell, I suggest to remove 20% and 30%.	Suggestion accepted and 20% and 30% *reference removed*.
23	Page 34, lines 24-26: I suggest specifying the number of DA source cells and the number of DA outside source.	We specified the number of DA outside source cells as 50,000 sample. The number of source cells was *added at 4318 grid cells on page 31, line 31*.

24	Figure 14a: I think there is an error in the plot. The sum of all the bars must be equal to 1. If this is true for Outside DA, it cannot be true for Source DA since for each bin the relative frequency is lower.	This *figure has been removed*.

Response to Anonymous Referee #2

	Comment	**Response**
25	The work is of high scientific value and the applied methodologies are scientifically robust. However, to my opinion, the paper ended up being excessively long, sometimes not immediately clear and the overall application not well focused on clear and simple targets. Moreover, given the numerous details of the developed numerical model system, I wonder if a journal which addresses to models development or environmental software would be more appropriate. Anyways, to my opinion, it needs major revision for it to be published in order to make it clearer, more fluent, to better define the aims of the application and to improve the literature review which lacks of some important contributions.	Please refer to response to referee #1 comment #1. Additional literature review with citation has been added, particularly based on the additional citations supplied by the referees. We also made the effort to improve clarity of the objectives of the paper, the purpose of different simulations, findings with respect to model results, and related observational inferences.
26	1. The manuscript is very long and sometimes repetitive, with English style a bit verbose. I have to read it a couple of times to get to the point. Some parts can be synthesized and stated more directly.	We agree that the article is long, but feel it reflex the necessary information to: (1) orient the reader, (2) describe the model framework and cyberinfrastructure designed for reproducibility, and (3) demonstrate a real-world application. Nevertheless, we reduced the length of the paper and made it more direct to point. Please refer to response to referee #1 comment #1.
27	2. Literature review is well done and comprehensive of various aspects involved in this work. However, it	Additional literature has been cited throughout the manuscript, in particular some of the literatures noted by referees. *Thirteen*

	also lacks of some important contributions in the specific field of physically based modeling for rainfall-triggered landslides, also with regard with the parameters uncertainty.	*additional citations* have been added to the references.
28	3. My main concern is whether simpler and more computationally efficient statistical approaches for susceptibility evaluation could be more appropriate for such regional and long term analysis. The methodology is based on the use of various simplified models which make it complex. The ultimate model performances are not very satisfactory in terms of ROC and AUC. The approach is classified as dynamic and processed- oriented; however it is not able to reproduce and simulate specific events due to the simplifications and the large temporal scale and can be used only for long term analysis, thus becoming a kind of 'static' approach. Statistical models are very robust and able to guarantee very satisfactory results (e.g. Lepore et al., 2012; Lee and Pradhan, 2007). Lepore C, SA Kamal, P Shanahan, RL Bras (2012). Rainfall-induced landslide susceptibility zonation of Puerto Rico. Environmental Earth Sciences 66 (6), 1667-1681 Lee, S., Pradhan, B. (2007). Landslide hazard mapping at Selangor, Malaysia using frequency ratio and logistic regression models. Landslides 4, 33-41	We are familiar with the literature provided and agree that statistical analysis is a powerful modeling technique for landslide hazard assessments for existing conditions. However, the aim of our research is different, as clearly indicated in the Introduction section. Statistical models are particularly useful for evaluating conditions conducive to different types of landslides. Indeed, some of the authors are completing a manuscript that compares a statistical approach to the physical model used in this paper, which will be submitted for peer review in the coming months. See also response to referee #1, comment #7. Our model can be used at event scales in addition to long term. When using for a particular event, the user would need to quantify the uncertainty for recharge and other soil parameters to reflect the conditions at the time of the event. The Landlab LandslideProbability component is based on a simple physical model and its lack of complexity facilitates its use in a wide variety of settings and situations. We agree that the performance against mapped debris avalanches with the physical model is modest based on ROC and AUC metrics, as stated on line 19 on page 32. Challenges in validating physical models with observations are described in lines 28-37, page 33. We believe the modest performance based on observed landslides does not discount the value of a predictive physical model, particularly where data are limited.
29	4. In the model system there is a mix of temporal and spatial resolutions	Yes, there is a mix of temporal and spatial resolutions used in the demonstration of the

	(soil depth evolution at yearly scale, hydrological model at daily and 6 kmq square, geomorphological model at 30 m). If I understood well the finest temporal resolution is the daily scale of the annual maximum recharge. However, the daily resolution misses the most intense events and moreover, the daily annual maximum recharge does not guarantee the worst 'hydrological conditions' since the antecedent soil moisture conditions are also influent. This why I am skeptical on the advantage of this approach instead of others (comment 3).	model. The hydrological model is a daily time-step, but only the annual maximum is used in the application. We agree that the daily hydrology time step misses the sub-daily intense storms, which may lead to some underestimate of instability. However, landslides driven by pore-water pressure as subsurface flow develops requires longer durations than short storm outbursts. The subsurface flow model is a steady-state model so no antecedent moisture conditions is required in the model. It assumes that the subsurface flow attains steady-state given the annual maximum recharge value. The spatial scale variety used in the model application is a result of the native resolution of the various data sources as well as the resolution chosen for the application. However, the model is flexible for use at other spatial and temporal resolutions.
30	5. Soil depth evolution: it is not totally clear to me whether the soil depth evolution model is run in conjunction with the stability module or it is run 'off line' and the final map is then fed to the slope stability module. Also, how the soil depth evolution influences the hydrological module? Theoretically, the soil evolution model itself should take into account the change in elevation due to the landslide. Is this done? Please make it clear.	We improved the description and application of the soil evolution model and how we used it. Section 2.4. describes broadly why we needed a soil evolution model, what we obtained from it, and how we used the modeled soil depth. It also provides a narrative of the soil production processes modeled. *Section 4.1.2. describes in more detail* how the model is implemented at select locations that represent the topography and vegetation of the domain and how this limited model information is used to make a map of mode of soil depth and set minimum and maximum parameters of the triangular distributions used in the Landlab LandslideProbability component. This section also clarifies the differences between M-SD and M-SD LT. The soil evolution model does not influence the hydrology model and landscape elevations are not changed with soil development and landslides.

31	6. Authors do not explicitly discuss the importance of the effect of matric suction and the 'apparent' cohesion which arises under unsaturated soil moisture conditions (e.g., Simoni et al., 2008; Baum et al., 2002) and which can be much higher than soil and also root cohesion (e.g., Arnone et al., 2016). They discuss clearly hypothesis of steady state conditions, but this does not justify the neglecting of the matric suction. Moreover, several procedure have been also proposed to predict shear strength under unsaturated soil (based on modified Mohr-Coulomb failure criterion (Vanapalli et al., 1996; Fredlund et al., 1996)), which have been used in various works (Montrasio and Valentino, 2008; Lepore et al., 2013). I suggest referring to Lepore et al., (2013) for a discussion on this point. Arnone E, Caracciolo D, Noto LV, Preti F, Bras RL (2016) Modeling the hydrological and mechanical effect of roots on shallow landslides. Water Resour Res 52(11):8590–8612 Baum, R. L., Savage, W. Z., and Godt, J. W. (2008) TRIGR-a Fortran program for transient rainfall infiltration and grid-based regional slope-stability analysis, US Geological Survey Open File Report 2008-1159, 75 pp. Fredlund, D. G., Xing, A., and Barbour, M. D.(1996). The relationship of the unsaturated soil shear strength to the soil water	We recognize and explicitly state that we neglect apparent cohesion on line 41 on page 33. In steep mountain terrain of the Pacific Northwest soils, are loosely developed and have large particles in hillslope soil mixtures. Earlier applications of similar model typically use cohesionless soils. However, we recognize the discoveries of the importance of matric suction, perhaps more important in well-developed soils, in stability analysis (e.g., citations referee listed) and highlight this opportunity for future advancements in the Landlab LandslideProbability model on page 34, line 5-6. We believe that comparison of our model with the tRIBS-VEGGIE model would be an interesting future study, but is beyond the scope of the current model version. We are familiar with many of the citations provide and appreciate exposure to the others. Some of these citations are already included in the manuscript, but the *literature review has been enhanced (13 more citations)* using these references as well as others. *Additional or modification of text from these references include: insensitivity to soil unit weight (Page 16, line 12), assumed negligible correlation between C and friction angle (Page 8, line 14), and hydrologic effect of roots drying out soils (Page 31, lines 15-17).*

	characteristic curve, Can. Geotech. J., 32, 440–448 Lepore C, Arnone E, Noto LV, Sivandran G, Bras RL. (2013). Physically based modeling of rainfall-triggered landslides: a case study in the Luquillo forest, Puerto Rico. Hydrology and Earth System Sciences 17: 3371–3387. DOI: 10.5194/hess-17-3371- 2013. Montrasio, L. and Valentino, R. (2008) A model for triggering mechanisms of shallow landslides, Nat. Hazards Earth Syst. Sci., 8, 1149–1159. Simoni, S., Zanotti, F., Bertoldi, G., and Rigon, R. (2008) Modelling the probability of occurrence of shallow landslides and channelized debris flows using GEOtop-FS, Hydrol. Process., 22, 532–545 Vanapalli, S. K., Fredlund, D. G., Pufahl, D. E., and Clifton, A. W.(1996) Model for the prediction of shear strength with respect to soil suction, Can. Geotech. J., 33, 379–392	
32	7. Distribution of soil and mechanical parameters are assumed triangular and then distributions of FS are estimated by means Monte Carlo approach. The approach is fine but clearly it increases the computational effort. Other approaches to estimate probability of FS have been proposed in the literature. For example, the First-Order Second Moment (FOSM) (Benjamin and Cornell, 1970) is commonly used to estimate analytical approximations of the	FOSM approach provides the moments of a random function. Given these moments, then a theoretical distribution of FS would need to be assumed at each grid cell. Monte Carlo simulation does not assume any distribution, but estimates probability of failure based on the calculated FS values <=1 from the distribution of FS given the distributions of input variables. Malkawi et al. (2000) compared FOSM and Monte Carlo simulation of slope stability and found good agreement between the two approaches using 2 to 3 slope stability methods; slight differences between the two approaches for the Spencer method was due to the need to

	spatio-temporal FS statistics (i.e. mean and variance), that can be used to fit a theoretical probability distribution for FS and estimate the spatio-temporal dynamics of probability of failure. Moreover, mechanical parameters are normally assumed to be described by the Normal distribution (Abbaszadeh et al., 2011; you can refer to Arnone et al., 2016 and references therein). Please, briefly discuss. Abbaszadeh M, Shahriar K, Sharifzadeh M, Heydari M. 2011. Uncertainty and re- liability analysis applied to slope stability: a case study from Sungun copper mine. Geotechnical and Geological Engineering 29: 581–596. Arnone E, Dialynas YG, Noto LV, Bras RL (2016) Accounting for soils parameter un- certainty in a physically-based and distributed approach for rainfall-triggered landslides. Hydrol Process 30:927–944	perform a numerical approximation of the first derivative of factor-of-safety required by FOSM, which isn't required using Monte Carlo simulation. They endorse the use of the Monte Carlo simulation approach given the capabilities of computers to handle data and computation. We did not find computational requirements limiting in our use of Monte Carlo simulation. In fact, once the model input is prepared, the model's Monte Carlo simulation with n=3,000 for an area of over 2,700 km2 runs in minutes. Malkawi, Abdallah I. Husein, Waleed F. Hassan, and Fayez A. Abdulla. "Uncertainty and reliability analysis applied to slope stability." *Structural safety* 22.2 (2000): 161-187. Regarding distributions of parameters, both normal and uniform distributions are often used in slope stability analysis, but we preferred to use triangle for *reasons given on page 8, lines 3-5.* This distribution has been used by others in slope stability modeling using Monte Carlo simulations (Cho, 2007; Dou et al., 2014; Hammond et al., 1992; El-Ramly et al., 2002; Strenk, 2010). Additionally, it gives the most weight to data and/or knowledge from the modeler in the form of mode, facilitates skewed distributions, and avoids extrapolations to extreme high or low (and negative) values. Observed/measured values of soil depth, cohesion, and friction angle are typically skewed and not normally distributed (Hammond et al. 1992).
33	8. Model application is a bit confusing. My impression is that it is mainly addressed to demonstrate the model capabilities instead of producing reliable landslide hazard maps for the study areas (AUC are low and FS parameters are not site-dependent). Please, state clearly the main targets of the model application.	The model was implemented at a national park to provide demonstration of the model and provide a stability analysis for the park. It was not to substantiate the current landslide inventory. Explicit targets of the application are provided with a *new sentence at lines 36-38, page 10.*

34	1. P9L6: I suggest moving this info (soil density) in the model application section. Please, specify what type of soil density this value accounts for (total, dry, wet, bulk density...)	Soil density is wet bulk density (see response to comment #2 of Referee #1. This *sentence was removed* as the value is listed in line 43 of page 15.
35	2. P9L20: how do you justify this low resolution of the hydrological model? Clearly, this is not able to simulate the 'local' moisture dynamics at hillslope scale . . .	The VIC hydrological model was used to obtain annual maximum daily recharge averaged over the upslope contributing area of each grid cell of the probabilistic landslide initiation model. Local relative wetness used in the infinite slope stability model was calculated from a steady-state subsurface flow model, which is a function of local slope and transmissivity at the resolution of the landslide model. The steady-state subsurface model does not consider the local soil moisture dynamics. Additional justification for using VIC in our application is *provided in Sect. 3.2.2 on page 17*.
36	3. P15L7: working resolution is 30 m. However, if I understood well some components of the system (e.g. VIC) work at coarser resolution ... Is any interpolation method being used?	Recharge at the 30-m grid resolution is provided by routing the upstream fractional area of the coarse 1/16° resolution VIC grid cells to calculate the upstream proportionally-averaged maximum recharge for each year. These time series are used in an interpolation step within the component to generate a cumulative distribution of recharge equal to the length of the number of Monte Carlo iterations used in the simulation. This is *clarified with revisions to page 8, lines 37-40.* More detail on this is also provided in the User Manual as mentioned on line 23, page 9.
37	4. P16Table1: maximum values of friction angle seem to be very high . . . Do you have references?	Source for friction angle is provided in line 42, page 15; highest values are based on the ranges in the literature. See also *response to comment # 6* of Referee #1.
38	5. P16L9: The estimation of root cohesion belong to a further 'branch' of scientific literature of this field which here seems to be significantly simplified (e.g. Pollen and Simon 2005; Preti et al., 2010; Schwarz et al., 2013). . .	We agree that estimating root cohesion is a 'branch' of research by itself and represents one of the more challenging variables to represent in a landslide model. Our landslide research aims for regional application and was not focused on this branch of study. We believe basing root cohesion estimates on vegetation and used in a Monte Carlo simulation is a

	Schwarz, M., F. Giadrossich, and D. Cohen (2013), Modeling root reinforcement using a root-failure Weibull survival function, Hydrol. Earth Syst. Sci., 17, 4367–4377. Pollen, N., and A. Simon (2005), Estimating the mechanical effects of riparian vegetation on stream bank stability using a fiber bundle model, Water Resour. Res., 41, W07025	straightforward approach that can be easily implemented in other locations; however, the model is capable of operating with detailed estimates of root cohesion provided by the user. Citations provided offer approaches for estimating root cohesion based on quantification or parameterization of detailed root strength that is beyond the regional approach we take in our model. However, recognition of these techniques was *added to the paper for exposure to interested readers on page 14, line 11*.
39	6. P19sec3.2.2: please give some synthesis of the characteristics of the hydro-climatology forcing for the area (e.g. some characteristic time series ...).	The seasonality and range of precipitation is discussed on page 11, lines 6-13 and mean annual precipitation is spatially depicted in Fig. 2c, which was *moved up a page*. *Additional characterization of recharge was provided in a sentence on page 17, lines 14-16.*
40	7. Figure 4: how about the map of soil evolution model?	A map of a portion (close up) of the evolved soil depth product is in Fig. 7; however, the *Fig. 7 was revised to match the color palette of Fig. 4*'s SSURGO soil depth map. A relative histogram of a spatial soil depth product is also provided in same figure. We believe this information is sufficient to provide characterization for the comparison with the SSURGO soil depth product. Given the sample topography, details of the influence of converging and diverging morphologies on soil depth can be more clearly seen in a close-up figure than in the map of the entire domain.
41	8. Figure 5: which soil properties did you use for this figure? I don't see much difference in concavity between zone (2) and zone (3). I suggest adding the degree axis in y, slope is not easily readable. Please, specify what the angle values stand for.	Soil properties are *listed in figure caption*, but include friction angle of 34 degrees and dimensionless cohesion values listed in legend. The break in concavity between zone 2 and 3 is subtle, but was guided by the source cells (triangles) and the saturation line. We prefer to retain slope as m/m rather than degrees to facilitate comparison with other slope-area geomorphic analyses such as Montgomery and Dietrich (1994) and Pack et al. (1998). However,

		the labeled angles in degrees on the plot should help orient the reader. Assuming the angle values referee is referring to are 17, 35, and 50 degrees.
42	9. P20L7: please, specify the color of the dot lines.	We believe this refers to Fig. 5. *Caption amended to include color of vertical lines.*
43	10. P21L15: why is it tan(theta)< ½ tan(phi) ....From eq. (1) it should be simply tan(theta)<tan(phi).	Solving the FS equation (Eq. 1a) for tan(θ), given FS=1, relative wetness=1, cohesionless soil, and a water to soil density ratio= ½, yields tan(θ) ≤ ½ tan(ø) for unconditionally stable conditions.
44	11. P21L18: I don't see where theta=17 degree is in the figure 5	θ=17° in Fig. 5 is noted next to the cyan line. Updated figure caption *based on comment #41* eases the visibility of this threshold.
45	12. P22L5: specify color of the lines?	*Colors added.*
46	13. Figure 6a,c: Relative frequency is in time or space?	This is in time. *Clarified in Fig. 6 caption.*
47	14. Figure 6b,d: consider to cut the FS values ad significantly 'stable' values, e.g. > 10 (no matter if Fs is 10 or 200)! Otherwise make FS in logarithm scale (interesting values are those close to 1).	Incorporated referee's comment and *converted FS (2nd Y-axis) to logarithm scale* to emphasize the values closer to 1.
48	15. Figure 6: Interesting questions here could be: which is the soil depth which causes a 'critical change in FS, i.e. that lead the FS going from stability to instability. And in which time window this is reached?	The referee presents interesting questions that could be addressed in the soil evolution model. However, the soil evolution model is not the focus of our research, but provides a mechanism to estimate soil depth to compare with soil surveys or to use in areas lacking soil depth estimates.
49	16. Figure 12: make figure 5 and figure 12 consistent to facilitate the comparison.	*Partially adjusted Fig. 5* to reflect the same maximum Y-axis limit as Fig. 12 *at 10^{1} and improved legend.* Otherwise retained the figure limits to maximize the display of data within the axes limits.
50	17. Please, note that the obtained values of AUC are very low ... Are you able to identify which landslides are you missing?	We recognize and report that the AUC values indicate modest model performance with observed debris avalanches on page 32, line 19. We have examined the landslides that the model did not identified as high probability as well as areas not mapped as landslides, but with high probabilities. We have not identified a consistent pattern in apparent "mis-matches".

		Additional evaluation of these areas is noted as future work on page 33, lines 24-26. For more discussion about performance, *see comment #7.*
51	18. Figure 15: I suggest reporting the AUC values of the ROC curves.	We report the AUC values in the text on page 32, line 20; however, we *repeated the range in the Fig. 14 caption*.

A hydro-climatological approach to predicting regional landslide probability using Landlab

Comment [RS1]: VERSION WITH TRACK CHANGES

Ronda Strauch[1], Erkan Istanbulluoglu[1], Sai Siddhartha Nudurupati[1], Christina Bandaragoda[1], Nicole M. Gasparini[2], and Gregory E. Tucker[3]

1. Civil and Environmental Engineering, University of Washington, Seattle, WA

2. Earth and Environmental Sciences, Tulane University, New Orleans, LA, USA

3. Cooperative Institute for Research in Environmental Sciences (CIRES) and Department of Geological Sciences, University of Colorado Boulder, Boulder, CO, USA

Corresponding to: Ronda Strauch (rstrauch@u.washington.edu)

Abstract

We develop a hydro-climatological approach to modeling of regional shallow landslide initiation that integrates spatial and temporal dimensions of parameter~~variable~~ uncertainty to estimate an annual probability of landslide initiation based on Monte Carlo simulations. The physically-based model couples the infinite slope stability model with a steady-state subsurface flow representation and operates on a digital elevation model. Spatially distributed ~~raster~~ gridded data for soil properties ~~and a soil evolution model~~ and vegetation classification ~~from National Land Cover Data~~ are used for parameter estimation of~~to derive variables for~~ probability distributions ~~to represent input uncertainty~~for~~that~~ characterize model ~~parameters~~input uncertainty. Hydrologic forcing to the model is through annual maximum daily recharge to subsurface flow obtained from a macroscale hydrologic model~~, routed on raster grid to develop subsurface flow. A Monte Carlo approach is used to generate model parameter~~variables ~~at each grid cell and calculate probability of shallow landsliding.~~ We demonstrate the model in a steep mountainous region in northern Washington, U.S.A.~~, using 30-m grid resolution~~ over 2,700 km^2. The influence of soil depth on the probability of landslide initiation is investigated through comparisons among model output produced using three different soil depth scenarios reflecting uncertainty of soil depth and its potential long-term variability. We found elevation dependent patterns in probability of landslide initiation that showed the stabilizing effects of forests in low elevations, an increased landslide probability with forest decline at mid elevations (1,400 to 2,400 m), and soil limitation and steep topographic controls at high alpine elevations and post-glacial landscapes. These dominant controls manifest in a bimodal

distribution of spatial annual landslide probability. Model testing with limited observations revealed similarly moderate model confidence for the three hazard maps, suggesting suitable use as relative hazard products. ~~Validation of the model with observed landslides is hindered by the completeness and accuracy of the inventory, estimation of source areas, and unmapped landslides.~~ The model is available as a component in Landlab, an open-source, Python-based landscape earth systems modeling environment, and is designed to be easily reproduced utilizing HydroShare cyberinfrastructure.

1 Introduction

In steep mountainous landscapes, episodic shallow landslides (generally <2 m depth; Bordoni et al, 2015) and landslide-triggered debris flows are often the dominant form of hillside erosion and major source of sediment into streams (Benda and Dunne, 1997a, b; Goode et al., 2012). Where landslide processes intersect with human development, they cause property damage, disruption of infrastructure, injury, and loss of life (Taylor and Brabb, 1986; Baum et al., 2008a), contribute to sedimentation in reservoirs (Bathurst et al., 2005), and may even lead to dam failures (Ghirotti, 2012). Landslides provide punctuated sediment input to streams, affecting stream geomorphology (Benda and Dunne, 1997a, 1997b) and ecosystem dynamics (Pollock, 1998; May et al., 2009). Landslide hazard maps are a common tool used to characterize the relative potential for landslide occurrence in space, either qualitatively (using susceptibility levels) or quantitatively (using modeled landslide probabilities) (van Westen et al., 2006; Raia et al., 2014).

Our objective is to develop a parsimonious probabilistic model of regional shallow landslide initiation that can be implemented with minimal calibration for landslide hazard mapping using regionally available, spatially distributed input data for soil, vegetation type, ~~local~~ topography, and hydroclimatology. Based on the literature review presented below, we propose that a regional landslide hazard model should: (1) be flexible enough to incorporate changes in intrinsic and extrinsic conditions, such as vegetation and climate; (2) account for spatial variability in model parameters and forcings, and (3) integrate spatial and temporal dimensions of uncertainty to quantify landslide probability. With these principles in mind, we develop a hydro-climatological approach to modeling regional landslide hazard using the Landlab earth surface modeling toolkit - an open-source, Python-based earth surface modeling framework that provides flexible model customization and coupling (Hobley et al., 2017). Next, we provide a short literature review that guides the design of our landslide modeling approach.

1.1 Geomorphology and Modeling Background

Landslides occur when destabilizing forces due to gravity and pore-water pressure exceed the resisting forces of friction and cohesion over a failure plane. These forces are controlled by intrinsic hillslope conditions, including attributes of topography, such as local slope and upslope contributing area, and properties of rock, soil, and vegetation root cohesion; and extrinsic drivers of rainfall, snowmelt, and earthquakes (Crozier, 1986; Wu and Sidle, 1995; van Beek, 2002; Naudet et al., 2008). There are three primary components of a landslide: (1) a source

area or landslide scar where the initial failure begins, (2) a transmission or scour zone, such as a debris flow channel, and (3) a toe or zone of deposition (Lu and Godt, 2013).

Landslide susceptibility can be identified through numerous methods, which can be broadly grouped into empirical methods and process-based numerical models (Hammond et al., 1992; Wu and Sidle, 1995; Sidle and Ochiai, 2006). Data-driven empirical approaches relate the number and frequency of historical landslide observations in a region to triggering events (Caine, 1980; Crozier, 1999; Glade, 2001), landscape attributes (Carrara et al., 1995; Chung et al., 1995; Lee et al., 2007), or a combination of both (Kirschbaum et al., 2012) using threshold relations and various statistical models such as logistic regression, fuzzy logic, artificial neural networks, and support vector machine (Lee et al., 2007; Pardeshi et al., 2013; Chen et al., 2014). ~~Empirical methods have been used for landslide susceptibility zonation or categorizing the landscape into relative landslide hazards (Sidle and Ochiai 2006).~~

Process-based models employ effective stress principles to characterize the destabilizing and resisting forces under hydrologic drivers (Iverson, 2000; Montrasio and Valentino 2016), offering the ability to explore changes in environmental and climatic conditions, critical for~~.~~ ~~Such process-based models are especially useful in~~ areas with limited landslide inventories (Pardeshi et al., 2013). Recent process-based numerical models have largely focused on improving the characterization of the space-time dynamics of subsurface flow as a driver of pore-water pressure (e.g., Baum et al., 2008b; Raia et al., 2014; Anagnostopoulos et al., 2015; Montrasio and Valentino, 2016). Distributed hydrology models that use steady-state or transient solutions for subsurface flow depth were coupled with an infinite-slope stability model that solves the ratio of stabilizing to destabilizing forces on a failure plane parallel to the land surface (Montgomery and Dietrich, 1994; Miller, 1995; Wu and Sidle, 1995; Pack et al., 1998; Borga et al., 1998; Casadei et al., 2003; Tarolli and Tarboton, 2006; Baum et al., 2008b).

Steady-state models assume that lateral subsurface flow, driven by the topographic gradient, at each point on the landscape is in equilibrium with a steady-state recharge rate (Montgomery and Dietrich, 1994; Pack et al., 1998). The degree of soil saturation is predicted proportional to the ratio of upslope contributing area to local slope, and a ratio of watershed recharge and local soil transmissivity, following TOPMODEL assumptions (Beven and Kirkby, 1979; O'Loughlin, 1986; Pack et al., 1998). More recent efforts have focused on the development of transient flow models in various complexities by coupling vertical infiltration and redistribution processes in the unsaturated zone, using the Richards equation for unsaturated flow (Richards, 1931) or its variants, with lateral flow parameterizations such as kinematic wave in 1- and 2-dimensions (Iverson, 2000; Casadei et al., 2003; Baum et al., 2008b; Godt and McKenna, 2008; Raia et al., 2014; Alvioli et al., 2014; Anagnostopoulos et al., 2015).

While transient flow models have contributed to improved understanding of the influence of weather forcing and temporal variability in precipitation on landslide initiation, they remain tools typically applied for relatively small-scale assessments (Iverson, 2000; Raia et al., 2014). Transient models require a large number of hydrologic soil and vegetation parameters that are

highly variable, uncertain, and difficult to measure or estimate (Godt and McKenna 2008; Baum et al., 2008b). In addition, in most steep forested mountains where landslide risk is high, the presence of macropores due to connected root structures, biological activity, fractures, large clasts, and lenses, leads to preferential and funneled flows that violate the assumptions of most matrix-flow models (Nimmo, 2005; Sidle et al., 2001; Gabet et al., 2003; Montrasio and Valentino 2008; Beven and Germann 2013). Numerical solutions to flow equations also present a major computational bottleneck in large-scale applications for probabilistic quantification of landslide hazard.

~~Comparison of steady-state and transient models using case studies with known extreme rainfall events that caused widespread landsliding involve statistical model performance evaluation (Zizioli et al., 2013).~~ While using transient hydrologic models provided slight improvements in the prediction of landslide locations, overall, statistical comparisons of model outputs between steady-state and transient models revealed fairly similar degrees of success (Gorsevski et al., 2006; Zizioli et al., 2013; Anagnostopoulos et al., 2015; Boroni et al., 2015; Formetta et al., 2016). In some applications, model complexity increased the accuracy of predicted landslide locations at the expense of overestimating instability on unsaturated hillslopes (e.g., Godt et al., 2008; Bellugi 2011). In other cases, model precision increased while accuracy decreased (Gorsevski et al., 2006).

Data uncertainty due to spatial and temporal variability of parameter~~variable~~s continues to be one of the major challenges in predicting landslides over broad regions (Crozier, 1986; Sidle and Ochiai, 2006; van Westen et. al., 2006; Baum et al., 2014; Anagnostopoulos et al., 2015). ~~These~~ Parameter uncertainties ~~and variabilities~~ can develop from geological anomalies, inherent spatial heterogeneities in soil and vegetation properties and their changes over time, and sampling limitations (El-Ramly et al., 2002; Cho, 2007; Baum et al., 2014). Uncertainties in hydro-climatic~~e~~ variables~~quantities~~, such as precipitation, air temperature, and resulting hydrologic fluxes ~~and recharge~~, are particularly pronounced in steep high mountain regions due to lack of observations to capture~~and~~ complex ~~spatial and temporal~~ atmospheric processes (Roe, 2005; Wayland et al., 2016). Designating landslide hazard as a probability, rather than an index, systematically accounts for uncertainty and variability in stability analysis (Hammond et al., 1992; Simoni et al., 2008; Arnone et al., 2014) and more appropriately represents complex systems (Berti et al., 2012). ~~Currently, only limited~~Recently, some promising advances have been made in process-based models accounting for data uncertainty in landslide hazard mapping (e.g., ~~Pack et al., 1998;~~ Raia et al., 2014; Arnone et al., 2016a).

~~Observations and model experiments suggest that the largest landslides are usually associated with the largest rainfall events (e.g., Page et al. 1994; Gorsevski et al., 2006). Considering that hillslope hydrology is more likely to attain equilibrium conditions during prolonged wet conditions (e.g., Barling et al., 1994; Borga et al., 2002), a steady-state representation of subsurface flow hydrology, coupled with a process-based infinite slope stability model is an efficient approach for predicting the likelihood of landslide hazard at regional scales.~~

Lastly, most landslide hazard methods disregard a temporal dimension over which landslide probability is defined (Wu and Sidle, 1995; van Westen et al, 2006). As a result of that, instead of using estimated probabilities directly in the form of return periods of observed landslides or expected values for risks resulting from landslides, models use probability estimates as relative indices (eg., Pack et al., 1998) that can be used for hazard zonation (Pardeshi et al., 2013). Lack of temporal dimension limits the incorporation of model results into risks assessments and the decision-making processes in high-risk regions.

1.2 Approach Overview

We develop a process-based modeling approach for shallow landslide initiation that incorporates imprecision ~~s~~ and uncertainty~~ies~~ in hydro-climatological forcing, soils, and ~~land cover properties~~vegetation parameters using ~~a~~ Monte Carlo simulation~~ approach~~. ~~Rather than predicting critical rainfall intensity necessary to destabilize hillslopes (Montgomery and Dietrich 1994) or a terrain stability index map (Pack et al. et al., 2001, 2005), O~~our approach aims to develop a spatially continuous probability of landslide *initiation* that can be updated as conditions and triggers change~~evolve~~. ~~The~~ model evaluates factor of safety using ~~the~~ infinite slope stability equation ~~at~~ the scale of a grid cell from a Digital Elevation Model (DEM) through Mont~~.~~e Carlo simulation and calculates the probability of landslide initiation (Hammond et al., 1992; Raia et al., 2014). A Landlab component (LandslideProbablity) and a model "driver" that runs the component are written and a workflow is developed for mapping shallow landslide probability. The model driver and data are deployed on HydroShare (www.hydroshare.org), an online collaboration environment for sharing data, models, and code (Horsburgh et al., 2016; Idaszak et al., 2016), and made available for cloud computing via HydroShare JupyterHub infrastructure using a web browser (see Sect. 2.5).

In this work we explore the following question using Landlab and regional landslide observations: How do spatial patterns in hydro-climatology, vegetation, and soil depth influence shallow landslide initiation over large geographic scales? We demonstrate our approach in a mountainous region of Washington, USA. This Pacific Northwest (PNW) region is naturally susceptible to landslides because of high and intense rainfall, steep mountains, active tectonics, and geologic and glacial history (Nadim et al., 2006; Sidle and Ochiai, 2006). The Oso landslide, which occurred in the vicinity of our study area in 2014, resulting in 43 fatalities and over $50 million in economic losses (Wartman et al., 2016).

~~et al. et al., 1994) as used in our regional application, or assigned as parameters by the user. Raster grids derived from soil texture and vegetation cover classes are used with look-up tables to estimate model variables ranges obtained from the literature to quantify uncertainty. Through Monte Carlo simulation (Raia et al., 2014), we calculate the probability of landslide initiation at each landscape grid cell. Our probability is further refined by a geomorphic soil evolution model that estimates soil depth with greater spatial heterogeneity than conventional soil survey map units, which is critical for slope stability analysis (Dietrich et al., 1995). This soil evolution model estimates long-term soil depth based primarily on soil mass production and~~

Formatted: Font: Not Italic

Formatted: Highlight

~~slope-dependent sediment transport rules.~~

~~In this work we explore the questions (1) How does regional hydro-climatology influence the spatial patterns of shallow landslide initiation over large geographic scales? and (2) How does distributed soil depth influence the probabilistic nature of landslide initiation compared to coarse-scale, homogenous soil depth estimates? We demonstrate our approach in a mountainous region of Washington, USA. This Pacific Northwest (PNW) region is naturally susceptible to landslides because of high and intense rainfall, steep mountains, active tectonics, and geologic and glacial history (Nadim et al., 2006; Sidle and Ochiai, 2006). The Oso landslide, which occurred in the vicinity of our study area in 2014, resulting in 43 fatalities and over $50 million in economic losses, provides a solemn reminder of the hazard landslides present (Wartman et al., 2016). Although the Oso landslide was a deep-seated type, the greater frequency of shallow landslides affords utility and relevance to our model.~~

2 Methodology

2.1 Probabilistic approach to landslide initiation

~~Our approach is based on t~~The infinite slope stability equation, derived from the Mohr-Coulomb failure law, ~~that~~ predicts the factor-of-safety (FS) ~~stability index of a hillslope parcel~~of an infinite plane from the ratio of stabilizing forces of ~~soil~~ cohesion and friction, reduced by pore-water pressure ~~of subsurface flow~~, to destabilizing forces of gravity (Hammond et al., 1992; Wu and Sidle, 1995). The model as given by Pack et al. (1998) is:

$$\square\square = \frac{(\square_{\square} + \square_{\square})/h}{\sin} + \frac{\cos \quad \tan \quad (1- \qquad / \quad)}{\sin} \qquad (1a)$$

$$* = (\quad + \quad)/h \qquad (1b)$$

Formatted: Space Before: 6 pt

Formatted: Space After: 6 pt

C* is a dimensionless cohesion (Eq. 1b) embodying the relative contribution of cohesive forces to slope stability. When C*>1, cohesion is sufficient to hold the soil slab vertically (Pack et al., 1998). *Cr* and *Cs* are root and soil cohesion respectively [Pa], h_s is the soil depth perpendicular to slope [m], ρ_s and ρ_w are saturated soil bulk density and water density [kg/m^3], respectively, *g* is acceleration due to gravity [m/s^2], θ is slope angle of the ground, and ø is soil internal friction angle [°]. Relative wetness, R_w, is defined as the ratio of subsurface flow depth, h_w, flowing parallel to the soil surface, to h_s. Deterministically, a hillslope element is unstable if *FS* < 1 and stable if *FS* > 1 (Sidle and Ochiai, 2006; Shelby, 1993). When FS = 1, the slope is "just-stable" or in a state of "limited equilibrium" (Lu and Godt, 2013).

Relative wetness is arguably the most dynamic factor at short time scales, relating to water table depth and to recharge rate. Considering that hillslope hydrology is more likely to attain equilibrium conditions during prolonged wet conditions (e.g., Barling et al., 1994; Borga et al., 2002), a steady-state representation of subsurface flow is used. It is derived from local subsurface lateral flow, q_s [m^2 d^{-1}], represented by a 1-D (i.e., flow parallel to bedrock) form of

the kinematic wave approximated by Darcy's law using topographic gradient of hillslope, $q_s=K_s h_w \sin\theta$ (Wu and Sidle, 1995). Under a steady-state assumption, lateral flow is in balance with the rate of water input, q_r [$m^2\ d^{-1}$], through a uniform rate of recharge, R [$m\ d^{-1}$], defined across the upslope specific contributing area, a [m], $q_r=Ra$. This assumption gives: $Ra=K_s h_w \sin\theta$, where K_s is saturated hydraulic conductivity [$m\ d^{-1}$]. Solving this equation for h_w and dividing both sides by h_s gives R_w (Montgomery and Dietrich, 1994; Pack et al., 1998):

$$\square_{\square} = \frac{h}{h} = \min\left(\frac{\quad}{\sin}, 1\right) \qquad (2)$$

Here T is local soil transmissivity [$m^2\ d^{-1}$], which is depth-integrated saturated hydraulic conductivity, K_s. For uniform K_s within the soil profile~~,~~ overlying ~~a~~ impermeable bedrock $T=K_s h_s$. Ground saturates when R_w = 1, ~~which represents hydrostatic conditions and~~ the maximum value for R_w. ~~Options for user-provided T or K_s are accepted by the component; although comparison of resulting probabilities were found to be similar given that the value of T was derived from h_s. We assume uniform conductivity within the soil profile overlying a relatively impermeable layer such as bedrock, and subsurface flow direction parallel to this drainage barrier~~ (Montgomery and Dietrich, 1994). These assumptions are appropriate for ~~relatively~~ steep topography ~~and~~ to efficiently characterize wetness over large areas (Tarolli and Tarboton, 2006; van Westen et. al., 2006).

A Monte Carlo simulation is used with equation (1a) by assuming R, T, C ($C=C_r+C_s$), h_s and ϕ as random variables represented by probability distributions (Tobutt, 1982; Hammond et al., 1992). ~~One benefit of Monte Carlo simulation is that many of the sources of inaccuracy (e.g., nonlinearity, input uncertainties) are overcome (Strenk, 2010; El-Ramly et al., 2002) by generating a distribution of samples over a plausible range for selected variables.~~ The uncertainty in R is ~~defined~~ represented ~~by~~ using a ~~time series~~dataset of the maximum daily recharge in each year (e.g., Benda and Dunne, 1997a; Borga et al., 2002; Istanbulluoglu et al., 2004). The model includes both spatially uniform and spatially distributed options for sampling recharge (described further in Sect. 2.3). Using sampled random variables in Eq. (1a), FS is calculated in each model iteration, i, during the simulation. Annual probability of failure P(F) and landslide return period (RP) at each grid cell are defined as (Hammond et al., 1992; Cullen and Frey, 1999):

$$P(F) = P(FS \le 1) = n(FS \le 1)/N \qquad (3a)$$

$$RP = P(F)^{-1} \qquad (3b)$$

Comment [RS2]: We don't multiply n times FS<1. We sum up the FS<1 (count)

~~*~~

~~( ) = (≤ 1) = (≤ 1)** USE THE ORIGINAL EQUATION the revised equation is not correct there is the summation version of it too in the drop box that is not right**.~~

where n() is the number of conditions met in brackets and N is the number of iterations. Our model does not predict the size of a probable landslide at the initiation point, which can be smaller or larger than the size of a DEM grid. P(F) gives a relative propensity that a landslide could initiate within the grid cell. ~~The design of the model reflects the uncertainty of soil and vegetation within a grid cell. Therefore, l~~if some random samples lead to a low deterministic FS, they contribute to an increase of the P(F) within that cell. ~~S~~sensitivity analysis of the infinite slope stability model was shown in the literature ~~input values in the infinite slope approach have been performed elsewhere~~ (see: Sidle 1984; Hammond et al., 1992).

Formatted: No Spacing

2.2 Model Development in Landlab

~~The landslide modeling approach presented above is implemented in Landlab (landlab.github.io). Landlab is an open-source modeling toolkit written in Python for building and running two-dimensional numerical models of Earth-surface dynamics (Tucker et al., 2016; Hobley et al., 2017; Adams et al., 2017). A detailed explanation of the Landlab framework is provided in Hobley et al. (2017).~~ Landlab is a python-based earth surface modeling toolkit (landlab.github.io). It provides a grid architecture, a suite of pre-built components for modeling surface or near-surface processes, and utilities that handle data creation, management, and interoperability among process components (Tucker et al., 2016; Hobley et al., 2017; Adams et al., 2017). ~~The Landlab design allows for a "plug-and-play" style of model development, where process "components" can be coupled together in a user-customized "model driver". Each component is a set of code functions that represent an individual process; the model driver has code used to import or generate required data, execute the component or set of components used in the model, and to visualize results. For example, once a DEM is imported as a Landlab grid instance, any Landlab component can be used with interoperable methods to attach data and perform operations. Landlab landslide modeling code developed for this work is explained in detail in the user manual supportingof the Landlab LandslideProbability component available from eSurf and the Landlab github website(see Sect. 6).~~

The LandslideProbability component is written in python and implemented with a model "driver" (written as a Jupyter Notebook) using ~~Landlab~~the workflow ~~developed in this regional landslide probability mapping study uses the LandslideProbability component presented in Fig. 1. The workflow includes preparing~~shown in Fig. 1 of the~~(~~see component's User Manual (See Sect. 6). The driver imports Landlab and necessary Python libraries, loads and processes data, and executes the LandslideProbability component on RasterModelGrid (RMG), which is a Landlab class for creating raster grid objects. A structured grid is generated by the RMG class that covers the model domain. The spatial model parameters~~variables~~ and model forcing data are completed in preprocessing steps outside of Landlab. ~~A model driver is written to run the LandslideProbability component on RasterModelGrid (RMG) instance only. RMG is a Landlab class for creating raster grids and representing the connections among grid elements. A structured grid is generated that covers the model domain. Spatial model parameter~~variables ~~and forcing variables~~They ~~supplied by the user~~ are loaded and stored on grid~~the~~ nodes (the central point of grid cells) of the ~~grid~~ RMG~~elements~~ as Landlab data fields, ~~which are~~composed of NumPy arrays ~~containing data associated with grid elements (in this case nodes, which~~

Formatted: Font: 12 pt, Font color: Black

Formatted: Font: 12 pt, Font color: Black

~~represent the central point of grid cells)~~.

The LandslideProbability component is instantiated by passing four arguments: the grid, number of iterations, recharge distribution, and recharge parameters. Once the component has been instantiated, the component's method *calculate_landslide_probability*() is executed in a for loop that performs the calculations at each node. The number of iterations in the range of 700 (Malkawi et al., 2000) to >1,200 (Abbaszadeh et al., 2011) were found sufficient in the literature. We used 3,000 in this study. At each node the method generates unique model parameters, and calculates the relative wetness (Eq. 2) and FS (Eq. 1a) for~~t~~ each iteration. At the end of the iterations, probability of saturation and probability of failure are calculated at each node. ~~The driver imports Landlab and necessary Python libraries as well as loads and processes data required for the LandslideProbability component.~~

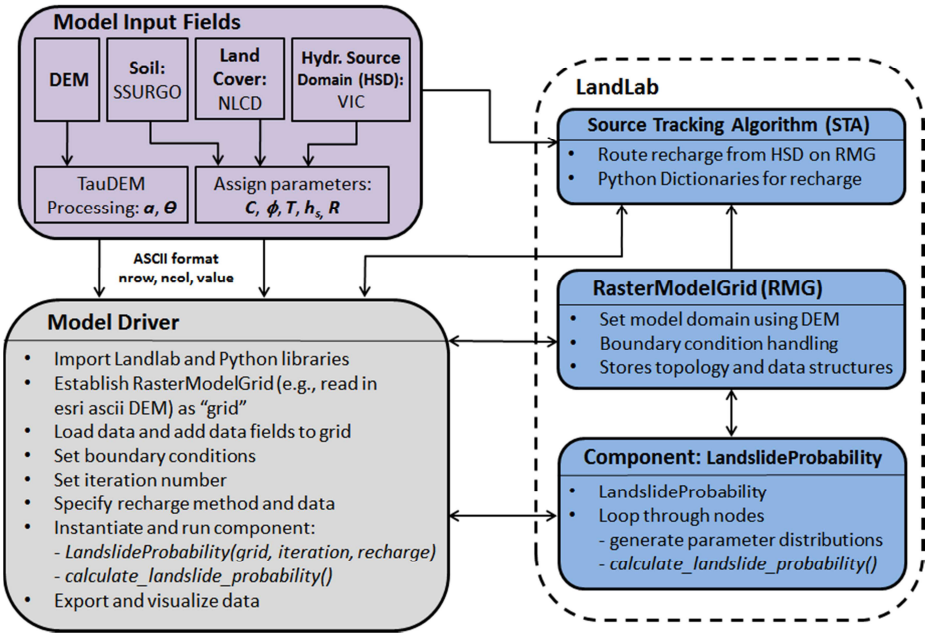

Figure 1. Workflow for landslide modeling using the Landlab LandslideProbability component. The user creates input parameter fields (purple box). The model driver (gray) imports Landlab, Python libraries, and model parameter fields~~:~~; instantiates (e.g., create an instance) the RasterModelGrid and the component; and runs utilities and the Landlab component (blue inside dashed box).

Slope angle and specific contributing area are static parameters derived from a DEM in pre-processing steps. Total cohesion, C (i.e., C_r+C_s), $\varnothing$, h_s, and T are treated as random variables following a triangular distribution specified with three parameters (minimum, mode, and

Formatted: No widow/orphan control, Don't adjust space between Latin and Asian text, Don't adjust space between Asian text and numbers

Formatted: Font: +Body (Calibri)

Formatted: Font: +Body (Calibri), Italic

Formatted: Font: +Body (Calibri)

Formatted: Font: +Body (Calibri)

Formatted: Font: (Default) Times New Roman

maximum) ~~to represent spatial and temporal uncertainties in these parameters on the landscape~~ (Cho, 2007; Dou et al., 2014). Options for user-provided T or K_s are accepted by the component; although comparison of resulting landslide probabilities were found to be similar given that the value of T was derived from h_s. Triangular distributions give weight to the most likely value (i.e., mode) and have been proposed in other Monte Carlo simulation studies for slope stability (Hammond et al., 1992; El-Ramly et al., 2002; Strenk, 2010).

Mode parameters of the triangular distribution used for all soil and vegetation parameters are developed as raster grids as part of preprocessing steps, loaded to Landlab, and assigned to nodes of the RMG (Fig. 1). For root cohesion we used ~~Parameters of the triangular distribution can be assigned by relating~~ vegetation types from the ~~categorical vegetation cover variables, for example the~~ National Land Cover Data (NLCD) (Jin, 2013; USGS, 2014b) ~~or other map sources~~, with a lookup table for cohesion obtained from the literature (Table 1). Only for cohesion, minimum and maximum parameters are also provided as raster grids to represent distributed variation with vegetation. ~~and using available soils data such as gridded~~Gridded Soil Survey Geographic Database (SSURGO) (*DOA-NRCS* 2016) is used~~,~~ to assign ~~ϕ internal friction angle~~, h_s ~~soil depth~~, and T ~~transmissivity~~ (see 3.2.1~~3~~ for details). The current model design assumes negligible correlation between C and ϕ as assumed in other studies (e.g., Abbaszadeh et al., 2011; Arnone et al., 2016a). Other spatial soil and vegetation datasets can be used in the preprocessing of the model. Exposed bedrock and glaciated surfaces can be excluded from the model domain by user. ~~Soil density is set as a constant field, 2,000 kg m^{-3} in our application.~~

In each Monte Carlo iteration, we ~~characterize recharge as an~~use annual maximum daily recharge, R, which represents a steady-state uniform recharge rate defined for the upslope contributing area of each RMG node ~~event~~. Local recharge (i.e., flux of water entering saturated zone) within the upslope contributing area of RMG nodes can be incorporated from a variety of grid resolutions from hydrologic models, referred to as a Hydrologic Source Domain (HSD). A "Source Tracking Algorithm" (STA) is developed that uses spatially variable recharge data from a HSD, re-sampled to the grid resolution of slope stability calculations, and routes local recharge in the downstream direction following the steepest descend until a target cell is reached. Then it calculates the spatially-averaged upslope recharge for each node of the RMG, used as R in the model. STA is described in more detail in the component's User Manual (See Supplement).

Four options for sampling ~~recharge~~ R are provided for Monte Carlo simulation~~s~~ at each node, ~~which are~~ identified in the model driver by selecting a probability distribution: *uniform, lognormal, lognormal_spatial,* and *data_driven_spatial*. The first two options assign spatially uniform random variables of R across the whole model domain with respective parameters of minimum and maximum, and mean and standard deviation. The latter two "spatial" options are designed to represent spatial variability in R~~recharge~~, constructed based on the statistics of annual maximum R obtained from a HSD using the STA utility~~historical annual maximum daily recharge. routed to each node of the model domain.~~ The *lognormal_spatial* option assigns mean and standard deviation of R at each node derived from the modeled R data, while the

Formatted: No widow/orphan control

Formatted: Font: 12 pt, Not Italic, Font color: Black

data_driven_spatial option uses a non-parametric sampling approach to sample from the cumulative distribution of R data produced for each node of the RMG. In this regional application of the landslide component, the VIC macroscale (1/16° or 5x6 km grid cell) hydrology model is used as HSD. annual maximum recharge and uses a lognormal distribution of recharge for simulation. The *data_driven_spatial* option calculates uses a non-parametric Monte Carlo sampling approach to sample directly from historical a recharge data distribution of . Uupslope-averaged recharge for each grid node is calculated with the Landlab Source Tracking Algorithm (STA) utility using recharge from a HSD, which in this study issuch as the VIC macroscale (1/16° or 5x6 km grid cell) hydrology model, and by interpolating a cumulative distribution of recharge equal to the length of the number of Monte Carlo iterations used in the simulation .

Within the model driver, the user also sets any boundary conditions, such as areas to exclude (i.e., bedrock outcrops, glaciers) and assigning the number of Monte Carlo iterations (n>>1,000, Hammond et al., 1992). The seed random number generator does not appear to affect Monte Carlo simulation results and n>700 (Malkawi et al., 2000) or n>1,200 (Abbaszadeh et al., 2011) is sufficient to converge to the same probability of failure. The LandslideProbability component is instantiated by passing four arguments: the grid, number of iterations, recharge distribution, and recharge parameters. Multiple instances of the LandslideProbability class can be established in one driver to compare the results from different recharge specifications. Once the component has been instantiated, the component's method *calculate_landslide_probability()* is run. For each iteration, this method loops through each core node, generates unique model parametervariables, and calculates the relative wetness (Eq. 2) and deterministic FS index (Eq. 1a) at each iteration. At the end of the iterations, the P(F) at the node is calculated as the number of iterations in which FS≤1 divided by the number of iterations (n). Variables output by the component at each core node include calculated probability of saturation and P(F), which can be queried at each node or visualized across the entire grid within the driver or using a command line terminal to execute commands.

Formatted: Font: 12 pt, Font color: Black

2.3 Hydrologic Data Processing

A key aspect of the regional landslide modeling approach is the linking of landslide hazard to hydro-climatological forcing at regional scales. The Landlab LandslideProbabilty component is written with the capability to accept input from hydrologic model outputs, such as. We used the VIC macroscale hydrologic model (Liang et al., 1994) we to demonstrate in this paper. this capability because it VIC is semi-distributed, predominantly physics-based macro-scale hydrology model that characterizes elevation-dependent differences in regional precipitation and temperature forcings and their influence on recharge through regulating rain-on-snow, snow accumulation and melt, rain-on-snow, evapotranspiration, and soil moisture. VIC is semi-distributed, predominantly physics-based macro-scale hydrology model, which is advantageous for representing distributed parameters of hydro-climatology that are not stationary in time over large regional areas (Hamlet et al., 2013).

~~The VIC model simulates the land surface as a large, flat, uniform grid with sub-grid heterogeneity (e.g., vegetation and elevation) based on statistical distributions. Daily or sub-daily meteorological drivers (e.g., temperature and precipitation) influence the fluxes of water and energy near the land surface. Each grid is simulated independently and flows between grid cells are ignored (e.g., unrouted). Precipitation enters the upper of typically three layers of soil and infiltrates to lower layers via a variable infiltration curve. Soil water can move between layers vertically and is lost through evapotranspiration and from the third layer as base/subsurface flow via non-linear recession. Water input in excess of infiltration forms surface runoff.~~

The steady-state subsurface model coupled with the infinite slope stability equation in our model requires a steady-state recharge rate as input. Recharge refers to the input of water to subsurface flow from precipitation and snowmelt less ~~of~~ evapotranspiration and soil storage. In a VIC model simulation, this condition can be obtained by adding baseflow and surface runoff. Observations and model experiments suggest that widespread landslides ~~is~~ are usually associated with the largest rainfall events (e.g., Page et al., 1994; Gorsevski et al., 2006). To characterize ~~the annual probability~~ when the ground is likely to be the most saturated each year, daily baseflow and surface runoff are summed at each VIC grid cell to represent daily recharge [mm d^{-1}] and the annual maximum daily value is selected for each ~~model~~ year of the dataset, similar to others (e.g., Benda and Dunne, 1997a; Borga et al., 2002; Istanbulluoglu et al., 2004). ~~Observations and model experiments suggest that the largest landslides are usually associated with the largest rainfall events (e.g., Page et al., 1994; Gorsevski et al., 2006). The recharge data arrays are keyed to latitude, longitude, and grid cell ID (a user-defined ID for each VIC grid cell, in our case) packaged as Python dictionaries (see Fig 1. of User Manual). To help account for lateral fluxes in groundwater (van Beek, 2002)~~To obtain a steady-state average recharge rate in the upslope contributing area of each RMG, ~~VIC recharge is routed to each node in the model grid using~~ the ~~STA~~ Landlab STA utility is used ~~, which also addresses the different spatial resolutions of VIC and the RMG~~ (see S~~s~~ect~~ion~~. 2.2., and Fig 1. of User Manual link provide in Sect. 6). ~~This Landlab utility was developed to derive the fraction of annual maximum recharge from each VIC grid cell within the upslope contributing area of each Landlab grid node. The fractions and VIC IDs are saved as values for two Python dictionaries keyed to the RMG node ID. At each node, these dictionaries are used to calculate the upstream proportionally averaged maximum recharge for each year.~~

Formatted: No widow/orphan control

2.4 Soil ~~Depth Evolution~~Evolution Model

Soil depth controls the temporal and spatial patterns of landsliding over geomorphic time scales and is considered one of the most significant ~~parameter~~variables controlling the FS stability index, especially at depths less than 1.5 m (Benda and Dunne, 1997a; Istanbulluoglu et al., 2004; Catani et al., 2010; Sidle and Ochiai, 2006). Soil depth can vary in space and time as a function of weathering and sediment transport in relation to climate, lithology, topographic position, and vegetation cover (Dietrich et al., 1995). Despite its fine grid resolution, the SSURGO database (*DOA-NRCS* 2016) only broadly captures topographic controls on soil depth and reflect existing conditions in the field ~~as it's~~ based on soil surveys. In an attempt to

improve the representation of spatial granularity and local uncertainties of soil depth, ~~As an alternative to spatial soil maps such as the SSURGO database (*DOA-NRCS* 2016), which are often produced at the soil pedon level, we developed a soil depth map~~ a soil evolution model is used ~~using a simple soil evolution model and topographic and land cover attributes~~ (Dietrich et al., 1995; Simoni et al., 2008; Pelletier and Rasmussen, 2009; Tesfa et al., 2009; Bellugi et al., 2015). The model is run to develop time series of soil depth from which triangular distribution parameters for soil depth (mode, minimum and maximum) can be obtained and used in Landlab LandslideProbability component.

In the soil evolution model, change in soil depth is modeled as the annual sum of local soil production, divergence of sediment flux due to soil creep, and soil removal by landslides (e.g., Tucker and Slingerland, 1997; Heimsath et al., 1997; Braun et al., 2001; Istanbulluoglu et al., 2004; Nicótina et al., 2011). The rate of soil production is related exponentially to local soil depth (Heimsath et al., 1997). Soil creep is linearly related to local elevation gradient (e.g., McKean et al., 1993). Soil removal by landslide initiation is modeled with the infinite slope stability equation, implemented with representative parameters (Table 2~~).~~ When FS≤ 1, ~~).~~ ~~When FS<1, Change in soil depth depends on soil production by bedrock weathering and slope-dependent sediment transport expressed as (Nicótina et al., 2011; Tucker and Slingerland, 1997; Heimsath et al., 1997):~~

~~$$\frac{\partial z_b}{\partial t} = -P_0 e^{-\alpha h_z} \quad (5)$$~~

~~where P_o is the soil production rate from exposed bedrock (i.e., no soil cover) and α is the rate of exponential decay with depth. Diffusive sediment transport characterized in the second term on the right side of Eq. (4) can be represented by a simple soil creep function dominant in convex hillslopes as (Nicótina et al., 2011; Istanbulluoglu et al., 2004):~~

~~$$\nabla q_s = -K_d \nabla^2 z \quad (6)$$~~

~~where K_d is a linear hillslope diffusion coefficient and ∇^2 is Laplacian of elevation. Dividing Eq. (4) by ρ_s, multiplying by the ratio of ρ_r / ρ_s, and substituting Eq. (5) and Eq. (6) into Eq. (4), yields the following instantaneous soil depth equation:~~

~~$$\frac{\partial h_z}{\partial t} = \frac{\rho_r}{\rho_s} P_0 e^{-\alpha h_z} + K_d \nabla^2 z \quad (7)$$~~ ~~Variable curvature profiles, steep and planar hillslopes, and abrupt knife edge drainage divides indicate nonlinear transport processes such as mass wasting (Roering et al., 2004, 1999). These landscape characteristics are common in the steep terrain; therefore, in every iteration of the model, Eq. (1a) and Eq. (2) are used to calculate FS within the soil evolution model. This deterministic FS is independent of the FS values calculated during the Monte Carlo simulations described in Sect. 2.2. When FS≤1,~~ soil is removed to bedrock by setting it to a very small value ~~of~~ (0.005 m) ~~to be consistent with the creep equation~~. In each model iteration~~,~~ C and T~~,~~ were randomly sampled and used ~~deterministically~~ in the FS Eq. (1a). Calibration of the soil evolution model is done by adjusting ~~P_o~~ soil production rate and ~~K_d~~ hillslope ~~diffusion coefficient~~diffusivity parameter to obtain long-term soil loss consistent with ~~for the location of the landslide analysis based on published~~ long-term regional ~~rates of~~ erosion rates ~~and diffusion~~. Details on model application and the utilization of model outputs are presented in ~~Creation, calibration, and application of the soil evolution model are detailed in~~ Sect. 4.1.2.

Formatted: Highlight

Formatted ... [1]

Formatted: Left, Indent: Left: 0 cm, Space Before: 0 pt, After: 0 pt, Tab stops: Not at 12.7 cm

Formatted: Font: Cambria Math, Highlight

Formatted: Left, Indent: Left: 0 cm, Space Before: 0 pt, After: 0 pt, Tab stops: Not at 12.7 cm

Formatted ... [2]

Formatted ... [3]

Formatted ... [4]

Formatted ... [5]

2.5 Reproducibility

To publish a reproducible version of this research, we used the HydroShare (www.hydroshare.org) cyberinfrastructure platform, ~~which is~~ designed ~~explicitly to encourage the~~for reproducing, reusing and sharing ~~of~~ models (Tarboton et al., 2014; Horsburgh et al., 2016; Morsy et al., 2017). Steps that supported reproducibility included using the HydroShare sharing settings with a workflow that started with *Private* while data and models were developed, *Discoverable* while research was being shared with colleagues for review, and *Public*, once our results were accepted for publication. We used the *Select a license* function to add No Commercial (NC) use to our Creative Commons license. We made use of the *Groups* social collaboration, by making early versions of our research results available to invited participants of workshops and tutorial demonstrations to our Landlab group in HydroShare. The data and model are accessed by launching Jupyter Notebooks that access Landlab installed on JupyterHub servers at the National Center for Supercomputing Applications (Yin et al, 2017; Castranova, 2017). HydroShare features enable our current and future researchers to use the *Copy Resource* function to replicate our published resource (i.e., the landslide model) in their own account with *Derived from* metadata that references back to the published resource DOI, to serve as a starting point for their work. The Supplement provides instructions on how to access Hydroshare and run a Jupyter Notebook that reproduces portions of the application below.

3 Model A~~a~~pplication

3.1 Study Area

The model described above is applied within the geographical limits of the North Cascades National Park Complex (NOCA) in the state of Washington, U.S.A, managed by the U.S. National Park Service (Fig. 2). In recent decades, NOCA has experienced damaging and disruptive landslides that have impacted infrastructure and the public. Furthermore, the park area is covered by a recent soil survey between 2003 and 2009, including field investigation (DOA-NRCS and DOI-NPS, 2012), and has a complete map of mass wasting processes visually observed in the field (Riedel and Probala, 2005). The application is designed to demonstrate the potential capability of Landlab LandslideProbability component using existing data in a real setting and to provide a site-specific stability analysis for landslide susceptibility ~~that indicates potential areas susceptible to landsliding~~ for NOCA land management.

NOCA is approximately 2,757 km^2, with 93% wilderness, ~~(in which no permission for~~where motorized or mechanized devices are not allowed ~~are permitted;(~~ DOI-NPS, 2012), which is ideal for studying naturally triggered landslides. The elevation ranges from about 100 m to 2,800 m (Fig. 2a). The terrain is composed of rock slopes at the highest elevations, short (<100 m) soil-mantled hillslopes, and landslides upslope of relatively straight debris flow channels connected to the fluvial system. Over 300 glaciers occupy mountain peaks in NOCA. The influence of the Pacific Ocean, approximately 80 km to the west, provides a humid temperate

climate. However, the north-south oriented Cascade Mountains create an effective orographic climate boundary, separating a wetter west side from a drier east side. Reported mean annual precipitation ranges from about 708 mm in the low elevations of the eastern slopes to 4,575 mm at the highest mountain elevations west of the Cascade crest, with about 70% falling in November through March (Fig. 2b). This spatial precipitation gradient is the result of orographically-enhanced precipitation that leads to a strong rain shadow (Roe 2005). Average annual air temperatures range from -2 to 11°C, depending on elevation (DOA-NRCS and DOI-NPS, 2012).

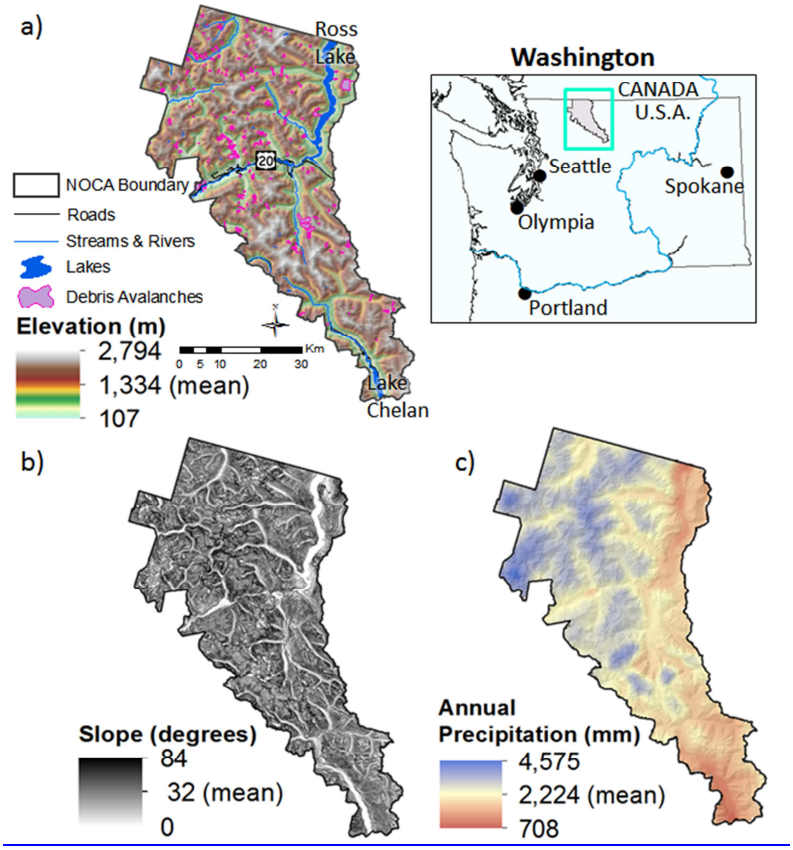

Figure 2. North Cascades National Park Complex (NOCA) in northern Washington state, U.S.A: **(a)** a 30-m DEM of the domain overlain by debris avalanches and major water bodies; **(b)** slope derived from DEM; and **(c)** mean annual precipitation (1981-2010 average) mapped at 800-m resolution from PRISM (Daly et al., 2008). ~~Is this how PRISM data is cited..?~~

~~Vegetation is mainly coniferous trees, with deciduous trees along river floodplains, and shrubs, meadows, and barren land in the subalpine and alpine environments.~~ In this study vegetation classes were grouped into herbaceous, shrubland, and forest using the 2014 NLCD data, ~~which~~

Formatted: Centered

~~is~~ based on the land use/land cover (LULC) classification of 2011 Landsat satellite imagery (Jin, 2013; USGS, 2014b). Other LULC types include water, wetland, snow/ice, barren, and developed (e.g., roads, campgrounds), covering about 13% of NOCA. Based on this classification, forest, shrubland~~s~~, and herbaceous vegetation represent 58%, 17%, and 12% of the park, respectively. Elevation ranges for these vegetation classes are from 106 to 2363 m (forest), 110 to 2465 m (shrubs), and 121 to 2759 m (herbaceous), showing vegetation co-existence. ~~OTHER TYPES OCCUPY X%.~~

Formatted: Highlight

The park geology is composed of a complex mosaic that includes mostly ~~complexly~~ faulted and folded sedimentary and volcanic rocks on the west side, unmetamorphosed sedimentary and volcanic rock on the eastern edge, and highly squeezed and recrystallized metamorphic rock originating from great depth in middle (Haugerud and Tabor, 2009). Alpine and continental glaciation, along with rivers and mass-wasting processes linking peaks with rivers, have created the landscape ~~we observe today~~. The glaciers eroded U-shaped valleys with steep valley walls prone to landslides and flat valley floors with gravel-bed rivers. The lower ends of many valleys on the east side with lower precipitation were not covered in alpine glaciers and have narrow, winding V-shaped canyons and steep, narrow rivers.

A park-wide landform mapping study identified six different types of mass wasting landforms: rock fall/topple, debris avalanche, debris torrent, slump/creep, sackung, and snow avalanche-impacted landforms (Riedel et al., 2015). Mass wasting landforms were identified ~~in the landform mapping~~ using 1998 air photos at 1:12,000 scale, 7.5 minute topographic maps, bedrock geology maps, and field investigations. The minimum mapping unit was approximately 1,000 m^2, except for a few smaller slump units. In this study, we only used mapped debris avalanches for model confirmation as they often initiate by a shallow landslide ~~processes~~. Debris avalanches typically represent a mixture of failed rock and debris. T~~and t~~heir mapping included ~~mapped~~ polygons that combine ~~included~~ head scars, transport and scour channel~~s~~s, and deposition zone~~s represented~~ in a single polygon (Fig 3a). We extract the highest 10% of the elevations in the mapped debris avalanche polygons as landslide source areas through comparison to aerial imagery (Tarolli and Tarboton, 2006). This analysis located 75% of landslide source areas ~~Landslide sources are more frequent~~ in ~~the~~ intermediate elevations from 1,200 m to 2,000 i~~. I~~n ~~the~~ NOCA ~~region, 75% of landslide source areas are located in the 1,200 m to 2,000 m elevation range~~ (Fig. 3b).

Formatted: Space After: 0 pt, Widow/Orphan control

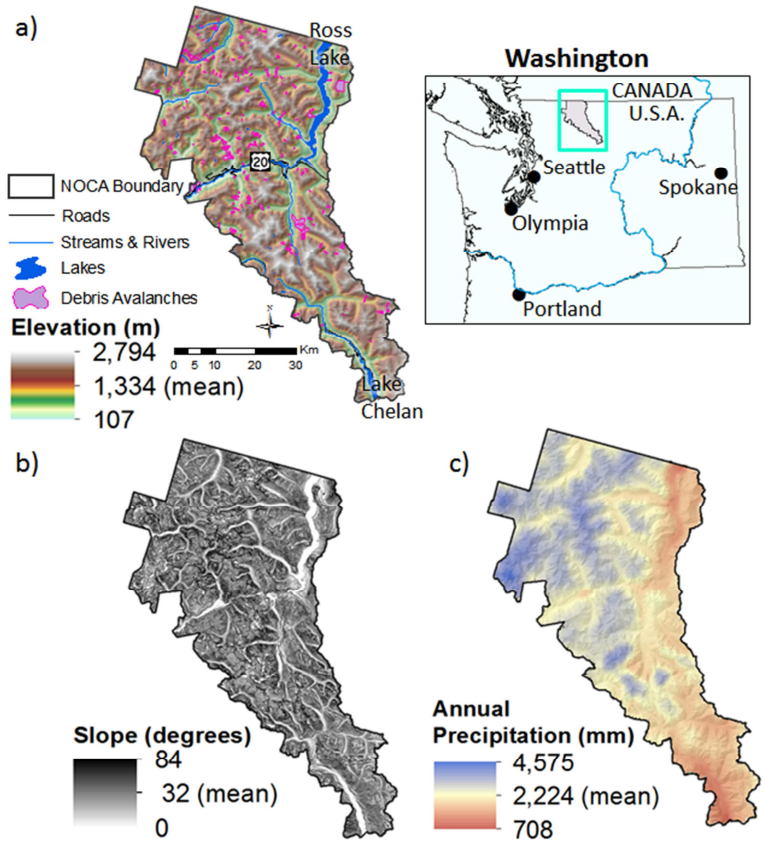

~~**Figure 2.** North Cascades National Park Complex (NOCA) in northern Washington state, U.S.A: **(a)** a 30-m DEM of the domain overlain by debris avalanches and major water bodies; **(b)** slope derived from DEM; and **(c)** mean annual precipitation (1981-2010 average) mapped at 800-m resolution from PRISM (PRISM Climate Group, 2004).~~

Some areas in mountainous regions are covered by glaciers, permanent snowfields, and exposed bedrock, which are unsuitable locations to model landslides ~~on soil-mantled hillslopes using the~~with the infinite slope model (Borga et al., 2002). These landforms~~. Furthermore, they are not expected to be destabilized by precipitation, although other forces could cause failures (e.g., earthquake, volcanic activity, and temperature). We exclude high elevation areas covered by glaciers, permanent snowfields and exposed bedrock (Fig 3c),~~ as well as wetlands and other water surfaces are excluded ~~, based on landform mapping and maps of lithology and LULC,~~ from our modeling domain~~ and geomorphic analysis because shallow landslides are not typically observed on these landforms~~. The total area excluded from the stability analysis accounts for about 21% of NOCA's land area.

Formatted: Left

Formatted: Space After: 0 pt, Widow/Orphan control

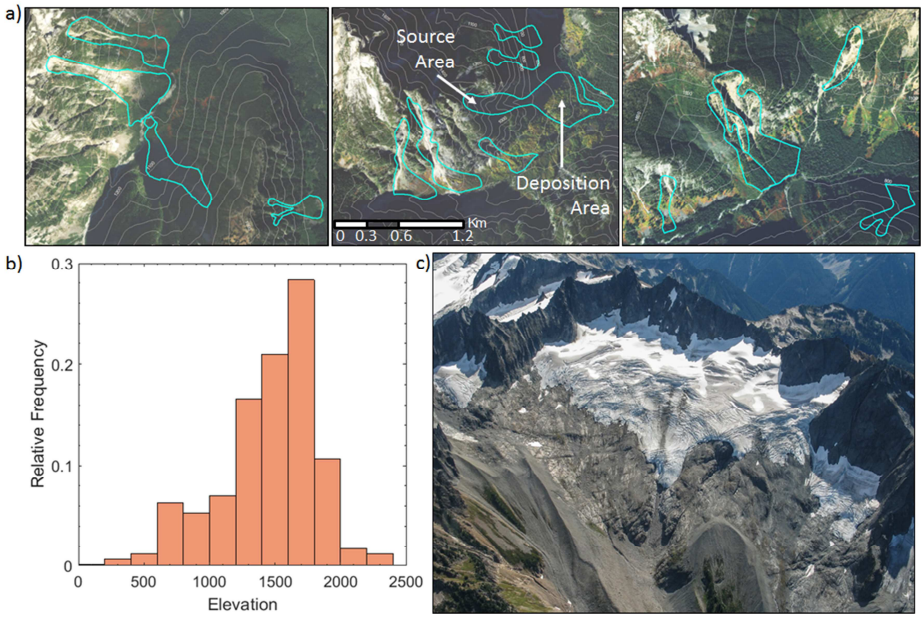

Figure 3. (a) Example debris avalanches (cyan) mapped in three areas within NOCA. Contours are in 100-m intervals. Aerial image source from World Imagery, Esri Inc.[1]; **(b)** elevation distribution of the relative frequency of mapped debris avalanche source areas (upper 10%); and **(c)** High elevation rock and glacier mapped surrounding Spiral Glacier in North Cascades showing a bedrock glacier cirque with thin barren soils and moraine deposits (photo by John Scurlock used with permission).

3.2 Model Input Fields

We used a grid resolution of 30 m from the National Elevation Dataset (NED) (USGS, 2014a) ~~to evaluate and compare our regional model of landslide probability to a limited set of landslide observations~~. Evaluation of model performance was intended at this resolution for regional modeling as NASA's Shuttle Radar Topography Mission (SRTM) DEM is available globally at a 30-m resolution. ~~A 30-m grid cell size is consistent with the~~The minimum mapping unit used for landslide~~s~~ is ~~-~~30 m for NOCA ~~-~~(Riedel et al., 2015~~; see also Regmi et al., 2014; Arnone et al., 2016~~). Slope (S=$\tan\theta$), ~~combined~~ total curvature (Curv) (i.e., both planar and profile), and contributing area (CA) attributes were derived ~~from a 30-m DEM acquired from *National Elevation Dataset* (NED) (USGS, 2014a)~~ from the DEM (Fig. 2a). ~~In addition, the NLCD data for vegetation classification and the SSURGO soils database we used in this study both have available 30-m grid resolutions. To show the model potential for regional applications, a global coverage of 30-m DEM from the NASA Shuttle Radar Topography Mission (SRTM) is available~~

Formatted: Font: Not Italic

[1] Images created using ArcGIS® software by Esri. ArcGIS® and ArcMap™ are the intellectual property of Esri and are used herein under license. Copyright © Esri. All rights reserved. For more information about Esri® software, please visit www.esri.com.

~~(USGS 2017). Thus, showing the model's potential at this resolution is intended in this paper, especially for regional applications beyond the use in a single watershed across the globe.~~

3.2.1. Vegetation and Soil parameters

Vegetation classes are obtained from the ~~National Land Cover Data (~~NLCD ~~201X)~~ in 30 m resolution (Jin, 2013; USGS, 2014b). Parameters of a triangular distribution for *C, ø, T, and* h_s are provided in Table 1. In our case study, *C* represents root cohesion. Soils across the study domain are assumed ~~because we assumed soils to be primarily~~ cohesionless, due to low clay content (<10%) ~~in~~ this mountain substrate with large clasts (Kulhawy et al., 1990)~~, particularly in comparison to root cohesion~~. Estimating root cohesion is challenging~~challenge~~ because of temporal and spatial variability in root~~s~~ density and size, differential breakage or pullout mechanisms, interaction among roots, and difficulty in measuring at a field scale (Pollen and Simon 2005; Schwarz et al., 2013). We developed ~~simple~~ spatial coverages for minimum, mode, and maximum C for NOCA by relating vegetation classes with corresponding published C values in the literature (Table 1), where field observations suggest right-skewed distribution (Hammond et al., 1992; Schmidt et al., 2001; Gabet and Dunne 2002; Hales ~~et al.~~ et al., 2013). Based on ranges available in the literature, we selected a mode value as a commonly reported value, minimum parameter as 30% of the mode, representing death and loss of productivity (Sidle, 1991; 1992), and a maximum near the highest reported value for C. Forest have higher C than shrubland because of the greater root area and deeper root~~s~~s (Arnone et al., 2016b). ~~Other LULC types include water, wetland, snow/ice, barren, and developed (e.g., roads, campground).~~ Small C values are assigned for barren and developed land uses (~14% of the domain) having minimal vegetation. Mode values of C mapped over NOCA are ~~given~~ shown in Fig. 4b. Forest communities of the valley bottom and lower valley walls show high values of C, which declines as vegetation transitions from forests to shrublands to herbaceous communities with increasing elevation.

Table 1. Parameters defined for vegetation and soil types in the study region. For spatially continuous ~~parameter~~variables T and h_s obtained directly from SSURGO, values represent spatial ~~the~~ statistics ~~for the model domain with *(mean)* values in parentheses~~.

~~Parameter~~Variable	Minimum	Mode *(Mean)*	Maximum
Root Cohesion [kPa]			
Barren/Developed	0.03	0.10	0.15
Forest (coniferous)	3	10	20
Shrubland	1.2	4	10
Herbaceous	0.6	2	5
Internal angle of friction [°][1]			
Loamy sand	26.2	32	42.2
Sandy loam	28.7	35	46.2
Developed areas (loamy, sandy)	28.7, 31.2	35, 38	46.2, 50.2
Transmissivity [m^2 d^{-1}][2]	0.42	*(3.39)*	16.4
Soil depth [m]~~[1]~~[2]	0.09	*(0.62)*	2.01

Formatted: Normal
Formatted: Font color: Black
Formatted: Not Highlight
Formatted: Font color: Black
Formatted: Font color: Black, Highlight
Formatted: Subscript
Formatted: Font: Not Italic, Font color: Black

[1] Developed areas within the two soil types, respectively, have mode values 3° larger due to compaction.
[2] Values for the continuous variables, transmissivity and soil depth, represent the minimum, mean, and maximum for spatial statistics for the study area, not individual soil map units.

~~Despite the aggregation of plant types into functional plant communities (Fig. 4a), considerable spatial variability in C is present within the park (Fig. 4b), with the greatest values in the forest communities of the valley bottom and lower valley walls. C declines aAs vegetation communities transitions from forests to shrublands to herbaceous species communities with increasing elevation, C declines. Note that herbaceous species are likely composed of considerable woody vegetation in this alpine region, but of diminutive stature.~~

In order to investigate the contribution of soil depth to mapping landslide probability, we developed and used two alternative soil depth products: 1) based on SSURGO and 2) based on a soil evolution model. The nationally available SSURGO database maintained by the Natural Resources Conservation Service (NRCS) is a readily available data source that includes depth-to-restrictive layer (*DOA-NRCS* 2016), which we used to specify the mode of soil depth (Fig. 4c). Using the *Soil Data Viewer* of Esri ArcGIS (DOA-NRCS, 2015a), the weighted-average aggregation option is used to extract soil depth within each soil map unit (DOA-NRCS and DOI-NPS, 2012). SSURGO soil depth (SSURGO-SD) is uniform for each soil map unit and thus, lacks finer scale spatial heterogeneity and create edge incongruities (Fig. 4c), a limitation ~~also~~ identified previously for landslide modeling~~in other landslide modeling studies~~ (Bordoni et al., 2015). A ~~smoother and~~ more spatially ~~consistent~~ heterogeneous soil depth map is developed~~achieved~~ using the output of a soil evolution model.

SSURGO-SD represents the recent conditions in soil depth. The difference between the actual soil depth in the field and the SSURGO reported soil depth will likely be associated with the limited number of soil depth measurements used to develop SSURGO maps, measurement errors, and spatial interpolation assumptions. In addition, for the locations that have already produced landslides before SSURGO mapping, we assume that the maximum value of the triangular distribution represents the soil depth prior to a landslide. To represent uncertainty, minimum h_s is assumed to be 70% of the mode and maximum h_s adds 10% to the mode value. These values give a left-skewed triangular distribution, commonly ~~used~~ observed for soil depth ~~in probabilistic landslide models~~ (Hammond et. al., 1992). The s~~S~~elected skewed ~~ranges~~distribution was ~~were~~ confirmed by the soil evolution model discussed in Sect. 4.1.2.

Transmissivity is derived as the product of weighted-average aggregated K_s of all soil layers above the restrictive layer and h_s for each soil map unit (DOA-NRCS, 2015a). Similar to h_s, this T value was considered the mode (Fig. 4d) and the minimum and maximum values needed for an asymmetrical triangular distribution calculated as: $T_{min} = T_{mode} - 0.3*T_{mode}$ and $T_{max} = T_{mode} + 0.1*T_{mode}$. Closely related to soil depth, ~~transmissivity~~ T is high in valley bottoms as well on plateaus because of deeper soils, thus, more water can move through the soil when saturated (Fig. 4d). ~~Transmissivity~~ T is low in the thin veneer soils below retreating glaciers as well on steeper side slopes.

~~Soil surface texture is a grouping used to describe the particle size distribution of granular media, and can be used as an indicator of ø (Nimmo, 2005).~~ The percent sand, silt, and clay ~~(weighted-average aggregation)~~ for each soil map unit in NOCA were derived from SSURGO data using Soil Data Viewer (DOA-NRCS, 2015b). This revealed largely sandy loam or loamy sand soil textures, based on USDA classification, across the NOCA. These soil textures corresponded to Unified Soil Classification System (USCS) soil types silty sand and well-graded (diverse particle size) fine to coarse sand, respectively. Reported ø values for these USCS soil types were assigned as the mode of ø, $ø_{mode}$ used in triangular distributions~~(i.e., Table 5.5 in Hammond et al., 1992 and Table 5.2 in Shelby, 1993)~~. Developed land cover type was assigned an additional 3° to the mode to compensate for higher soil density from development activity, such as compaction (Sidle and Ochiai, 2006). ~~The map of ø exhibits the least variability in NOCA due to the relatively narrow range of soil textures, with lower angles typical at higher elevation and higher angles farther downslope (figure not shown).~~ Given the mode and ranges of ø for these soil types, minimum and maximum ø were calculated to generate right-skewed distributions for both soil types as: $ø_{min} = ø_{mode} - 0.18*ø_{mode}$ and $ø_{max} = ø_{mode} + 0.32*ø_{mode}$~~,~~ based on literatures review (i.e., Table 5.5 in Hammond et al., 1992 and Table 5.2 in Shelby, 1993). The soil and water density terms in Eq. (1a), were assigned a constant value of 2,000 kg m^{-3} and 1,000 kg m^{-3}, respectively similar to ~~(~~Pack et al.~~,~~ (2005). Factor-of-safety has been found to be insensitive to soil density (Hammond et al., 1992; Lepore et al., 2013).

Formatted: Font color: Black

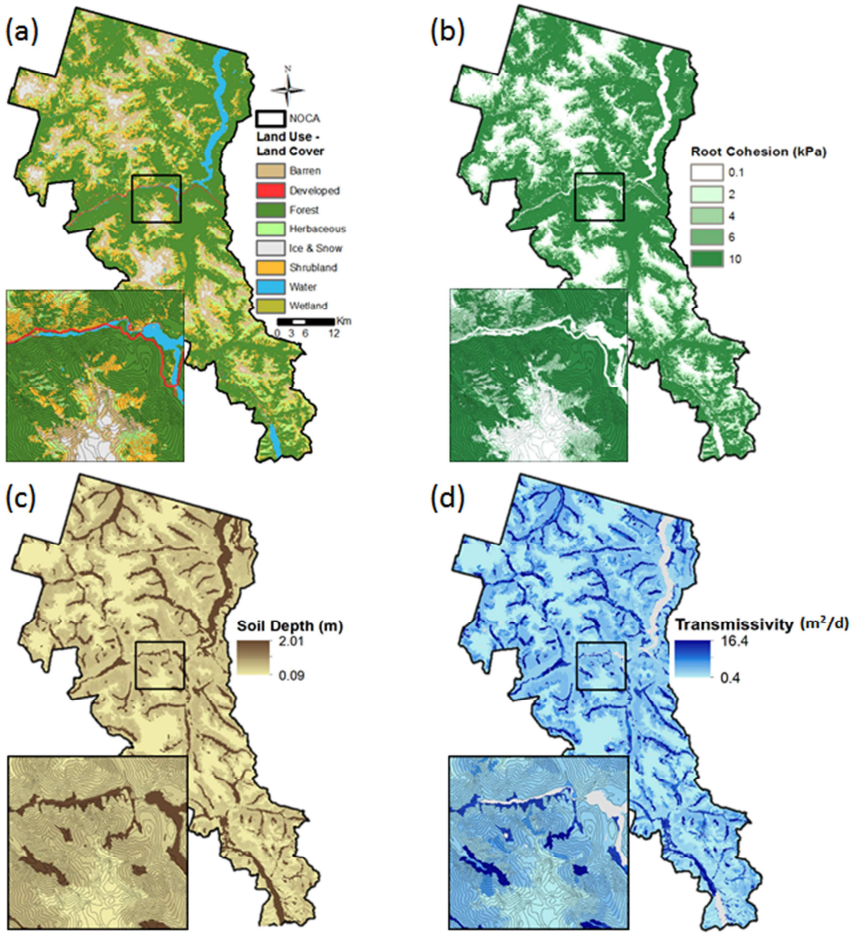

Figure 4. NOCA ~~Distributed parameter~~variables~~ used in the landslide model over NOCA, including~~maps for: **(a)** LULC classified from NLCD (2014); **(b)** root cohesion based on LULC; **(c)** soil depth from SSURGO; and **(d)** transmissivity based on SSURGO soil depth. Mapped values in (b) through (d) represent the mode values used in triangular distribution for Monte Carlo simulations~~the parameter~~variable ~~distributions~~. Insert shows zoomed-in area with 100 m contours.

3.2.2. Model Recharge

~~E~~We used existing ~~The model is designed with a flexible approach to parameterizing recharge. Available probability distributions include uniform, lognormal, lognormal spatial, and data driven spatial. Supplemental materials include a Jupyter Notebook that reproduces these four recharge options on a synthetic grid. To provide the hydro-climatology forcing to drive our landslide model, our model application leverages the existing detailed simulations of~~ VIC model

runs for ~~in~~ the PNW region developed through the Columbia Basin Climate Change Scenarios Project (Elsner et al., 2010; Hamlet et al., 2013). The project developed a calibrated implementation of VIC (1/16° or 5x7 km grid resolution) covering the Columbia River basin in Washington to produce validated historical hydrologic simulations (water years 1916-2006) driven by spatially interpolated daily station observations of temperature and precipitation (Hamlet et al., 2013). Archived model output at a daily-time-step includes gridded baseflow and runoff. Hydrologic simulations using VIC have also been run for all of the contiguous United States (CONUS) (Data available from:~~,~~ Livneh et al., 2013, 2015). ~~Thus, acquisition of hydrologic model output is readily available to apply the landslide model anywhere throughout the CONUS.~~ We determined the maximum daily recharge for each year to generate a 91-year long time series to ~~calculate represent a surrogate for~~characterize the wettest ground saturation conditions for shallow landsliding ~~the annual highest pore water pressure at each VIC grid cell~~. ~~.~~ Modeling with maximum recharge provides an indicator of individual storm events that typically trigger shallow landslides (Lu and Godt, 2013), although lesser amounts of recharge may also be sufficient to trigger landslides in some locations. The average annual maximum daily recharge over NOCA is about 35 mm/d (± 15 mm/d), ranging from a low of 7 mm/d along the eastern edge of the park to a high of 79 mm/d on the western edge and at higher elevation peaks.

Formatted: Font: Not Italic, Font color: Black

Formatted: Font: Not Italic, Not Highlight

4 Results and Discussion

4.1. Geomorphic Analysis and Soil Evolution

Understanding the spatial distribution of dominant geomorphic processes can aid the development of landslide hazard maps consistent with geomorphic theory. In this section, we discuss the mapping of dominant processes on the landscape on the slope and area domain, and explore the proposed soil evolution model to develop modeled soil depth maps.

4.1.1. Investigation of Process Domains

Hillslope diffusion, landslide, debris flow, and fluvial transport processes leave unique imprints on landforms, manifested in the slope-contributing area (S-CA) domain as different scaling relationships (Montgomery and Dietrich, 1992; Tucker and Bras, 1998; Montgomery, 2001; Stock and Dietrich, 2003; Tarolli and Fontana, 2009). The infinite-slope factor-of-safety model is only applicable to the initiation of landslides. Therefore, hazards associated with debris flow scour and deposition cannot be predicted by this model. We used a S-CA plot and the infinite slope stability theory to: (1) identify process domains and limit the analysis of the landscape to slopes where there is shallow landslide potential, (2) evaluate observations of debris avalanches to identify landslide source areas, and (3) infer plausible ranges of the infinite slope stability model parameters to corroborate those we compiled from the literature for NOCA (Table 1).

Our geomorphic analysis was based on plotting, in log-log scale, S~~,~~ ~~(=~~(as tan(θ)~~,~~ and CA pairs of each DEM grid cell in NOCA, cells within mapped debris avalanches (including depositional

areas), and most likely source areas of landslides identified as the single highest elevation grid cell within each mapped debris avalanche (Fig. 5). The general trend in the S-CA relationship is acquired for all grid cells of NOCA as well as debris avalanche (DA) cells by binning the data with respect to CA and calculating the mean S for each CA bin. The negative linear relation in the log-log plot suggest a power-law scaling in the form of $S \sim CA^{-B}$ where B is the slope of the S-CA relation on the log-log domain, which reflects channel longitudinal profile concavity. Concavity is generally associated with fluid driven processes ~~fluvial processes (including debris flows) the role of discharge (CA is used as a surrogate in this plot) in enhancing sediment transport~~, while the degree of concavity is tightly related to ~~how~~ the nonlinearity of ~~the dominant~~ fluvial transport ~~is~~ with respect to S and CA (Roering et al, 1999; Montgomery 2001; Stock and Dietrich 2003; Istanbulluoglu 2009). ~~the~~ Based on the scaling transitions that mark changes in concavity, process domains interpreted in Fig 5 are ~~Geomorphic process domains interpreted from the binned S-CA plot portrayed in Fig. 5 include~~: (1) a hillslope zone where slope-dependent processes such as dry ravel and soil creep dominate, leading to convex slopes, (2) a landsliding zone where pore-pressure driven slope failures introduce concavity as landslides arise with shallower slopes as recharge CA grows, (3) a debris flow or saturated landslide zone in headwater channels where mass wasting processes ~~are supplemented with higher fluidity and~~in saturated ground ~~saturation leading to S and CA driven~~evolve into high-concentration transport (Iverson et al., 1997), and (4) a fluvial region ~~where stream-dominated erosion and transport processes ensue~~ (Montgomery and Foufoula-Georgiou, 1993; Tucker and Bras, 1998). ~~Dominant process domains in the S-CA plot are identified by visual inspection of the scaling transitions that mark changes in concavity~~. ~~It is well documented that d~~Debris flow-dominated slopes~~s~~ were shown to exhibit reduced concavity relative to ~~both~~ channels and pore-pressure driven landslide zones in the S-CA domain (Montgomery and Foufoula-Georgiou, 1993; Tucker and Bras, 1998; Stock and Dietrich, 2003). ~~The highest profile concavity results from fluvial transport (Fig. 5).~~

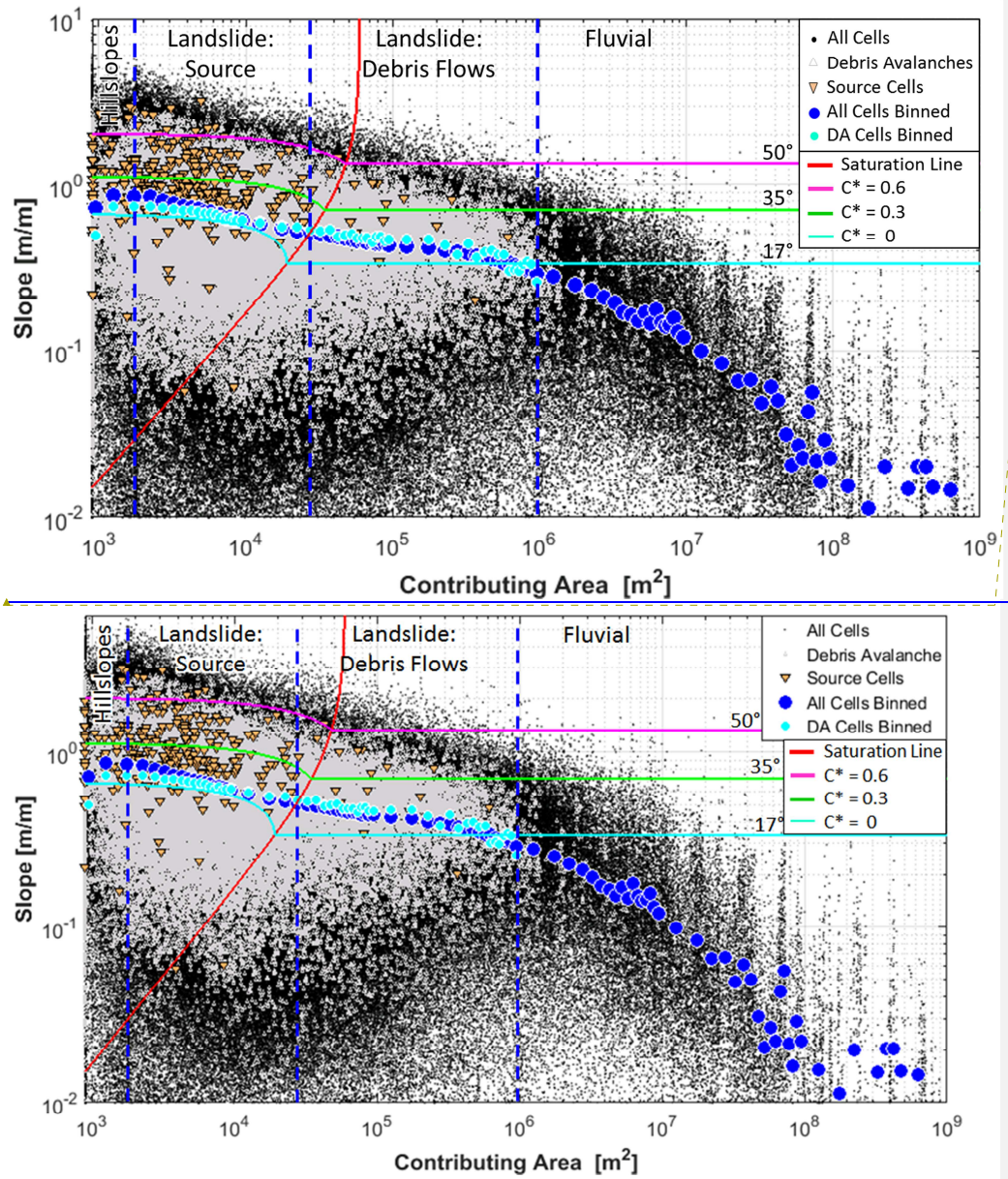

Figure 5. Slope-contributing area (S-CA) log-log plot for North Cascades National Park Complex. Mean S for bins of CA are indicated by blue dots and cyan dots for all cells and debris avalanche (DA) cells, respectively. DA source cells (orange triangles) are the single highest elevation grid cell within mapped debris avalanches (gray). Horizontal ~~s~~slope stability curves plot the solution of S (Eq. 1a and 2) as a function of CA, given FS=1, R/T=0.0005, ø=34° and select values of dimensionless cohesion, C*; S for

Formatted: Font color: Black

horizontal line portion (fully saturated regions) are labeled in ° for ease of understanding~~of Eq. (1a) for FS=1, given C* and ø=34°~~. Above each curve landscape is unstable for a given C*. Saturation line (red curve) separates partially saturated areas (left) from saturated areas (right). Blue ~~V~~vertical lines divide the plot into geomorphic process domains in relation to CA of the landscape (e.g., Montgomery 2001). Cyan horizontal line at 17° generally separates potential landslide dominated areas from fluvial dominated areas.

A threshold CA of approximately 1 km^2 and a slope threshold of θ=17° generally separates colluvial mass wasting and debris transport processes from fluvial processes (Fig. 5; see also Legg et al., 2014). Nearly all grid cells within mapped debris avalanches plot to the left of the 1 km^2 dashed line. An average θ value of 17° may also correspond to a low-end of a slope threshold for landsliding. Fully saturated cohesionless soils are unconditionally stable at tan(θ) ≤ ½ tan(ø) (i.e. half of ø), assuming a ratio of water to saturated soil density of 0.5 (e.g., Montgomery and Dietrich, 1994). Solving for ø when θ = 17° gives 34°, generally consistent with selected ø values from soil texture (Table 1) (Hammond et al., 1992). Approximately 85% of NOCA landscape lies above θ > 17°, suggesting a dominant role of mass wasting processes in this landscape. We included areas above this slope threshold in our landslide model domain.

The red saturation curve is calculated as aR/T, where R/T is calibrated to 0.0005 m^{-1} (e.g., $a/\sin\theta$ = 2000 m) to capture most of landslide source cells (left of curve) and a scaling break in the binned S-CA plot (Fig. 5). The saturation curve partitions the landscape into partially saturated (left) and saturated (right) areas, which generally delineates the S-CA pairs separating landsliding from debris flow tracks that form under full soil saturation. For a T = 10 m^2 d^{-1}, R is 5 mm d^{-1}, which is within the range of the lowest maximum annual modeled recharge values in most of the study area, indicating that the plotted saturation line could reasonably map regions that experience saturation annually.

The three lines stacked vertically (i.e., cyan, green, and pink) plot the solution of S in the infinite slope stability equation (Eq. 1a and 2) as a function of CA, and given FS=1, R/T=0.0005, ø=34° and select values of dimensionless cohesion, C*. Conditioned on the C* value, slopes that plot above the S-CA solution are unstable. Consistent with the binned S-CA data, the solution of the infinite slope stability equation curves down as a function of CA, and following soil saturation, a constant instability S threshold is reached. Root cohesion is approximately 6 kPa for C*=0.3 (middle green line) and 12 kPa for C*=0.6 (upper pink line), assuming a soil depth of 1 m and cohesionless soil. These root cohesion values are reasonable for shrub and mature forest vegetation found in the literature (Table 1) and they facilitate stability with steeper slopes. When C*=0 (bottom cyan line), landslides initiate at lower slopes than when cohesion is greater. This solution also envelops the low slope-end of nearly all landslide source S-CA pairs identified from debris avalanche data. Only a small portion of the unstable areas plot above the C*=0.6 solution of Eq. (1a), which implies areas with higher root cohesion.

4.1.2. ~~Evolved Soil Depth~~Modeled Soil Depth

We ran the soil evolution model described in Sect. 2.4 at a population of ~~at~~ representative topographic conditions and vegetation types (forest, shrub, herb) instead of running the simulations over the whole study domain. ~~and used the results in a nonlinear regression analysis to estimate soil depth from slope ({θ [°]}) and, and total curvatureCurv. As the study domain is large, we used a representative population of θ [°], CA, and Curv values to run the soil evolution model for different vegetation types. The resulting nonlinear equations were used to estimate the mode of modeled soil depth (M-SD) of each vegetated grid cell of the study domain.~~ Capitalizing on the S-CA analysis (see Sect. 4.1.1), local ~~({θ [°]})~~, CA, and Curv triplets in each of the CA bins are used from the landscape dominated by colluvial transport processes ($\theta > 17^{o}$ and $CA \leq 1\ km^2$). In order to further classify landscapes within each CA bin, θ and Curv pairs are grouped into shallow (θ ≤ the 10th percentile θ), moderately steep (between 10th and 90th percentiles of θ), and steep (θ ≥ the 90th percentile θ) slope classes. Within each class, θ and Curv are averaged. This led to 53 number of triplets used for the soil evolution model, with the assumption that landslides do not significantly change local θ and Curv, implying long-term equilibrium conditions. The model is run for 10,000 years to represent the postglacial landscape (i.e., roughly the current interglacial period or Holocene) using the calibrated parameters listed in Table 2.

Local erosion is calculated within the soil evolution model. Calibration of the soil evolution model was performed by adjusting model parameters from the literature (e.g., Tucker and Slingerland, 1997; Nicótina et al., 2011) and comparing the mean annual rock erosion rate estimated by the model to long-term average rock erosion rates published for the Cascade Mountains, which range from 0.02 to 0.5 mm y^{-1} over roughly the last several Ma (Reiners et al., 2002, 2003) and slightly higher rates over the last millennia of 0.08 to 0.57 mm y^{-1} (Moon et al., 2011). In addition to published erosion rates, the resulting soil depths were compared to the SSURGO-SD, which ranged from 0.09 to 2.01 m across NOCA.

In Fig. 6 we show modeled mean annual erosion rates in relation to mode of modeled soil depth (M-SD) for a steep and moderate slope class, and illustrate the local variability of modeled soil depth under forest and shrub conditions. The relative frequency histogram of local soil depth resembles a triangular distribution, with mode values generally higher than mean values, indicating a negatively (left) skewed distribution for soil depth (Fig. 6a, 6c). Therefore, there is a higher frequency of deeper soil relative to shallower soils. Soil creep fills hollows, thickening soils, as FS gradually drops, leading to episodic landslides that evacuate sediment (Fig. 6b, 6d).

Table 2. Model parameters used in the soil evolution model

Parameter	Value	Units
h(initial) – initial soil depth	0.01	m
α – rate of exponential decay with depth	3	m^{-1}
Po – soil production rate from exposed bedrock	0.0005	m yr^{-1}
Kd – linear hillslope diffusion coefficient	0.01	m^2 yr^{-1}
ρ_r / ρ_s – Rock to soil density ~~density~~	2.65/2	[-]
Ks – saturated hydraulic conductivity	7	m d^{-1}
ø – internal angle of friction	35	Degrees
Root cohesion[1]	Varies	kPa
Recharge (mean)[2] and Coefficient of variation	32, 0.35	mm d^{-1}

[1] Root cohesion varied by vegetation type based on Table 1 and soil cohesion was assumed to be zero.
[2] Recharge extracted from average values found at four representative VIC grid cells within NOCA.

Formatted: Font: Bold, Font color: Black
Formatted: Font: Bold
Formatted: Centered

Both θ and Curv have been found to be correlated with soil depth (Heimsath et al., 1997; Braun et al., 2001; Mitchell and Montgomery, 2006; Hren et al., 2007). A multivariate nonlinear regression in the form of $y=\beta_1 \cdot x_1^m + \beta_2 \cdot x_2 + C$ was fit to ~~mean and~~ mode of soil depth (predictand, *y*) given θ and Curv (predictors, x_1 and x_2) for each vegetation type with R^2 >0.9 for all slope classes (not reported). Maps for mode of the modeled soil depth (M-SD) were developed over the portion of the NOCA domain by applying the regression equations using the distributed θ and Curv ~~appropriate for~~and vegetation type at each grid cell. Minimum soil depth was set at 0.005 m ~~if the regression calculated negative depths~~ and maximum soil depth ~~were set at 0.005 and~~was set to 2 m~~, respectively~~. Outside the colluvial transport process domain are conditions outside the regression analysis; therefore, vegetated areas were assigned a depth of 0.5, 1, and 2 m for herbaceous, shrubland, and forest, respectively, to generate a contiguous soil depth map for NOCA consistent with SSURGO. Areas with barren land cover were assigned a soil depth of 0.05 m, representing the minimum range of modeled herbaceous areas. Developed areas were assigned a value of 0.5 m. Areas assigned ~~a such~~ fixed values are about 2% of the model domain.

~~As an alternative to the SSURGO-SD, the map of the mode values of M-SD was used to represent the most likely soil depth at each grid cell in the landslide probability model.~~ The evolved soil depth was also used to revise *T*, using the *Ks* provided by SSURGO, which provides a more-distributed continuous field of *T*. The revised *T* map is used when Landlab is run based on mode from M-SD.

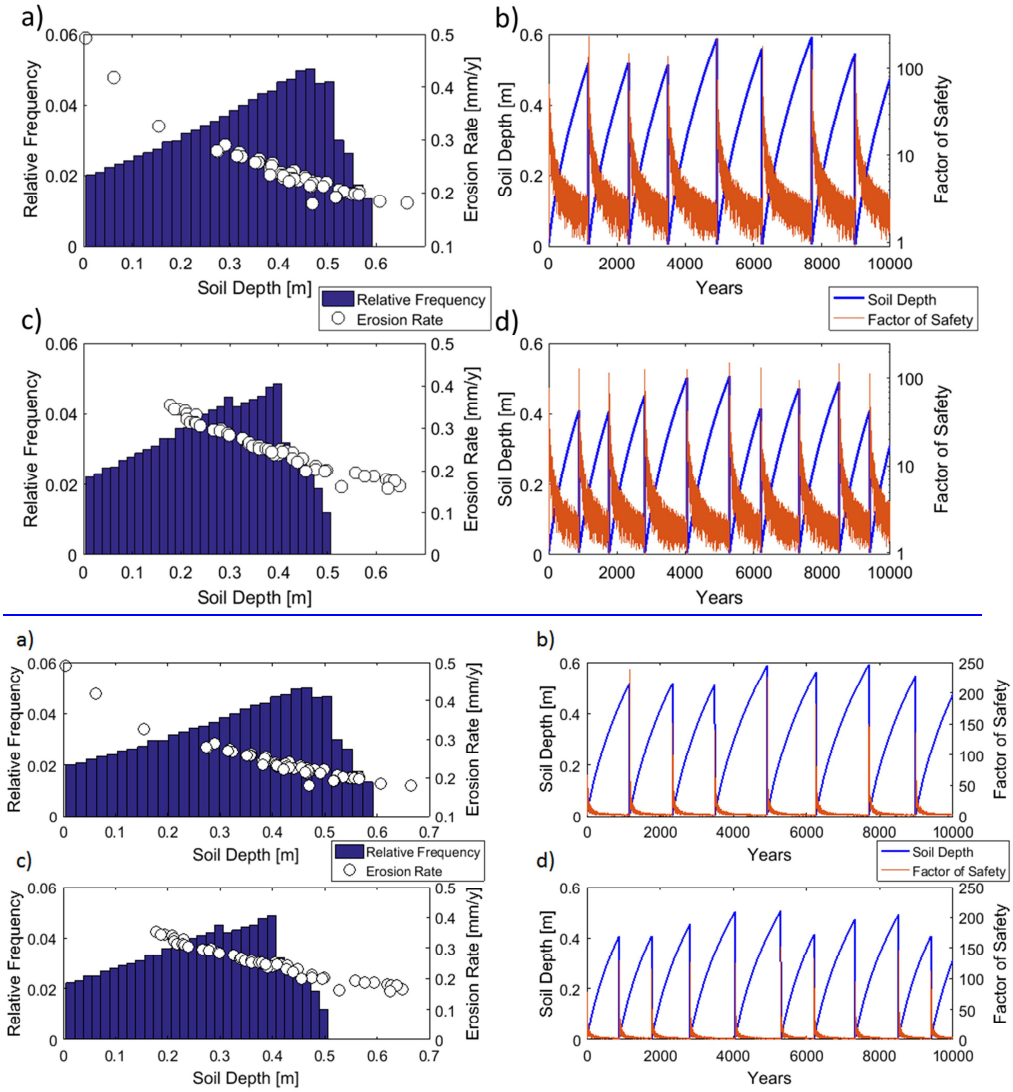

Figure 6. Illustration of the soil evolution model run using **(a, b)** steep slope class and forest vegetation and **(c, d)** moderately steep slope class and shrub vegetation. (a, c) Modeled mean annual erosion rates plotted with respect to model of modeled soil depth, along with soil depth temporal relative histogram for a representative convergent location. (b, d) Temporal evolution of soil depth and FS (logarithmic scale) for a representative convergent location with: (a) S=40° and Curv=-0.01; and (b) S=29° and Curv=-0.01.

~~Comparison of the SSURGO-SD with the M-SD indicates that there is value in a long-term geomorphic perspective in supplying a spatiospatial temporal soil depth.~~ M-SD exhibits

substantially more spatial variability than the SSURGO-SD (Fig. 7). While both spatial soil depth distributions have similar median values, M-SD has a wider distribution with a higher proportion of shallower and deeper soils than SSURGO-SD. In general, the M-SD is shallower than SSURGO-SD on steeper, convex hillslopes with herbaceous or shrub vegetation and deeper on gentler, concave hillslope with forest vegetation. For both ~~models~~datasets, soil depth is deeper~~greater~~ in the valleys and shallower near the ridge tops (Fig. 7c, d), consistent with other studies~~reporting~~ (Anagnostopoulos et al., 2015; Montgomery and Dietrich, 1994).

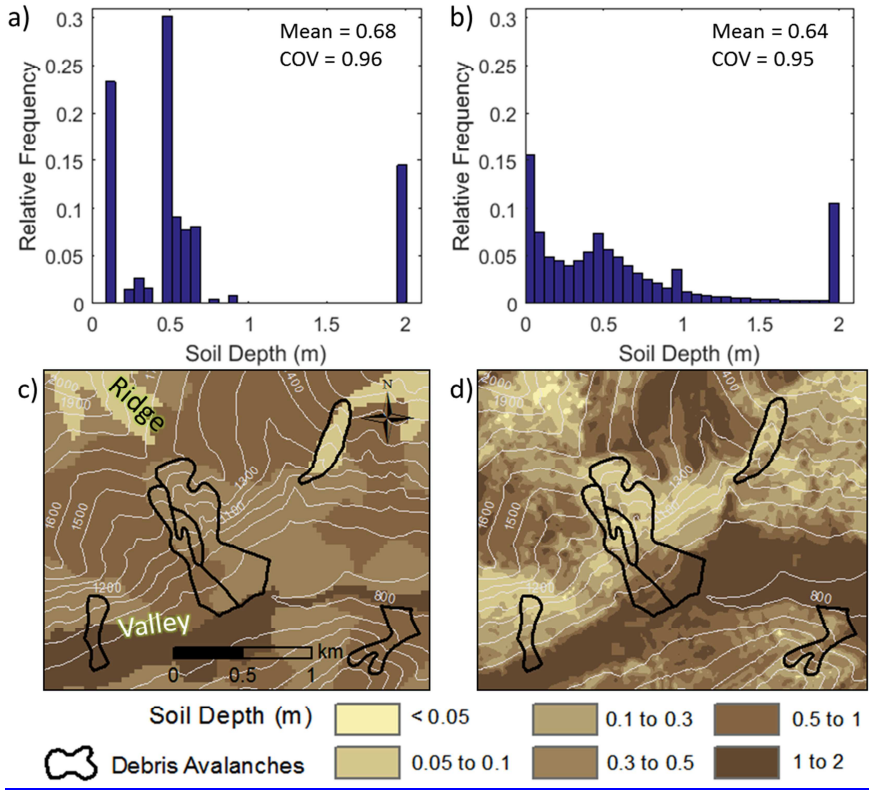
a)
Mean = 0.68
COV = 0.96
Relative Frequency
Soil Depth (m)
b)
Mean = 0.64
COV = 0.95
Relative Frequency
Soil Depth (m)
c)
Ridge
Valley
N
km
0
0.5
1
d)
Soil Depth (m)
< 0.05
0.05 to 0.1
0.1 to 0.3
0.3 to 0.5
0.5 to 1
1 to 2
Debris Avalanches

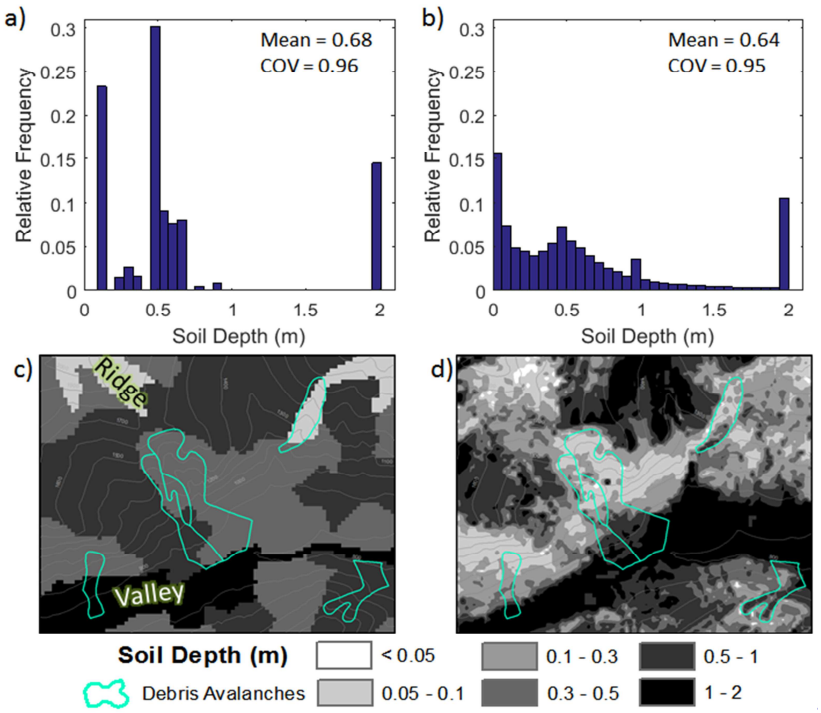

Figure 7. Sample illustration of the soil evolution model. Relative histograms of soil depths within NOCA: **(a)** SSURGO-SD and **(b)** mode of M-SD, with respective spatial mean and coefficient of variation (COV). ~~Example location (~6 km^2) within NOCA~~Mapped soil depth, with mapped debris avalanches outlined in black and contours are at 100-m for:
(c) SSURGO-SD and **(d)** M-SD.
~~Mapped debris avalanches are outlined in cyan black and contours are at 100-m.~~

The maximum and minimum soil depth parameters of the triangular distribution ~~to characterize soil depth variability~~ were obtained by analyzing soil evolution model results. At most θ, CA, and Curv triplets ~~using in the soil evolution model~~used, a landslide occurred at least once over the modeled duration. As described in Sect. 3.2.1, g~~G~~iven the negatively-skewed nature of the temporally evolved soil depth (Figure 6 a,c), the maximum ~~evolved~~ soil depth parameter of the triangular distribution was set equal to 10% of the mode in all model simulations. Two scenarios for the minimum parameter of the triangular distribution were used to reflect soil depth uncertainty for contemporary and long-term conditions. In the first case, we set the minimum parameter as 70% of the mode. The LandslideProbability model was run for this scenarios for both SSURGO (SSURGO-SD) and modeled soil depth (M-SD) input. In the long-term scenario, the minimum soil depth was set to 0.005 m, reflecting bedrock scour conditions by landslides. We argue that this assumption implicitly introduces a temporal uncertainty component to soil depth, which may be used to more accurately estimate landslide return

period over the long-term. The model run was called M-SD LT for this case. ~~Two scenarios for the minimum parameter of the triangular distribution were used M-SD. scenarios were developed to compare with SSURGO-SD In the first approach we focus on existing contemporary soil depth conditions in the field by running two simulations called SSURGO-SD and M-SD where we set the minimum parameter as 70% of the mode. Second, we aimed to reflect the longer-term perspective of soil evolution on the uncertainty of soil depth (called M-SD LT simulation) by setting the minimum soil depth to 0.005 m, reflecting bedrock scour conditions by landslides. This assumption implicitly introduces a temporal uncertainty component to soil depth, which can be used to more accurately estimate landslide return period over the long-term.~~

4.2 Probability of Failure

Modeled annual probability of failure of shallow landslides, P(F), for NOCA simulated by the Landlab LandslideProbability component using SSURGO-SD and two M-SD scenarios are shown in Fig. 8. ~~–~~In each ~~run~~model run~~simulation~~, 3,000 values were sampled (i.e., iterations) for model parameter~~variable~~s at each grid cell in the Monte Carlo simulations.

P(F) derived from simulations exhibit low probabilities where slopes are moderate and cohesion is high (e.g., forest). Highly unstable areas largely correspond to steep barren landscape (13% of the model domain) mostly located below retreating alpine glaciers, with steep glacial landforms, transitioning from glacier to colluvial processes (similar to Guthrie and Brown 2008; Tarolli et al., 2008; Legg et al., 2014) (Fig. 9). These areas with a thin veneer colluvium, except for moraines, appear to be “continuously sliding” (Borga et al., 2002) or “chronically unstable” (Montgomery, 2001). Frequent slides impede the colonization of vegetation (Dietrich et al., 1995; Istanbulluoglu and Bras, 2005). Slides in barren areas were not completely included in our landslide inventory as they do not pose major risks to humans and infrastructure.

~~s (i.e., 3,000 iterations in each simulation).~~

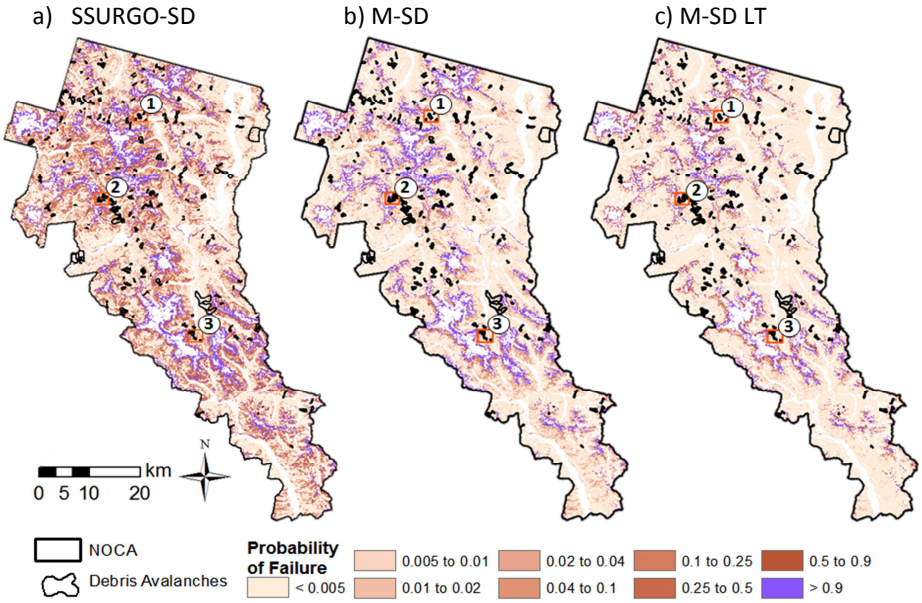

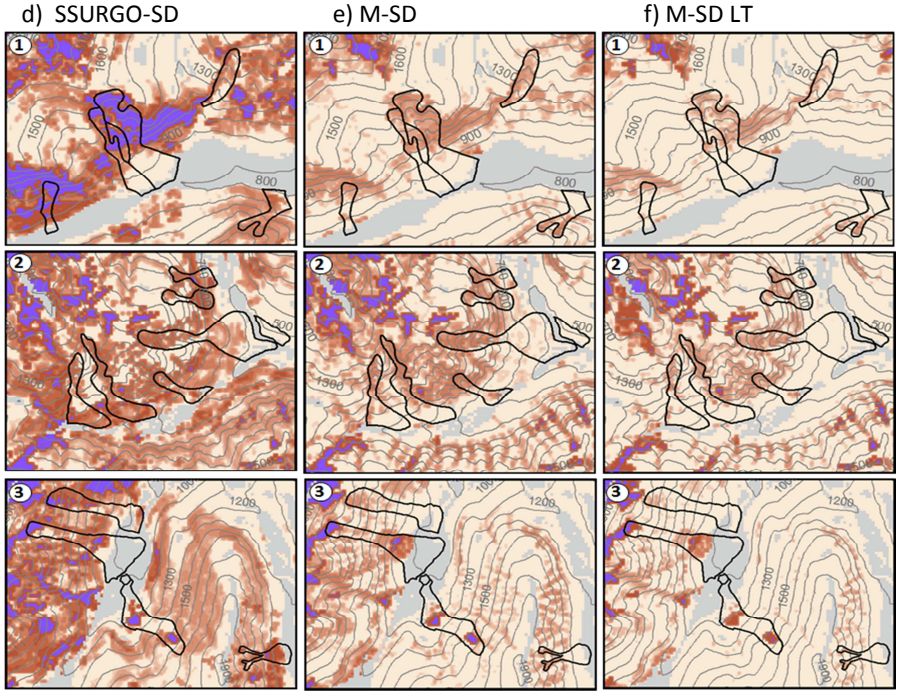

Figure 8. Landslide annual P(F) map for NOCA overlain with mapped debris avalanches for simulations with: **(a)** SSURGO-SD; **(b)** M-SD; **(c)** M-SD LT. Zoomed-in areas are shown for greater detail in the lower panel in the same order and according to number designated. Purple areas are considered chronically unstable and areas excluded from analysis are shown as gray. Contours are at 100 m. Aerial images of zoomed-in areas are provided in Fig. 3.

~~P(F) derived from simulations exhibit low probabilities where slopes are moderate and cohesion is high (e.g., forest). Highly unstable areas largely correspond to steep barren landscape (13% of the model domain) mostly located below retreating alpine glaciers, with steep glacial landforms, transitioning from glacier to colluvial processes (similar to Guthrie and Brown 2008; Tarolli et al., 2008; Legg et al., 2014) (Fig. 9). Barren areas cover ~13% of the modeled domain. These areas with a thin veneer colluvium, except for moraines, appear to be "continuously sliding" (Borga et al., 2002) or "chronically unstable" (Montgomery, 2001). Frequent slides, which also impedees the colonization of vegetation (Dietrich et al., 1995; Istanbulluoglu and Bras, 2005). Shallow soils can enhance the probability of saturation, leading to high pore-water pressure and saturated overland flows with moderate storms (Pelletier and Rasmussen 2009). Mass wasting activitySlides in barren areas were not completely included in our landslide inventory as they exhibit chronic small-scale slides that do not pose major risks or substantial deposition to humans and infrastructurezones.~~

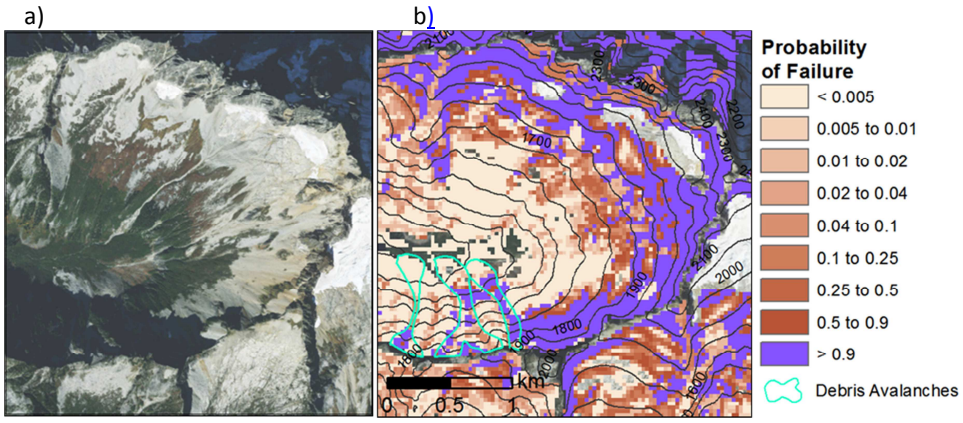

Figure 9. Illustration of highly unstable steep areas: **(a)** High resolution (0.3 m) imagery of a NOCA mountain (World Imagery, Esri Inc.)[1] compared to **(b)** P(F) simulated by M-SD with mapped debris avalanches. Contours at 100 m. Notice the barren areas below retreating glaciers with high P(F).

Other locations of higher P(F) are located in topographic hollows (Fig. 8, 9). These converging areas accumulate deeper soils, which decreases the effectiveness of root cohesion, and enhance pore pressure through ~~attract subsurface flow, leading to enhanced~~convergence of~~ing~~ subsurface flow ~~enhance pore pressure~~ (Dietrich et al., 1995). Converging areas often correspond to the upper portions of mapped debris avalanches, ~~which display~~thatwhich clearly

display higher landslide probabilities than the runout portions ~~in simulations~~downstream. Thus, the landslide probability visually appears to capture the source area of debris avalanches.

Substantial differences between P(F) derived with different soil depth maps are evident (Fig. 8 and Fig. 10) and corroborate previous studies showing the influence of various soil depth estimates on landslide susceptibility (Dietrich et al., 1995; Okimura, 1998). In general, probabilities are higher and more spatially extensive when the model is parameterized using SSURGO-SD compared to both M-SD scenarios. ~~Given that other parameter~~variables ~~are kept consistent, these differences are attributed to spatial variability of soil depth and related adjustments to transmissivity.~~

To investigate the spatial distribution of P(F) in relation to soil depth, we plot the cumulative distribution of P(F), referred to as the fraction of modeled area where P(F) is less than or equal to a given value, for each simulation (Fig 10a). We present our general observations of the spatial distribution of P(F) in the order of SSURGO-SD, M-SD, and M-SD LT as depicted in Fig 8. Simulations show approximately 26%, 38%, and 49% of the modeled domain (79% of NOCA, where θ>17°) as stable (i.e., P(F)=0) under the current vegetation cover and climate. We refer to these sites as unconditionally stable (i.e., stable even when saturated, and with minimum C and ø sampled) (Pack et al., 1998; Montgomery 2001). A bimodal spatial distribution for P(F) is evident (Fig. 10a, 10b). Areas with low probabilities, around P(F)≤0.1, dominate the spatial distribution of P(F), manifested with a steep rise in the fraction of area from P(F)=0 to P(F)=0.1 (Fig 10a). For P(F)≤0.1 (RP≥10 years), the order of aerial cover for the model domain, including the stable regions, is 72%, 85%, and 87%. When the unconditionally stable areas are excluded, the percentages become 46%, 47% and 38%, respectively, for the three soil depth products used. This region approximately marks the first peak of the relative histogram of P(F) (Fig. 10b).

In the broad 0.9>P(F)≥0.1 range, the increase in fraction of area with P(F) is gradual especially for the two M-SD simulations (Fig. 10a). In the highly unstable regions, with P(F)≥0.9 (RP≤1.1) as mapped in Fig. 8 and 9, the fractional area begins to rise again in all simulations (Fig 10a). P(F)=1 occupies 11% and 7% of the modeled area in the SSURGO-SD and M-SD simulations, which can be conceptually named as unconditionally unstable (i.e., unstable even when dry and with the highest combinations of C and ø sampled) (Pack et al., 1998; Montgomery 2001). The model run using M-SD LT soil scenario shows a smaller area percentage, ~6%, with P(F)≥0.9, while SSURGO-SD and M-SD had 16% and 10%. M-SD LT soil scenario provides a more realistic estimate as some locations are not likely to produce slope failures annually due to limited soil development. The second peak of the relative frequency histogram of P(F) appears when P(F)>0.9, largely associated with postglacial barren lands with steep mountain slopes, and converging topography, especially in the case of SSURGO-SD (Fig. 10b). Dominant factors that control the relative frequency of P(F) are labeled in Fig 10b, and further discussed in subsequent sections.

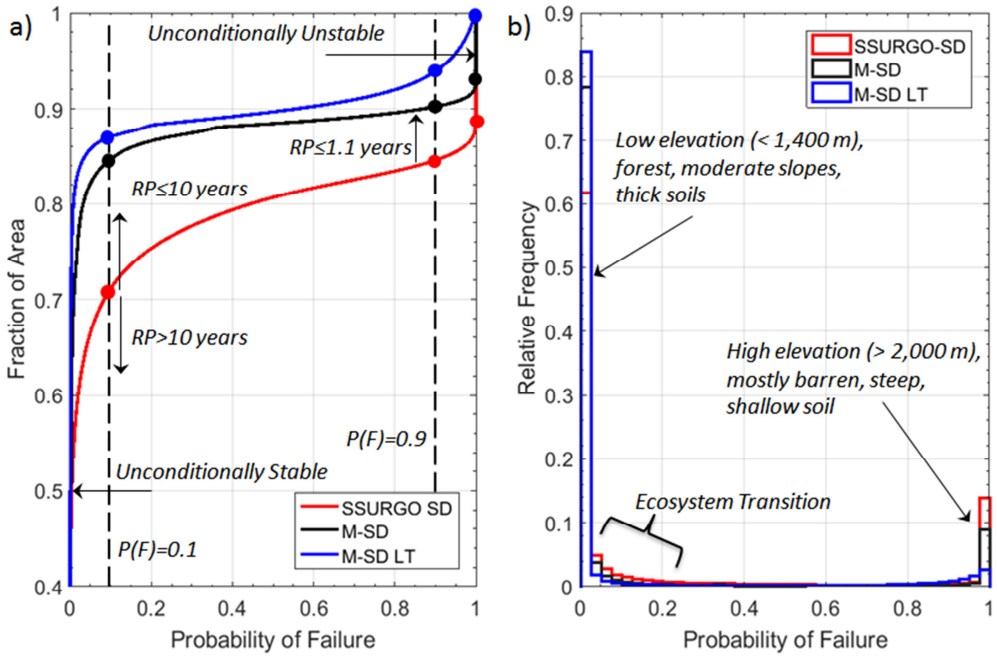

Figure 10. (a) Cumulative distribution and **(b)** relative frequency of P(F) (bin size ΔP(F)=0.025) mapped over NOCA from Landlab simulations using SSURGO-SD and two M-SD scenarios. Labels indicate dominant controls on the distribution of P(F) in (b). Fraction of area is used for cumulative spatial probability, plotted using the Weibull plotting position. Return Period for landslides are illustrated only for SSURGO-SD.

Comment [EI3]: I think the RP 10 arrows should be going along the curves – to the left RP<10 and to the right RP<10..

We expressed the annual probability of landsliding in the form of a RP, plotted with respect to fraction of area for all three simulations, and mapped RPs for the M-SD LT scenario in Fig. 11. The M-SD LT reduces the probability and increases the return period estimates of landslide initiation, revealing the influence of long-term memory of landsliding on the probability distribution of soil thickness obtained from the soil evolution model. Therefore, the M-SD LT scenario would better suit the definition of RP, while the other two simulations provide reference for relative comparisons. In general and in concert with the P(F), landslides at nearly all RPs affect a greater proportion of the domain when SSURGO-SD is used. Approximately 28% of the model domain is simulated to have a landslide return period of less than or equal to 10 years (i.e., P(F)≥0.1 or frequent slides) based on SSURGO-SD, compared to half as much area, 15%, for simulations using M-SD; M-SD LT had slightly less at 13%. Low return periods (i.e., < 10 years) coincide with steep slopes in barren areas that show chronic landsliding, low-cohesion vegetation type, such as herbaceous, as well as some steep hollows.

At the high end of the return period, 46% of the model domain was simulated to have landslides with a return period of ≥500 years for SSURGO-SD scenario, including stable areas,

compared to 52% and 70% for model runs that used M-SD and M-SD LT scenario, respectively (Fig. 11). High return periods (i.e., RP>500 years, P(F)< 0.002) are found where slopes are gentler, on divergent topography, and in ~~forest~~ forested areas. The fraction of the model domain with a landslide return period between 100 and 500 years is 10%, 18%, and 21% for SSURGO-SD, M-SD, and M-SD LT, respectively, showing a larger fraction in the M-SD products. These landslide frequency rates relate to long-term averages and the actual failures are likely to be clustered in space and time depending on triggering event and the time since the last landslide at the same location (Guthrie and Evans, 2004).

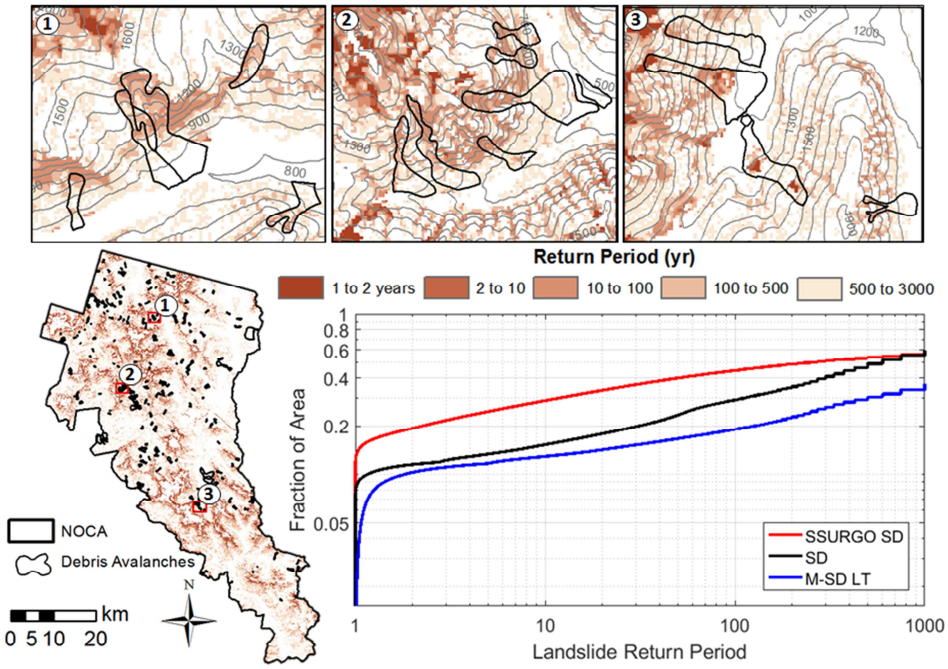

Figure 11. Modeled landslide return period simulations with M-SD LT for NOCA overlain with mapped debris avalanches, including zoomed in areas at top for greater detail. Cumulative distribution of return periods for SSURGO-SD, M-SD, and M-SD LT scenarios, plotted on a log-log scale using the Weibull plotting position.

As soils in landslide locations are formed by sediment accumulation from surrounding hillsides and weathering of the local bedrock, landslides can be the main source of denudation across landslide-prone regions. The expected values of mean annual denudation rate is approximated by the spatial mean of ~~: mean(~~$P(F)*h_s$~~)~~$/(\rho_r/\rho_s)$ for each simulation. This gives spatial average of the long-term denudation rates due to landslides as 51.9 mm y^{-1}, 7.06 mm y^{-1}, and 5.04 mm y^{-1} for SSURGO-SD, M-SD, and M-SD-LT scenarios, respectively. While these rates are higher than the reported mean annual denudation rates in this region over the last millennia of 0.08 to 0.57 mm y^{-1} (Moon et al., 2011), M-SD-LT clearly gives the closest estimates to observations among

the three soil depth scenarios. Over an order of magnitude variation in denudation rates is also common as part of long-term records of erosion rates (e.g., Molnar, 2004).

A critical question that remains is: what are the dominant controls that lead to the bimodal distribution of landslide probability in the modeled domain? First, we examined if topography alone, represented by S and CA pairs, can explain this behavior. The S-CA data pairs from each model grid cell are colored by the value of P(F) in the order from low to high value using output from the M-SD LT scenario (Fig. 12). As slopes get steeper (S>0.45 or 24.2^{o}), a relatively rapid increase in P(F) in relation to slope from P(F)=0.4 to 1.0 can be seen, surrounded with lower probabilities. CA does not seem to impose a visually detectable increase in P(F), which is likely largely due to the wet climate in region. The landslide source cells identified from the highest elevation of debris avalanche shapefiles fall in the "eye" of this high-P(F) region in the S-CA domain. Interestingly, P(F) diminishes in the steepest slopes of most CAs. While the trend of increasing P(F) as slope gets steeper generally shows the influence of slope in Eq. (1a), landscape with P(F)≥0.4 only constitute about 11% of the model domain (Fig. 10a). For comparison P(F)≥0.1 was 13%. On the other hand, about 57% of the domain has steeper slopes than 24.2^{o} (S=0.45m/m). ~~Locations with slopes less than this are rarely found with P(F)>0.4.~~ This suggest that the majority of the domain with similar pairs of S and CA exhibit lower landslide probability, which can be largely attributed to the spatial distribution and influence of vegetation type and soil depth (e.g., Roering et al., 2003).

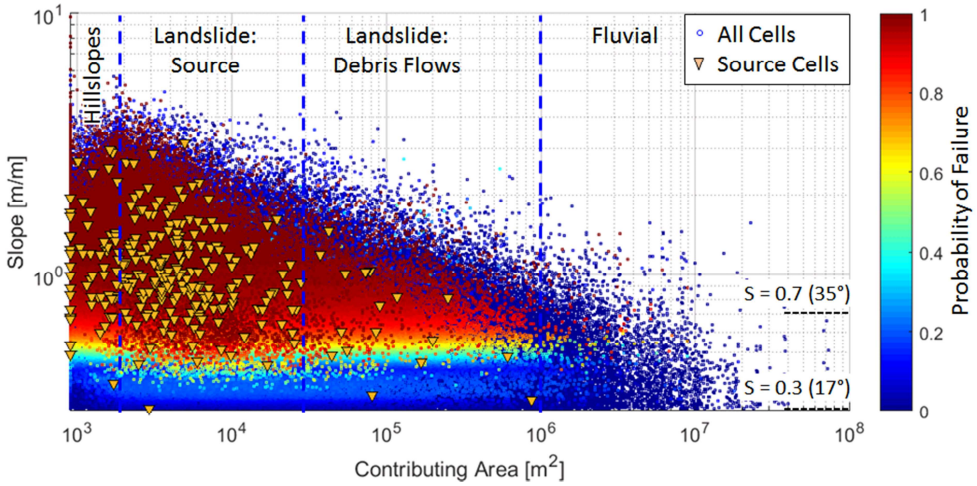

Figure 12. S-CA plot colored by the P(F) simulated with from the M-SD LT. Source cells (orange triangles) are the single highest-elevation grid cell within mapped debris avalanches. Comparable to Fig. 5. High probabilities plot over low probabilities.

We investigated the roles of vegetation, slope steepness, and soil depth on P(F) in relation to elevation (Fig 13). From low to high elevations, vegetation changes from predominantly forest (elevation <1,400 m) to coexisting shrub, herbaceous plants, and barren land (1,400 m to 2,200

m) as a result of elevation-dependent ecoclimatic controls (e.g., temperature) on vegetation survival and growth (Fig. 13a). In this region of ecosystem transition, the mean P(F) shows a persistent increase from 1,400 m until a maximum is reached between 2,200 and 2,400 m, depending on simulation (Fig. 13b, 13c). Observations of debris avalanche by elevation confirm the pattern of P(F) dependence on elevation in relation to ecosystem change; 75% of the extracted landslide initiation zones from mapped debris avalanches are located between 1,200 m to 2,000 m (Fig. 3b). In the 1,400 to 1,900 m elevation range of the ecosystem transition zone, mean slope is relatively constant ~0.75 m/m (~37^{o}), and rises up to 0.9 m/m (42^{o}) between 1,900 and 2,200 m (Fig 13c), consistent with the binned-averaged slopes of the landslide source area in the S-CA plot in Fig 5. Mean soil depth begins to drop in both SSURGO and modeled soil depth products above 2,200 m.

These ~~observations~~ model results confirm the strong control of ecosystem transition on landslide activity in the region. Below about 1,400 m (~40% of NOCA), forested vegetation combined with deeper soils and moderate slopes keep P(F) low. In the 1,400 to 2,200 m range, loss of root cohesion with ecosystem transition combined with gradual increase in landscape slopes contribute to increased P(F). Above 2,200 m elevation, soils become very shallow and slopes exhibit the steepest angles in the modeled domain. This combination leads to the largest variability in P(F), combining the highest P(F) values~~,~~ (P(F)≥0.9) mostly attributed to barren areas (~6% of the model domain in the M-SD LT scenario), with lower P(F) values where thinner soils reduce the driving force within Eq. (1a). Total cohesion has been found to affect FS estimates more on thin soil than on thick soils (Hammond et al., 1992). The sensitivity of FS to cohesion is even more pronounced on steep slopes, especially when saturated (Sidle 1984). Forest vegetation has also been found to stabilize slopes through the hydrological process or root water updake and transpiration, which leads to drier soil conditions (Arnone et al., 2016b). In aggregate, thinner soils at higher elevations lead to lower mean P(F), which we referred to as soil depth control (see also Sidle 1984). The general contribution of elevation on the spatial organization of P(F) is labeled in Fig 10b.

Comment [EI4]: What is this I would delte this where did this come from.. response to reviwer.. this read like a lit review.

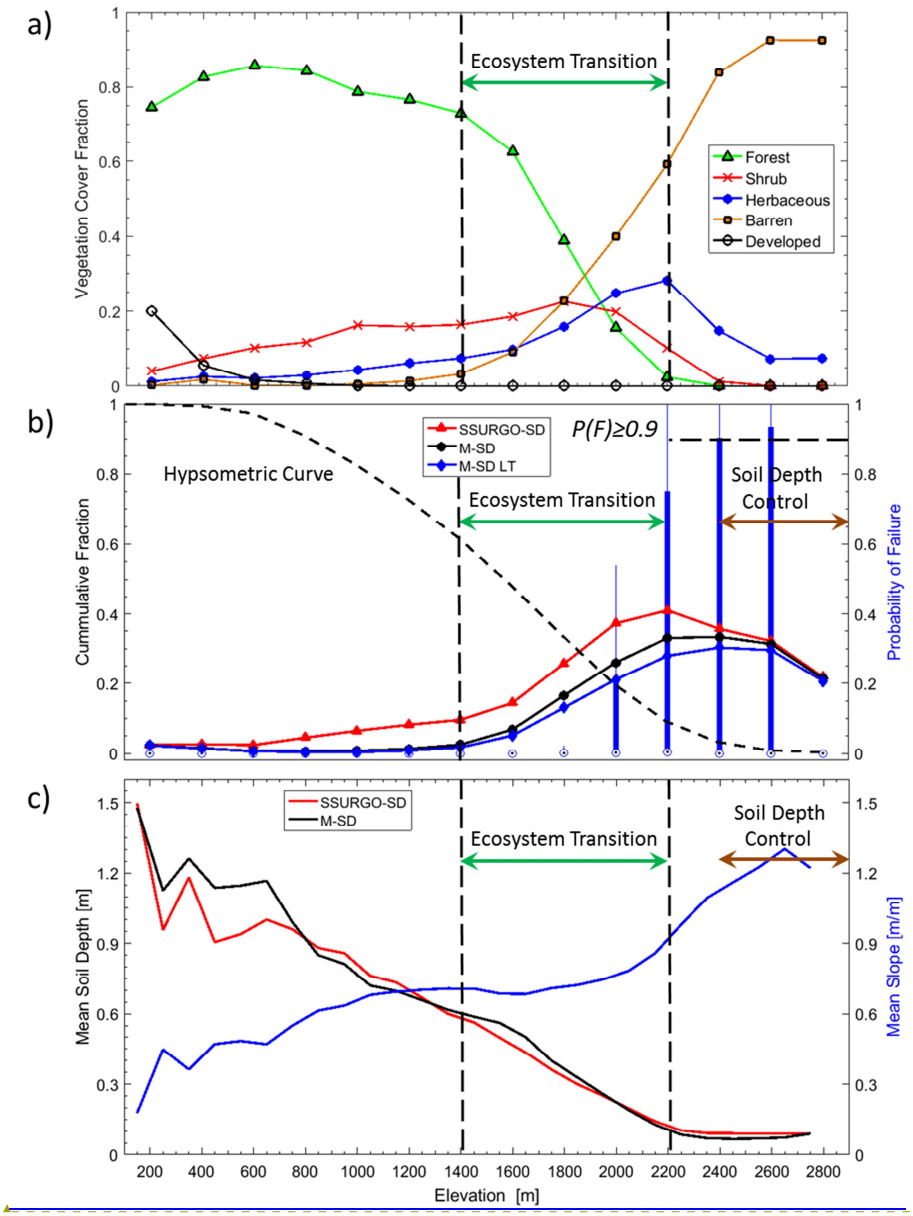

Formatted: Font: 11 pt, Font color: Custom Color(RGB(16,16,16))

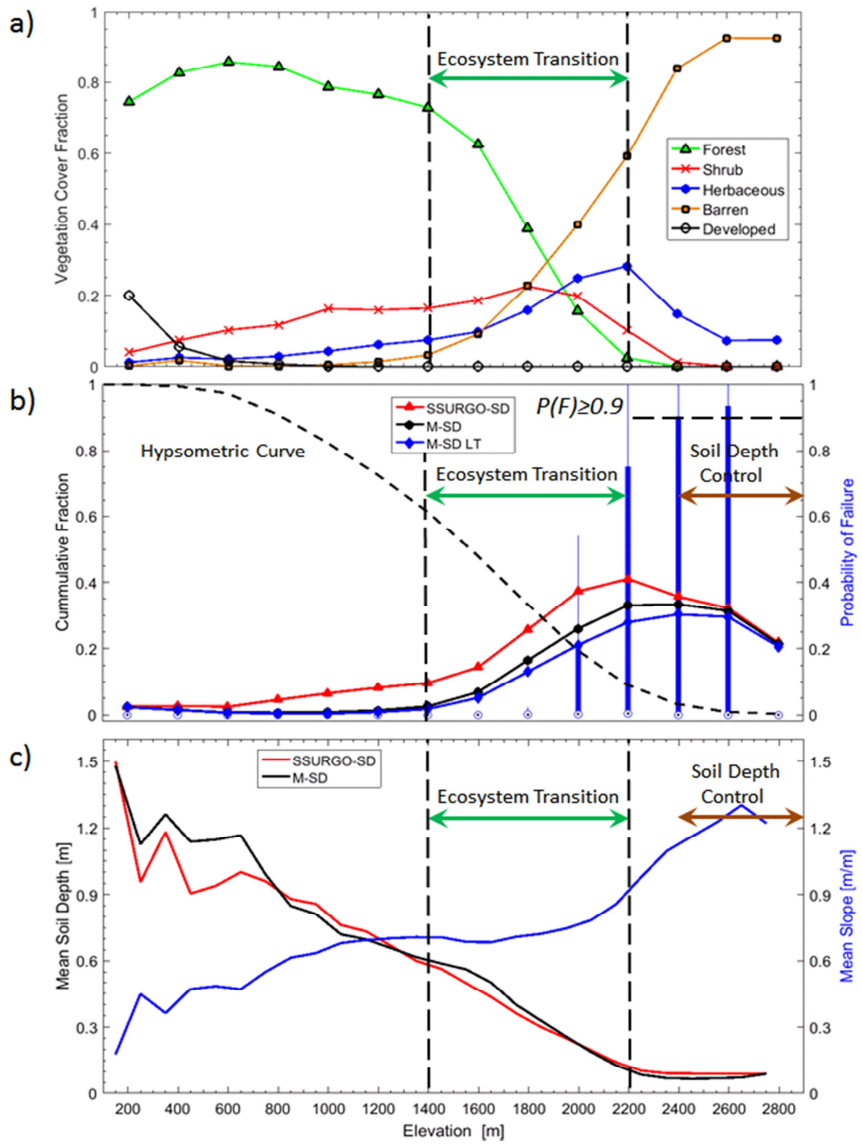

Figure 13. Elevation (200 m bands or bin) influence on: **(a)** vegetation cover fraction for NOCA, taken as fraction of vegetation type within each elevation band, **(b)** mean P(F) using SSURGO-SD and two M-SD scenarios, along with compact box-whisker plots for P(F) of M-SD LT scenario, ~~where~~ circle~~s~~ dot symbols represents median (outliers not shown~~, greater than 1.5 interquartile distance~~), overlaid with hypsometric curve for NOCA, and **(c)** mean soil depth for SSURGO-SD and M-SD products with mean slope. Mean values calculated within each 200-m elevation band.

4.3 Model Evaluation

The performance of a landslide model is often based on its ability to capture existing mapped landslides. W~~In Sect. 4.2 we evaluated our model through visual comparison of modeled P(F) to observed landslide locations (e.g., Fig. 8, 9). In this section, a more quantitative approach is presented for model evaluation. W~~e statistically evaluated our model using ~~multiple approaches, including cumulative distribution (CD) of P(F) comparisons as well as~~ Receiver Operating Characteristics (ROC) (Fawcett, 2006) and Success Rate (SR) curves (Bellugi et al., 2015).

~~For the statistical analysis, W~~we limited our performance assessment to the source areas of the mapped debris avalanches. Source areas of debris avalanches were not mapped separately from the remaining debris avalanche features (i.e., transition and deposition zones), hindering the evaluation of model predictions (Tarolli and Tarboton, 2006). ~~Because we anticipate that the source areas could originate from a neighboring grid cell, we considered source cells as a collection of grid cells in the upper 10, 20, and 30% highest elevation cells within each mapped debris avalanche shapefile.~~ Source areas we identified in relation to elevation~~These populations of source cells~~ (4318 samples) were treated as 'observed' landslide source cells during validation of the landslide probability using ~~CD, S~~ROC and SR~~OC~~ performance metrics. In this validation, we excluded barren areas with slopes ≥ 37° (~5% of the model domain), which characterizes slopes of active small-scale dry landslides (failure depth ≤ soil depth) more appropriately represented by nonlinear hillslope diffusion models (see Roering et al., 1999; DiBiase et al., 2010; Pelletier et al., 2013).

For comparison of P(F) with source area cells, we randomly sampled 50,000 grid cells outside mapped debris avalanches (~2% of the modeled domain), similar to the number of grid cells within entire mapped debris avalanche areas. ~~The majority of the source grid cells and outside debris avalanches cells are located at elevations between 1200 and 1800 m (Fig. 14a). Grid cells in the random sample outside debris avalanches were constrained to the elevation range of the source cells to allow unbiased comparison.~~ We recognize that the areas outside mapped debris avalanches have the potential to be unmapped landslides, other landslide types, or unstable areas deficient a triggering event; therefore, we interpret the test results conservatively. ~~We expect the simulated P(F) should estimate lower probability outside debris avalanches compared to source areas of mapped debris avalanches.~~

~~At low and mid elevations, simulations generally showed a greater fraction of high probabilities in source areas compared to outside of debris avalanches (Fig. 14b, c). However, when only high elevation (>1,800 m) data were considered, the pattern was reversed with a larger fraction of high probabilities found outside debris avalanches than source areas (Fig. 14d). At this higher elevation, much of the land cover is barren or herbaceous (i.e., low root cohesion), resulting in high probabilities of failure throughout the model domain (Fig. 12a). While there are extensive shallow failures in these regions only limited amount of those that turned into debris avalanches were mapped. This reverse pattern is also present at mid-elevations (~1,200~~

~~to 1,800) for both M-SD scenarios, only for 10% of the sample data, when P(F)>0.03 and P(F)>0.1 for M-SD and M-SD LT, respectively (note the crossing curves in Fig. 14b). At low elevation (~125 to 1,200 m), there were no source areas with P(F)>0.4 in M-SD and M-SD LT scenarios.~~

~~The performance of the model results we are presenting in this paper are specific to a sample comparison of 10% source area of mapped debris avalanches and random sampling outside debris avalanches. When examining the validation datasets in their entirety (i.e., regardless of elevation), the median P(F) of the 10% source DA cells is 13 times the median P(F) of outside DA for SSURGO-SD and four times the median P(F) for M-SD; median is zero for outside DA cells in the M-SD LT. The Kolmogorov-Smirnov test (Chakravart et al., 1967) test show paired comparison between DA source area cells and cells outside DA for all three scenarios are statistically different (p<<0.01).~~

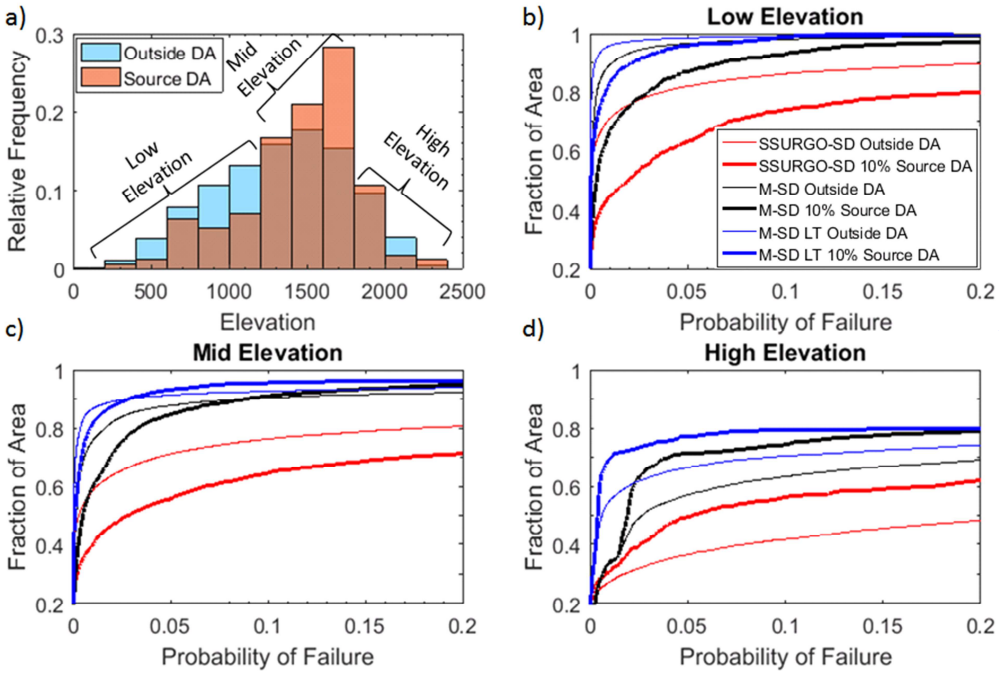

Formatted: Left

~~**Figure 14.** a) Relative histogram of source areas in upper 10% elevation of debris avalanches (DAs) and for 50,000 grid cells outside DAs. Cumulative distributions of P(F) plots limited to P(F) ≤ 0.2, or return period ≥ 5 years, to highlight detail in simulation using SSURGO-SD, M-SD, and M-SD LT at: b) low (<1,200 m), c) mid (1,200 to 1,800 m), and d) high (>1,800 m) elevations as depicted in a). Thicker lines represent probabilities for source areas of (DAs) and thin lines represent probabilities for cells outside DAs.~~

~~Another statistical analysis uses~~ ROC curves were~~are~~ used to examine how our model compares with randomly distributed landslides over the landscape. These curves are constructed from

confusion matrices generated from comparisons between observed and modeled landslides, based on varying P(F) threshold (e.g., 0.1, 0.2, 0.3, etc.). Details on calculating metrics used to generates these curves have been provided elsewhere (see: ~~True positives (TP) are those cases within observed landslides where probabilities are equal to or greater than threshold. False negatives (FN) are probabilities within landslides that fall below the threshold. False positives (FP) occur outside observed landslides with simulated probabilities equal to or above the threshold. True negatives (TN) are also outside observed landslides, but with probabilities below the threshold. From these metrics, true positive rate (TPR) or fraction of landslides captured and false positive rate (FPR) or fraction of false alarms can be calculated as follows:~~

~~$TRP = \frac{TP}{(TP+FN)}$ (8)~~

~~$FRP = \frac{FP}{(FP+TN)}$ (9)~~

~~The advantage of the ROC curve over a standard confusion matrix is the ability to vary the probability threshold for assigning model simulations to a modeled landslide (positive) or no landslide (negative) classification, generating different positive and negative comparisons~~ (~~Mancini et al., 2010; El-Ramly et al., 2002; Anagnostopoulos et al., 2015~~). A better performing model will exhibit a curve toward the upper left of a ~~FPR~~ false positive rate (x-axis) and ~~TPR~~ true positive rate (y-axis) plot. A 1:1 line in the plot represents a trivial model that randomly assigns stable and unstable cells. The area under the curve (AUC) generated by ROC curve quantifies the performance of a model for identifying landslide and non-landslide locations. The AUC statistic represents the probability of correctly ranking a landslide and non-landslide pair randomly selected from those two datasets (Hanley and McNeil, 1982). SR curves are similar to ROC curves, ~~with TPR as the y-axis,~~ but plot ~~compares this to~~ the fraction of landscape predicted as unstable (x-axis)~~, calculated as (TP+FP)/(TP+FP+TN+FN)~~. Again, a relatively well performing model would plots farther away from the 1:1 line representing a trivial model.

For this comparison, we used the same datasets used in the cumulative probability analysis discussed Sect. 4.2. Both simulations using SSURGO and M-SD modeled 10% source areas and non-landslide areas better than random selection as demonstrated by the curves plotted above the 1:1 line (Fig. ~~15~~14). ~~The classification is stronger as the source area fraction is reduced.~~ However, the model's strength in the classification is modest as indicated by the AUC values of between 0.60 and 0.61, compared to an AUC of 1 representing a perfect classification. The TRIGRS-P probabilistic landslide model tested by Raia et al. (2014) found higher AUC results (i.e., 0.65 to 0.73). However, their study tested small areas (3 to 6 km^2) that were well studied locations with detailed inventories of landslides resulting from one or two winter rainfall seasons and the entire landslide was tested rather than source areas only.

Formatted: Indent: Left: 0 cm, Space Before: 0 pt, Tab stops: Not at 13.97 cm

Formatted: Indent: Left: 0 cm, Space After: 0 pt, Tab stops: Not at 13.97 cm

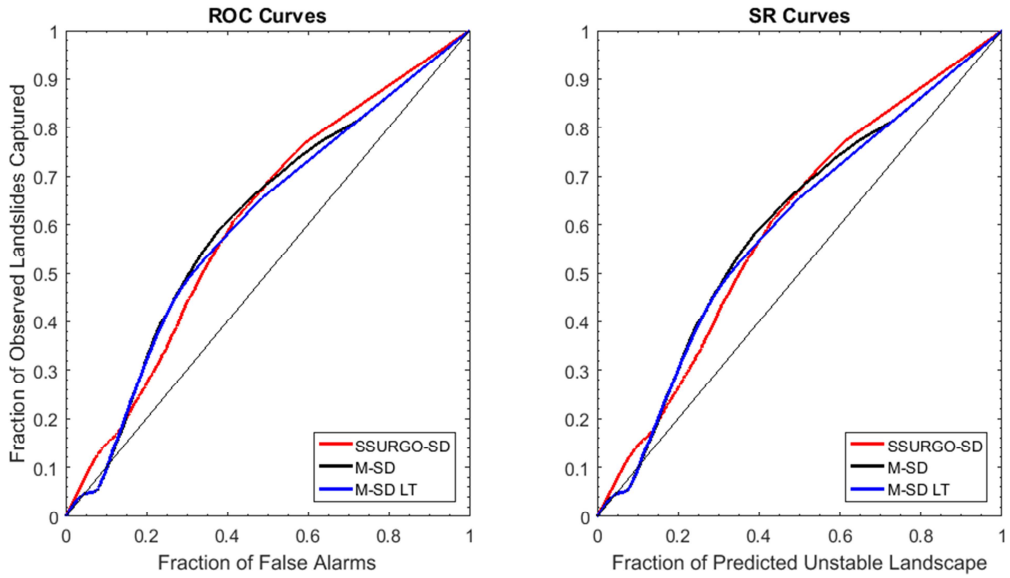

Figure ~~15~~14. a) ROC curves and b) SR curves for simulations using SSURGO-SD, M-SD, and M-SD long-term (LT). Comparison represent P(F) for the upper 10% of DA as observed landslides to a random sample of 5,000 cells outside DAs. Thresholds for simulated probabilities associated with positive classification of a source areas declines along the curves from lower left to upper right. Black diagonal line on a 1:1 line represents the case of a trivial or random classification model. AUC values range from 0.60 to 0.61.

ROC and SR curves provide an indication of how well the modeled simulations of P(F) classify both observed landslide source cells and non-landslide grid cells compared to random classification. The crossing of ROC and SR curves in the simulations with M-SD (Fig. ~~15~~14) implies that at higher probability thresholds, simulated probabilities delineate more false alarms (e.g., areas outside DAs as unstable) than capturing source areas. This may be indicative of the high probability values at high elevations even outside the debris avalanches where vegetation is sparse, as was indicated above in the analysis of cumulative distribution plots. We found for our case study that the optimal probability threshold to maximizing landslides captured and minimizing false alarms (i.e., point around the apex of the ROC curves) declines by half depending on the simulation: P(F)≥0.008 (i.e., RP≤125 years) for SSURGO-SD, P(F)≥0.004 (i.e., RP≤250 years) for M-SD, and P(F)≥0.002 (i.e., RP≤500 years) for M-SD LT.

The modeled potentially unstable landscape has generally been greater than observed landslides when infinite slope stability models are calibrated with limited observations (Sidle and Ochiai, 2006; Baum et al., 2010). As pointed out by Borga et al. (2002), concluding "overrepresentation" of areas potentially subject to shallow landsliding can be misleading because the absence of mapped landslides does not necessarily indicate an absence of

landslide hazard over time across the landscape. Locations with high landslide probability outside mapped landslides in both simulations could be indicators of where to conduct additional investigations for missed landslides or areas on the verge of failing.

Validating hazard maps is challenging, especially in large areas of remote mountainous regions, because inventories are typically incomplete, lack the date of landslide occurrence, different landslide types likely have different meteorological triggers, environmental conditions change after a landslide event, and unidentified high probability areas may fail in the near future even though they appear to be stable during an inventory (van Westen et al., 2006; Tarolli and Tarboton, 2006). Additional evaluation of model performance would benefit from field investigation in areas of high and low modeled P(F) to identify any landslides or instability that may have been missed during the original inventory. Future work that couples the volume of sediment available for landsliding will lead to further improvements in estimating hazards and potential impacts from landslides.

4.4. Model Limitations

For model design and computation efficiency, we made several simplifying assumptions. We neglect groundwater leakage to the bedrock in recharge estimation and apparent soil cohesion through the effect of surface tension in unsaturated zones (e.g., Lepore et al., 2013), both of which could be added to future updates to the component. Tree and snow surcharge is also disregarded, although it may have some stabilizing effect where soils are shallower than 1 m (Hammond et al., 1992). Our approach does not simulate the actual number of landslides, landslide type, nor the size of the landslide because the discretized nature of the failure field precludes specific knowledge of which and how many grid units may be involved in a failure at a particular time. These model omissions present opportunities for future customization of the component or coupling with other models.

Modeled probability does not capture the runout of debris avalanches, which can travel considerable distances in steep mountainous environments. Some unexpected results depicted higher probability in runout portions of some debris avalanches when using SSURGO-SD, but these probabilities were lower when M-SD scenarios were used (e.g., Fig. 8, middle zoomed-in panels). Mis-mapping of probabilities of failure and observed landslide are likely attributed to variations in soil depth, material properties, and hydrologic routing (Schmidt et al., 2001). Model ~~parameter~~variables such as slope derived from DEMs developed with post-landslide mapping can also contribute to reduced probabilities in observed landslides where slope and soil depth were reduced. Furthermore, inventories over broad areas are challenging as landslides are isolated processes that may occur with regularity, but may not be large in size (Van Westen et al., 2006). Finally, steady-state flow that we used for subsurface flow neglects transient processes and roles of macro-pores. Macropores from decayed roots or animal activity can be important in transporting water relatively quickly from the surface to deeper soil layers and groundwater (Sidle et at., 2001; Gabet et al., 2003; Beven and Germann, 2013).

5 Conclusion

We develop a regional model of probabilistic shallow landslide initiation based on the infinite slope stability equation coupled by steady-state subsurface hydrology driven by groundwater recharge. Uncertainty in model parameter~~variable~~s is explicitly accounted for through Monte Carlo simulation. A geomorphic soil evolution model provides a spatially-distributed soil depth alternative to homogeneous patches of soil depths provided by SSURGO. This feature allows the landslide model to be used where soil depth information is uncertain, sparse, or absent. Our model workflow ~~framework~~ developed in Landlab (Hobley et al., 2017) is made up of a landsliding component, a Landlab utility for hydrologic data processing, and a model driver that runs the component. The model driver can be run on personal computers or online via Hydroshare through cloud computing creating reproducible results. Our approach demonstrates:

- Regional maps of landslide hazard produced with three different soil depth scenarios reveal alternative simulations of probability of landslide initiation, reflecting the importance in soil depth in landslide hazard prediction.
- Simulations using SSURGO-SD returned higher probability of failures and shorter return periods than simulations using modeled soil depth products (M-SD and M-SD LT). The M-SD LT simulation further reduces the probability of failure and increases the return period. Mean annual denudation estimates from the M-SD LT scenario show closer estimates to published rates of denudation over the last millennia than the other simulations.
- SSURGO-SD scenario provide a short-term tool for high risk planning using conservative estimates of probability of failure, while M-SD LT provides long-term estimates arguably more consistent with landslide frequency in the region and useful for management of ecosystems and aquatic habitats, and estimation of sediment budgets for watershed planning.
- Elevation dependent patterns in probability of landslide initiation show the stabilizing effects of forests in low elevations, an increased landslide probability with forest decline at mid elevations (1,400 to 2,400 m), and soil limitation and steep topographic controls at high alpine elevations and post-glacial landscapes. These dominant controls manifest in a bimodal distribution of spatial annual landslide probability, ~~modes~~ peaks controlled by highly stable forested and chronically unstable post-glacial domains and other barren areas. This suggests that ~~further~~potential declines in forest cover with climate change could lead to widespread landslide activity.
- Model ~~testing~~ confirmation with limited observations revealed similar model confidence for the three hazard maps, suggesting suitable use as relative hazard products. Validation of the model with observed landslides is hindered by the completeness and accuracy of the inventory, estimation of source areas, and unmapped landslides.
- Our shallow landslide hazard model provides regional scale estimates of the relative annual probability of shallow landslide initiation as well as landslide return period,

which is useful for civil protection through land use planning to minimize geohazard consequences from precipitation triggers.

6 Data and Model Availability

To facilitate ease of use of the landslide hazard model, we developed the landslide model as a component of Landlab, an open-source Python toolkit for two-dimensional numerical modeling of Earth-surface dynamics available at GitHub: http://github.com/landlab/landlab (Hobley et al., 2017). Documentation, installation instructions, and software dependencies for the entire Landlab project can be found at: http://landlab.github.io/. The Landlab project is tested on recent-generation Mac, Linux and Windows platforms using Python versions 2.7, 3.4, and 3.5. The Landlab modeling framework is distributed under a MIT open-source license. A component ~~user~~ User ~~manual~~ Manual and driver scripts for the application of the Landlab LandsideProbability component can be found at https://github.com/RondaStrauch/pub_strauch_etal_esurf~~https://github.com/landlab/pub_strauch_etal_esurf (Strauch, GitHub Repository)~~.

Online access to the Landlab LandslideProbability model is freely provided through https://www.hydroshare.org, where data and code drivers are available to demonstrate and explore the model using interactive IPython notebooks in a JupyterHub. Thus, users can access, test, adapt, and apply the landslide model for their area of interest without downloading Landlab or the components. Data and driver code used in this analysis are available at hydroshare (Strauch et al., 2017). Existing demonstration driver codes can be adapted to fit data provided in raster format by the user to create distributed data fields used as ~~parameter~~variables in the component. Instructions for accessing HydroShare and the online demonstrations, codes, and data used in this paper are provided in the S~~s~~upplement~~al material~~.

Acknowledgements

This research was supported by the US National Science Foundation (CBET-1336725, OAC-1450412, 1450409, 1450338) and USGS Northwest Climate Science Center. We thank Dan Miller and two anonymous reviewers for helpful reviews of an earlier version of the manuscript. Technical editing on portions of the manuscript was provided by Brad Strauch and Diann Strom. We also appreciate the developers of Landlab, including open-source contributors to the earth surface processes modeling community. Data repository (Strauch et al., 2017), testing, and online reproducibility was facilitated by the cyber infrastructure of HydroShare services provided by researchers associated with the Consortium of Universities for the Advancement of Hydrologic Science, Inc. (CUAHSI), particularly the support of Tony Castronova, and the team at CyberGIS Center for Advanced Digital and Spatial Studies for their maintenance and support for our use of the ROGER Supercomputer at the National Center for Supercomputing Applications (NCSA) at University of Illinois at Urbana-Champaign.

~~7~~ References

Abbaszadeh M., Shahriar K., Sharifzadeh M., and Heydari M.: Uncertainty and re- liability analysis applied to slope stability: a case study from Sungun copper mine. Geotechnical and Geological Engineering 29: 581–596, 2011.

Adams, J.M., Gasparini, N.M., Hobley, D.E.J. Tucker, G.E., Hutton, E.W.H., Nudurupati, S.S., and Istanbulluoglu, E.: The Landlab v1. 0 OverlandFlow component: a Python tool for computing shallow-water flow across watersheds, Geoscientific Model Development, 10.4, 2017.

Alvioli, M., Guzzetti, F., and Rossi, M.: Scaling properties of rainfall induced landslides predicted by a physically based model, Geomorphology, 213:, 38-47, 2014.

Anagnostopoulos, G.G., Fatichi, S., and Burlando, P.: An advanced process-based distributed model for the investigation of rainfall-induced landslides: The effect of process representation and boundary conditions, Water Resources Research, 51(9): 7501-7523, 2015.

Arnone, E., Dialynas, Y.G., Noto, L.V., Bras, R.L.: Parameter Uncertainty in Shallow Rainfall-triggered Landslide Modeling at Basin Scale: A Probabilistic Approach. Procedia Earth and Planetary Science 9:101-111, 2014.

Arnone, E., Dialynas, Y.G., Noto, L.V., and Bras, R.L.: Accounting for soil parameter uncertainty in a physically based and distributed approach for rainfall-triggered landslides. Hydrological Processes 30(6): 927-944, 2016a.

Arnone E., Caracciolo D., Noto L.V., Preti, F., and Bras, R.L.; Modeling the hydrological and mechanical effect of roots on shallow landslides. Water Resour Res 52(11):8590–8612, 2016b.

Barling, R.D., Moore, I.D., and Grayson, R.B.: A quasi-dynamic wetness index for characterizing the spatial distribution of zones of surface saturation and soil water content, Water Resources Research, 30.4: 1029-1044, 1994.

Bathurst, J. C., Moretti, G., El-Hames, A., Moaven-Hashemi, A. and Burton, A.: Scenario modelling of basin-scale, shallow landslide sediment yield, Valsassina, Italian Southern Alps, Natural Hazards and Earth System Science, 5.2: 189-202, 2005.

Baum, R.L., Galloway, D.L., and Harp, E.L.: Landslide and land subsidence hazards to pipelines, U.S. Geological Survey Open-File Report 2008-1164, 192 pp., 2008a.

Baum, R., Savage, W., Godt, J.W.: TRIGRS — a fortran program for transient rainfall infiltration and grid-based regional slope-stability analysis, version 2.0, U.S. Geological Survey Open-File Report 2008-1159, 75 pp., 2008b.

Baum, R.L, Godt J.W., and Savage, W.Z.: Estimating the timing and location of shallow rainfall-induced landslides using a model for transient, unsaturated infiltration. Journal of Geophysical Research: Earth Surface, 115(F3), 2010.

Baum, R.L., Schulz, W.H., Brien, D.L., Burns, W.J., Reid, M.E., and Godt, J.W.: Plenary: Progress in Regional Landslide Hazard Assessment—Examples from the USA, In: Landslide Science for a Safer Geoenvironment, Springer International Publishing, 21-36, 2014.

Bellugi, D., Milledge, D.G., Dietrich, W.E., Perron, J.T., and McKean, J.: Predicting shallow landslide size and location across a natural landscape: Application of a spectral clustering search algorithm. Journal of Geophysical Research: Earth Surface, 120(12), 2552-2585, 2015.

Bellugi D., W.E. Dietrich, J. Stock, J. McKean, B. Kazian, and Hargrove, P.: Spatially explicit shallow landslide susceptibility mapping over large areas, Italian Journal of Engineering Geology and Environment, doi: 10.4408/IJEGE.2011-03.B-045, 2011.

Benda, L. and Dunne, T.: Stochastic forcing of sediment supply to channel networks from landsliding and debris flow, Water Resour. Res. 33(12): 2849-2863, 1997a.

Benda, L. and Dunne, T.: Stochastic forcing of sediment routing and storage in channel networks. Water

Formatted: Font: 11 pt, Font color: Custom Color(RGB(20,20,19))

Resour. Res. 33(12): 2865-2880, 1997b.
Berti, M., Martina, M.L.V., Franceschini, S., Pignone, S., Simoni, A., and Pizziolo, M.: Probabilistic rainfall thresholds for landslide occurrence using Bayesian approach, Journal of Geophysical Research 117:F04006, 2012.
Beven K.J. and Kirkby, N.J.: A physically based variable contributing area model of basin hydrology, Hydrological Sciences Bulletin 24: 43-69, 1979.
Beven, K., and Germann, P.: Macropores and water flow in soils revisited. Water Resour. Res., 49(6), 3071-3092, 2013.
Bordoni, M., Meisina, C., Valentino, R., Bittelli, M., and Chersich, S.: Site-specific to local-scale shallow landslides triggering zones assessment using TRIGRS, Natural Hazards & Earth System Sciences, 15(5): 1025-1050, 2015.
Borga, M., Fontana, G.D., and Cazorzi, F.: Analysis of topographic and climatic control on rainfall-triggered shallow landsliding using a quasi-dynamic wetness index. Journal of Hydrology, 268(1): 56-71, 2002.
Borga M., Fontana, G.D., Ros, D.D., Marchi, L.: Shallow landslide hazard assessment using a physically based model and digital elevation data, Environ Geol 35(2–3):81–88, 1998.
Braun, J., Heimsath, A.M., and Chappell, J.: Sediment transport mechanisms on soil-mantled hillslopes, Geology, 29(8): 683-686, 2001.
Caine, N. The rainfall intensity: duration control of shallow landslides and debris flows. Geografiska Annaler. Series A. Physical Geography, 23-27, 1980.
Carrara, A., M. Cardinali, F. Guzzetti, and Reichenback, P.: GIS technology in mapping landslide hazards. In: Carrara, A. and F. Guzzetti (eds.) Geographical Information System in Assessing Natural Hazard. Kluwer, New York, 107-134 pp., 1995.
Casadei, M., Dietrich, W.E. and Miller, N.L.: Testing a model for predicting the timing and location of shallow landslide initiation in soil-mantled landscapes, Earth Surf. Process. Landforms, 28: 925-950, 2003.
Castranova, T., Dockerfile for the HydroShare-JupyterHub base image, https://hub.docker.com/r/castrona/hydroshare-jupyterhub/ (Accessed April 4, 2017), 2017.
Catani F., Segoni, S., Falorni, G.: An empirical geomorphology-based approach to the spatial prediction of soil thickness at catchment scale, Water Resour Res 46, W05508, 2010.
Chakravarti, I. M., Roy, J.D., and Laha, R.G.: Handbook of Methods of Applied Statistics, Volume I, John Wiley and Sons, pp. 392-394, 1967.
Chen, W., Li, W., Hou, E., Zhao, Z., Deng, N., Bai, H., and Wang, D.: Landslide susceptibility mapping based on GIS and information value model for the Chencang District of Baoji, China, Arabian Journal of Geosciences 7(11): 4499-4511, 2014.
Cho, S.E.: Effects of spatial variability of soil properties on slope stability, Engineering Geology, 92(3): 97-109, 2007.
Chung, C.F., A.G. Fabbri, and Van Western. C.J.: Multivariate regression analysis for landslide hazard zonation. In: Carrara, A. and F. Guzzetti (eds.) Geographical Information System in Assessing Natural Hazard. Kluwer, New York: pp. 107-134, 1995.
Crozier, M.J. Prediction of a rainfall-triggered landslide: A test of the antecedent water status model. Earth Surf. Process. Landforms, 24: 825-83, 1999.
Crozier, M. J. Landslides Causes, Consequences, and Environment, Croom Helm, London, 252, pp.,1986.
Cullen, A.C. and Frey, H.C. Probabilistic techniques in exposure assessment: a handbook for dealing with variability and uncertainty in models and inputs, Springer Science & Business Media, 1999.
Daly, C., Halbleib, M., Smith, J.I., Gibson, W.P., Doggett, M.K., Taylor, G.H., Curtis, J. and Pasteris, P.P.: Physiographically sensitive mapping of climatological temperature and precipitation across the

conterminous United States. International Journal of Climatology, 28(15):2031-2064. 2008. (Data available at: PRISM Climate Group: Oregon State University, http://prism.oregonstate.edu).
DiBiase, R.A., Whipple, K.X., Heimsath, A.M. and Ouimet, W.B.: Landscape form and millennial erosion rates in the San Gabriel Mountains, CA, Earth and Planetary Science Letters, 289, 134–44, 2010.
Dietrich, W.E., R. Reiss, J. Hsu, and Montgomery, D.R.: A process-based model for colluvial soil depth and shallow landsliding using digital elevation data, Hydrological Processes 9: 383-400, 1995.
Dou, H.Q., Han T.C., Gong, X.N., and Zhang, J.: Probabilistic slope stability analysis considering the variability of hydraulic conductivity under rainfall infiltration–redistribution conditions, Engineering Geology, 183:1-13, 2014.
El-Ramly, H., Morgenstern, N.R., and Cruden, D.M.: Probabilistic slope stability analysis for practice, Canadian Geotechnical Journal, 39(3):665-683, 2002.
Elsner, M.M., Cuo, L., Voisin, N., Deems, J.S., Hamlet, A.F., Vano, J.A., Mickelson, K.E.B., Lee S., and Lettenmaier, D.P.: Implications of 21st century climate change for the hydrology of Washington State, Climatic Change, 102 (1-2): 225-260, doi: 10.1007/s10584-010-9855-0, 2010.
Fawcett, T.: An introduction to ROC analysis, Pattern recognition letters, 27(8):861-874, 2006.
Formetta, G., Capparelli, G., and Versace, P.: Evaluating performance of simplified physically based models for shallow landslide susceptibility, Hydrology and Earth System Sciences, 20(11): 4585, 2016.
Gabet, E.J., Reichman, O.J., and Seabloom, E.W.: The effects of bioturbation on soil processes and sediment transport, Annual Review of Earth and Planetary Sciences, 31(1):249-273, 2003.
Gabet, E.J., and Dunne, T.: Landslides on coastal sage-scrub and grassland hillslopes in a severe El Nino winter: The effects of vegetation conversion on sediment delivery, Geol. Soc. Am. Bull., 114(8):983–990, 2002.
Glade, T.: Landslide hazard assessment and historical landslide data—an inseparable couple? In The use of historical data in natural hazard assessments, Springer Netherlands, 153-168 pp., 2001.
Ghirotti, M.: The 1963 Vaiont landslide, Italy. In: J.J. Claque and D. Stead (eds.) Landslides: Types, mechanisms and modeling. Cambridge University Press, NY, 359 PP., 2012.
Godt, J.W., Schulz, W.H., Baum, R.L., and Savage, W.Z.: Modeling rainfall conditions for shallow landsliding in Seattle, Washington, Reviews in Engineering Geology, 20: 137-152, 2008.
Godt, J.W., and McKenna, J.P.: Numerical modeling of rainfall thresholds for shallow landsliding in the Seattle, Washington, area, Reviews in Engineering Geology, 20: 121-136, 2008.
Goode, J.R., Luce, C.H., and Buffington, J.M.: Enhanced sediment delivery in a changing climate in semi-arid mountain basins: Implications for water resource management and aquatic habitat in the northern Rocky Mountains, Geomorphology, 139: 1-15, 2012.
Gorsevski, P.V., Gessler, P.E., Boll, J., Elliot, W.J., and Foltz, R.B.: Spatially and temporally distributed modeling of landslide susceptibility, Geomorphology, 80.3: 178-198, 2006.
Guthrie, R.H., and Brown, J.K.: Denudation and landslides in coastal mountain watersheds: 10,000 years of erosion, Geographica Helvetica, 63(1): 26-35, 2008.
Guthrie, R.H., and Evans, S.G.: Analysis of landslide frequencies and characteristics in a natural system, coastal British Columbia, Earth Surface Processes and Landforms, 29(11): 1321-1339, 2004.
Hales, T.C., Cole-Hawthorne, C., Lovell, L., and Evans, S.L.: Assessing the accuracy of simple field based root strength measurements, Plant and soil, 372(1-2): 553-565, 2013.
Hamlet, A.F., M.M. Elsner, G. Mauger, S. Lee, and Tohver, I.: An Overview of the Columbia Basin Climate Change Scenarios Project: Approach, Methods, and Summary of Key Results, Atmosphere-Oceans, 51(4): 392-415, 2013.
Hammond, C., Hall, D., Miller, S., and Swetik, P.: Level 1 stability analysis (LISA), documentation for Version 2.0. USDA, For. Serv., Moscow, ID, Intermountain Res. Sta. Gen. Tech. Rep. INT-285, 1992.

Hanley, J.A., and McNeil, B.J.: The meaning and use of the area under a receiver operating characteristic (ROC) curve, Radiology, 143(1): 29-36, 1982.
Haugerud, R.A., and Tabor, R.W.: Geologic map of the North Cascade Range, Washington, US Department of the Interior, US Geological Survey, 29 pp., 2009.
Heimsath, A.M., Dietrich, W.E., Nishiizumi, K., and Finkel, R.C.: The soil production function and landscape equilibrium, Nature, 388(6640): 358-361, 1997.
Hobley, D.E.J., Adams, J.M., Nudurupati, S.S., Hutton, E.W.H., Gasparini, N.M., Istanbulluoglu, E., and Tucker, G. E.: Creative computing with Landlab: an open-source toolkit for building, coupling, and exploring two-dimensional numerical models of Earth-surface dynamics, Earth Surf. Dynam., 5(1): 21-46, doi:10.5194/esurf-5-21-2017, 2017.
Horsburgh, J.S., Morsy, M.M., Castronova, A.M., Goodall, J.L., Gan, T., Yi, H., Stealey, M.J., and Tarboton, D. G.: HydroShare: Sharing Diverse Environmental Data Types and Models as Social Objects with Application to the Hydrology Domain, JAWRA Journal of the American Water Resources Association, 52(4): 873-889, http://dx.doi.org/10.1111/1752-1688.12363, 2016.
Hren, M.T., Hilley, G.E., and Chamberlain, C.P.: The relationship between tectonic uplift and chemical weathering rates in the Washington Cascades: field measurements and model predictions, American Journal of Science, 307(9): 1041-1063, 2007.
Idaszak, R., Tarboton, D.G., Yi, H., Christopherson, L., Stealey, M.J., Miles, B., Dash, P., Couch, A., Spealman, C., Ames, D.P., and Horsburgh, J.S.: HydroShare - A case study of the application of modern software engineering to a large distributed federally-funded scientific software development project, Chapter 10 in Software Engineering for Science, Edited by J. Carver, N. P. Chue Hong and G. K. Thiruvathukal, Taylor and Francis CRC Press, 219-236 pp., 2016.
Islam, S.U., Déry, S.J., and Werner, A.T.: Future climate change impacts on snow and water resources of the Fraser River Basin, British Columbia. Journal of Hydrometeorology, 18: 473-496, doi: http://dx.doi.org/10.1175/JHM-D-16-0012.1, 2017.
Istanbulluoglu, E.: Modeling catchment evolution: from decoding geomorphic processes signatures toward predicting impacts of climate change. Geography Compass, 3(3): 1125-1150, 2009.
Istanbulluoglu, E., Tarboton, D.G., Pack R.T., and Luce, C.H.: Modeling of the interactions between forest vegetation, disturbances, and sediment yields. Journal of Geophysical Research: Earth Surface, 109(F1), 2004.
Istanbulluoglu, E., and Bras, R.L.: Vegetation-modulated landscape evolution: Effects of vegetation on landscape processes, drainage density, and topography, J. Geophys. Res., 110: F02012, doi:10.1029/2004JF000249, 2005.
Iverson, R.M., Reid, M.E., and LaHusen, R.G.: Debris-flow mobilization from landslides, Annual Review of Earth and Planetary Sciences, 25(1): 85-1, 1997.
Iverson, R. M.: Landslide triggering by rain infiltration, Water resources research, 36(7): 1897-1910, 2000.
Jin, S, Yang L, Danielson P, Homer C, Fry J, and Xian, G.: A comprehensive change detection method for updating the National Land Cover Database to circa 2011, Remote Sensing of Environment, 132: 159 175, 2013.
Kirschbaum, D.B., R. Adler, Y. Hong, S. Kumar, C. Peters-Lidard, and Lerner-Lam, A.: Advances in landslide nowcasting: evaluation of global and regional modeling approach. Environ. Earth. Sci. 66: 1683-1696, 2012.
Kulhawy, F.H., and Mayne, P.W.: Manual on estimating soil properties for foundation design. No. EPRI-EL-6800. Electric Power Research Inst., Palo Alto, CA (USA); Cornell Univ., Ithaca, NY (USA). Geotechnical Engineering Group, 1990.
Liang X., Lettenmaier D.P., Wood, E.F., and Burges, S.J.: A simple hydrologically based model of land

surface water and energy fluxes for GSMs, J Geophys Res 99(D7): 14,415–14,428, 1994.

Livneh B., Rosenberg, E.A., Lin, C., Nijssen, B., Mishra, V., Andreadis, K.M., Maurer, E.P., and Lettenmaier, D.P.: A Long-Term Hydrologically Based Dataset of Land Surface Fluxes and States for the Conterminous United States: Update and Extensions, Journal of Climate, 26: 9384–9392, 2013.

Livneh B., Bohn, T.J., Pierce, D.S., Munoz-Ariola, F., Nijssen, B., Vose, R., Cayan, D., and Brekke, L.D.: A spatially comprehensive, hydrometeorological data set for Mexico, the U.S., and southern Canada 1950-2013, Nature Scientific Data, 5:150042, doi:10.1038/sdata.2015.42, 2015.

Lee S., Ryu, J-H., and Kim, I-S.: Landslide susceptibility analysis and its verification using likelihood ratio, logistic regression, and artificial neural network models: Case study of Youngin, Korea. Landslides, 4:327–338, 2007.

Legg, N.T., Meigs, A.J., Grant, G.E., and Kennard, P.: Debris flow initiation in proglacial gullies on Mount Rainier, Washington, Geomorphology, 226, 249-260, 2014.

Lepore, C., Arnone, E., Noto, L.V., Sivandran, G. and Bras, R.L.: Physically based modeling of rainfall-triggered landslides: a case study in the Luquillo forest, Puerto Rico. Hydrology and Earth System Sciences 17: 3371–3387, 2013.

Löffler, J.: The influence of micro-climate, snow cover, and soil moisture on ecosystem functioning in high mountains, Journal of Geographical Sciences, 17(1), 3-19, 2007.

Lu, N., and Godt, J.W.: Hillslope hydrology and stability, Cambridge University Press, 2013.

Malkawi, A.I.H., Hassan, W.F. and Abdulla, F.A.: Uncertainty and reliability analysis applied to slope stability. Structural safety 22(2): 161-187, 2000.

May, C.L., Pryor, B., Lisle, T.E., and Lang, M.: Coupling hydrodynamic modeling and empirical measures of bed mobility to predict the risk of scour and fill of salmon redds in a large regulated river, Water Resources Research 45, W05402, 2009.

McKean, J.A., Dietrich, W.E., Finkel, R.C., Southon, J.R., and Caffee, M.W., 1993, Quantification of soil production and downslope creep rates from cosmogenic ^{10}Be accumulations on a hillslope profile: Geology, v. 21, p. 343-346.

Miller D.J.: Coupling GIS with physical models to assess deep-seated landslide hazards, Environ. Eng. Geosci., 1(3): 263–276, 1995.

Mancini, F., Ceppi, C., and Ritrovato, G.: GIS and statistical analysis for landslide susceptibility mapping in the Daunia area, Italy, Natural Hazards and Earth System Sciences, 10(9): 1851, 2010.

Mitchell, S.G., and Montgomery, D.R.: Influence of a glacial buzzsaw on the height and morphology of the Cascade Range in central Washington State, USA. Quaternary Research, 65(1): 96-107, 2006.

Molnar, P.: Late Cenozoic increase in accumulation rates of terrestrial sediment: How might climate change have affected erosion rates?, Annu. Rev. Earth Planet. Sci., 32, 67-89, 2004.

Montgomery, D.R.: Slope distributions, threshold hillslopes, and steady-state topography. American Journal of science, 301(4-5), 432-454, 2001.

Montgomery, D.R. and Dietrich, W.E.: A Physically Based Model for the Topographic Control on Shallow Landsliding, Water Resources Research, 30(4): 1153-1171, 1994.

Montgomery, D.R., and Foufoula-Georgiou, E.: Channel network source representation using digital elevation models. Water Resources Research, 29(12): 3925-3934, 1993.

Montrasio, L., and Valentino, R.: Modelling Rainfall-induced Shallow Landslides at Different Scales Using SLIP-Part I. Procedia Engineering, 158: 476-481, 2016.

Moon, S., Chamberlain, C.P., Blisniuk, K., Levine, N., Rood, D.H., and Hilley, G.E.: Climatic control of denudation in the deglaciated landscape of the Washington Cascades, Nature Geoscience, 4(7): 469-473, 2011.

Morsy, M.M., Goodall, J.L., Castronova, A.M., Dash, P., Merwade, V., Sadler, J.M., Rajib, M.A.,

Formatted: Font: (Default) +Body (Calibri), 11 pt, Font color: Custom Color(RGB(20,20,19)), Pattern: Clear

Formatted: Font: (Default) +Body (Calibri), 11 pt, Font color: Custom Color(RGB(20,20,19)), Pattern: Clear

Formatted: Font: (Default) +Body (Calibri), 11 pt, Font color: Custom Color(RGB(20,20,19)), Pattern: Clear

Formatted: Font: (Default) +Body (Calibri), 11 pt, Font color: Custom Color(RGB(20,20,19)), Pattern: Clear

Formatted: Font: (Default) +Body (Calibri), 11 pt, Font color: Custom Color(RGB(20,20,19)), Pattern: Clear

Formatted: Font: (Default) +Body (Calibri), 11 pt, Font color: Custom Color(RGB(20,20,19)), Pattern: Clear

Formatted: References, Indent: Left: 0 cm, Hanging: 0.76 cm, Widow/Orphan control

Horsburgh, J.S., and Tarboton, D.G.: Design of a metadata framework for environmental models with an example hydrologic application in HydroShare, Environmental Modelling & Software, 93: 13-28, http://dx.doi.org/10.1016/j.envsoft.2017.02.028, 2017.

Naudet, V., Lazzari, M., Perrone, A., Loperte, A., Piscitelli, S., and Lapenna, V.: Integrated geophysical and geomorphological approach to investigate the snowmelt-triggered landslide of Bosco Piccolo village (Basilicata, southern Italy), Engineering Geology, 98(3): 156-167, 2008.

Nadim, F., Kjekstad, O., Peduzzi, P., Herold, C., and Jaedicke, C.: Global landslide and avalanche hotspots, Landslides, 3(2): 159-173, 2006.

Nicótina, L., Tarboton, D. G., Tesfa, T. K., and Rinaldo, A.: Hydrologic controls on equilibrium soil depths, Water Resources Research, 47(4), 2011.

Nimmo, J.R.: Unsaturated Zone Flow Processes, in Anderson, M.G., and Bear, J., eds., Encyclopedia of HydrologicalSciences: Part 13--Groundwater: Chichester, UK, Wiley, v. 4, p. 2299-2322, doi:10.1002/0470848944.hsa161, 2005.

Okimura, T.: Prediction of slope failure using the estimated depth of the potential failure layer, J. Natural Disaster Sci., 11(1):67-89, 1989.

O'loughlin, E. M.: Prediction of surface saturation zones in natural catchments by topographic analysis. Water Resources Research, 22(5): 794-804, 1986.

Pack, R.T., Tarboton, D.G., and Goodwin, C.: SINMAP 2.0-A Stability Index Approach to Terrain Stability Hazard Mapping, User's Manual. Available online: http://www.engineering.usu.edu/dtarb/sinmap.html [Accessed 30 Jan. 1916], 2005.

Pack, R.T., D.G. Tarboton, and Goodwin, C.N.: Assessing Terrain Stability in a GIS using SINMAP, 15th Annual GIS Conference, Vancouver: http://hydrology.usu.edu/sinmap/gis2001.pdf, 2001.

Pack R.T., Tarboton, D.G., and Goodwin, C.N.: The SINMAP approach to terrain stability mapping. In: Proceedings of the 8th international congress of the international association of engineering geology and the environment, Vancouver, British Columbia, Canada, September 21–25, vol 2. AA Balkema, Rotterdam, pp 1157–1165, 1998.

Page, M.J., Trustrum, N.A., and DeRose, R.C.: A high-resolution record of storm-induced erosion from lake sediments, New Zealand, Journal of Paleolimnology, 11: 333-348, 1994.

Pardeshi, S.D., Autade, S.E., and Pardeshi, S.S.: Landslide hazard assessment: recent trends and techniques, SpringerPlus, 2(1): 523, 2013.

Pelletier, J.D., Barron-Gafford, G.A., Breshears, D.D., Brooks, P.D., Chorover, J., Durcik, M., Harman, C.J., Huxman, T.E., Lohse, K.A., Lybrand, R. and Meixner, T.: Coevolution of nonlinear trends in vegetation, soils, and topography with elevation and slope aspect: a case study in the sky islands of southern Arizona, Journal of Geophysical Research-Earth Surface, 118: 741–58, 2013.

Pelletier, J.D., and Rasmussen, C.: Geomorphically based predictive mapping of soil thickness in upland watersheds, Water Resources Research, 45(9): W09417, doi:10.1029/2008WR007319, 2009.

Pollen, N., and A. Simon (2005), Estimating the mechanical effects of riparian vegetation on stream bank stability using a fiber bundle model, Water Resour. Res., 41, W07025

Pollok, M.M.: Biodiversity, In: R. J. Naiman and R. E. Bilby (eds.) River Ecology and Management: Lessons from the Pacific Coastal Ecoregion, Springer-Verlag, New York, 430–452 pp., 1998.

~~PRISM Climate Group: Oregon State University, http://prism.oregonstate.edu, created 4 Feb 2004.~~

Raia S, Alvioli M, Rossi M, Baum RL, Godt JW, and Guzzetti, F.: Improving predictive power of physically based rainfall-induced shallow landslide models: A probabilistic approach, Geosci Model Dev Discuss, 6:1367–1426, 2014.

Regmi, N.R., Giardino, J.R., McDonald, E.V., and Vitek, J.D.: A comparison of logistic regression-based models of susceptibility to landslides in western Colorado, USA. Landslides, 11(2): 247-262, 2014.

Reiners, P.W., Ehlers, T.A., Mitchell, S.G., and Montgomery, D.R.: Coupled spatial variations in

precipitation and long-term erosion rates across the Washington Cascades, Nature, 426(6967), 645-647, 2003.
Reiners, P.W., Ehlers, T.A., Garver, J.I., Mitchell, S.G., Montgomery, D.R., Vance, J.A., and Nicolescu, S.: Late Miocene exhumation and uplift of the Washington Cascade Range, Geology, 30(9): 767-770, 2002.
Richards, L.A.: Capillary conduction of liquids in porous mediums, Physics, 1, 318–333, 1931.
Riedel, J, Brady S, Dorsch S, and Wegner, J.: Geomorphology of the Thunder Creek Watershed: Landform Mapping at North Cascades National Park Service Complex, Washington. Natural Resource Technical Report NPS/NCCN/NRTR—2012/567. National Park Service, Fort Collins, Colorado, 2015.
Riedel, J, and Probala, J.: Mapping ecosystems at the landform scale in Washington state, Park Science 23-2: 37-42, 2005.
Roe, G.H.: Orographic Precipitation. Annu. Rev. Earth Planet. Sci., 33:645–71, 2005.
Roering, J.J.: Soil creep and convex-upward velocity profiles: Theoretical and experimental investigation of disturbance-driven sediment transport on hillslopes, Earth Surface Processes and Landforms, 29(13): 1597-1612, 2004.
Roering, J.J., Schmidt, K.M., Stock, J.D., Dietrich, W.E., and Montgomery, D.R.: Shallow landsliding, root reinforcement, and the spatial distribution of trees in the Oregon Coast Range, Canadian Geotechnical Journal, 40(2): 237-253, 2003.
Roering, J.J., Kirchner, J.W., and Dietrich, W.E.: Evidence for nonlinear, diffusive sediment transport on hillslopes and implications for landscape morphology, Water Resources Research, 35(3): 853-870. 1999.
Schmidt, K.M., Roering, J.J., Stock, J.D., Dietrich, W.E., Montgomery, D.R., and Schaub, T.: The variability of root cohesion as an influence on shallow landslide susceptibility in the Oregon Coast Range, Canadian Geotechnical Journal, 38(5), 995-1024, 2001.
Schwarz, M., Giadrossich, F., and Cohen, D.: Modeling root reinforcement using a root-failure Weibull survival function, Hydrol. Earth Syst. Sci., 17: 4367–4377, 2013.
Selby, M.J.: Hillslope Materials and Processes. 2nd edit., Oxford University Press, 1993.
Sidle, R. C.: Relative importance of factors influencing landsliding in coastal Alaska. In 21st Annual engineering geology and soils engineering symposium. University of Idaho, Moscow, ID., 311-325, pp., 1984.
Sidle, R.C.: A conceptual model of changes in root cohesion in response to vegetation management, Journal of Environmental Quality, 20(1): 43-52, 1991.
Sidle, R.C.: A theoretical model of the effects of timber harvesting on slope stability, Water Resources Research, 28(7): 1897-1910, 1992.
Sidle, R.C., Noguchi, S., Tsuboyama, Y., and Laursen, K.: A conceptual model of preferential flow systems in forested hillslopes: Evidence of self-organization, Hydrological Processes, 15(10): 1675-1692, 2001.
Sidle, R.C., and Ochiai, H.: Landslides: processes, prediction, and land use, Water Resources Monogram 18, American Geophysical Union, Washington DC, 2006.
Simoni, S., Zanotti, F., Bertoldi, G., and Rigon, R.: Modelling the probability of occurrence of shallow landslides and channelized debris flows using GEOtop-FS, Hydrol. Process. 22:532–545, 2008.
Smith, K.: Mass movement hazards (Ch. 8), In: Environmental hazards: Assessing risk and reducing disasters (6th edition). Routledge, New York, NY., 205-234 pp., 2013.
Strenk, P.M.: Evaluation of analytical procedures for estimating seismically induced permanent deformations in slopes, Doctoral Thesis, Dexel University, 2010.
Stock, J., and Dietrich, W.E.: Valley incision by debris flows: Evidence of a topographic signature, Water Resources Research 39.4, 2003.

Strauch, R., E. Istanbulluoglu, S. S. Nudurupati, C. Bandaragoda (2017). Regional landslide hazard using Landlab - NOCA Data, HydroShare, http://www.hydroshare.org/resource/a5b52c0e1493401a815f4e77b09d352b

Sweeney, K.E., Roering, J.J., and Ellis, C.: Experimental evidence for hillslope control of landscape scale. Science, 349(6243), 51-53, 2015.

Tarboton, D.G., Idaszak, R., Horsburgh, J.S., Heard, J., Ames, D., Goodall, J.L., Band, L., Merwade, V., Couch, A., Arrigo, J., Hooper, R., Valentine, D., and Maidment, D.: HydroShare: Advancing Collaboration through Hydrologic Data and Model Sharing, in D. P. Ames, N. W. T. Quinn and A. E. Rizzoli (eds), Proceedings of the 7th International Congress on Environmental Modelling and Software, San Diego, California, USA, International Environmental Modelling and Software Society (iEMSs), ISBN: 978-88-9035-744-2, 2014. http://www.iemss.org/sites/iemss2014/papers/iemss2014_submission_243.pdf, 2014.

Tarolli, P., Borga, M., and Dalla Fontana, G.: Analysing the influence of upslope bedrock outcrops on shallow landsliding, Geomorphology, 93(3): 186-200, 2008.

Tarolli, P., and Dalla Fontana, G.: Hillslope-to-valley transition morphology: new opportunities from high resolution DTMs, Geomorphology, 113(1), 47-56, 2009.

Tarolli, P. and Tarboton, D.G.: A new method for determination of most likely landslide initiation points and the evaluation of digital terrain model scale in terrain stability mapping, Hydrol. Earth Syst. Sci. 10: 663-677, 2006.

Taylor, F., and Brabb, E.E.: Map showing the status of landslide inventory and susceptibility mapping in California (No. 86-100). US Geological Survey,1986.

Tesfa, T.K., Tarboton, D.G., Chandler, D.G., and McNamara, J.P.: Modeling soil depth from topographic and land cover attributes. Water Resources Research, 45(10), 2009.

Tobutt D.C.: Monte Carlo simulation methods for slope stability. Comput. Geosci., 8(2): 199–208, 1982.

Tucker, G.E., Hobley, D.E., Hutton, E.W.H., Gasparini, N.M., Istanbulluoglu, E., Adams, J.M., and Nudurupati, S.S.: CellLab-CTS 2015: a Python library for continuous-time stochastic cellular automaton modeling using Landlab., Geoscientific Model Development, 8: 9507-9552, doi:10.5194/gmd-9-823-2016, 2016.

Tucker, G.E., and Bras, R.L.: Hillslope processes, drainage density, and landscape morphology. Water Resources Research, 34(10), 2751-2764, 1998.

Tucker, G.E., and Slingerland, R.: Drainage basin responses to climate change. Water Resources Research, 33(8), 2031-2047, 1997.

United States Department of the Interior, National Park Service (DOI-NPS).: Foundation Document, North Cascades National Park Complex, Washington. Available from: https://www.nps.gov/noca/learn/management/upload/North-Cascades-NP-Complex-Foundation-Document_small.pdf (Accessed 23 January 2017), 2012.

United States Department of Agriculture, Natural Resources Conservation Service (DOA-NRCS), and United States Department of the Interior, National Park Service (DOI-NPS).: Soil survey of North Cascades National Park Complex, Washington, 2012.

United States Department of Agriculture, Natural Resources Conservation Service (DOA-NRCS).: United States Department of Agriculture. Web Soil Survey. Available from: http://websoilsurvey.nrcs.usda.gov/. (Accessed 23 January 2017), 2016.

DOA-NRCS.: Soil Data Viewer software. Available from: www.nrcs.usda.gov/wps/portal/nrcs/detailfull/soils/home/?cid=nrcs142p2_053620 [Accessed 23 June 1915], 2015a.

DOA-NRCS.: Soil Texture Calculator software. Available from: www.nrcs.usda.gov/wps/portal/nrcs/detail/soils/survey/?cid=nrcs142p2_054167 [Accessed 24 June

1915], 2015b.
United States Geological Survey (USGS).: Shuttle Radar Topography Mission (STRM) 1 arc-second global, Joint NASA-NGA partnership, data distributed and archived by USGS EROS Data Center, Available online at https://lta.cr.usgs.gov/SRTM1Arc. (Accessed 26 April 2017), 2017.
USGS.: National Elevation Data last modified March 6, 2014, National Map Viewer (Accessed 24 November 2014), 2014a.
USGS.: National Land Cover Data (NLCD) version Marched 31, 2014, National Map Viewer (Accessed 25 November 2014), 2014b.
Van Westen, C.J., Van Asch, T.W., and Soeters, R.: Landslide hazard and risk zonation—why is it still so difficult? Bulletin of Engineering geology and the Environment, 65(2), 167-184, 2006.
Van Beek, L.P.H.: Assessment of the influence of changes in land use and climate on landslide activity in a Mediterranean environment (Doctoral dissertation), Nederlandse Georafische Studies, Universiteit Utrecht. pp 294, 2002.
Yin, D., Liu, Y.Y., Padmanabhan, A., Terstriep, J., Rush, J., and Wang, S.: A CyberGIS-Jupyter Framework for Geospatial Analytics at Scale. The First Practice & Experience in Advanced Research Computing (PEARC) Conference, Under review, 2017.
Wayand, N., Stimberis, J., Zagrodnik, J., Mass, C.F. and Lundquist, J.D.: Improving Simulations of Precipitation Phase and Snowpack at a Site Subject to Cold Air Intrusions: Snoqualmie Pass, WA, J. of Geophysical Research, Atmospheres, 121, doi: 10.1002/2016JD025387, 2016.
Wartman, J., Montgomery, D.R., Anderson, S.A., Keaton, J.R., Benoît, J., dela Chapelle, J., and Gilbert, R.: The 22 March 2014 Oso landslide, Washington, USA. Geomorphology, 253: 275-288, 2016.
Wu, W. and Sidle, R.C.: A Distributed Slope Stability Model for Steep Forested Watersheds, Water Resour. Res., 31(8): 2097– 2110, 1995.
Zizioli, D., Meisina, C., Valentino, R., and Montrasio, L.: Comparison between different approaches to modeling shallow landslide susceptibility: a case history in Oltrepo Pavese, Northern Italy, Natural Hazards and Earth System Sciences 13(3): 559, 2013.

Page 13: [1] Formatted	Erkan Istanbulluoglu	09/10/2017 21:04:00

Font: Cambria Math, Highlight

Page 13: [1] Formatted	Erkan Istanbulluoglu	09/10/2017 21:04:00

Font: Cambria Math, Highlight

Page 13: [1] Formatted	Erkan Istanbulluoglu	09/10/2017 21:04:00

Font: Cambria Math, Highlight

Page 13: [1] Formatted	Erkan Istanbulluoglu	09/10/2017 21:04:00

Font: Cambria Math, Highlight

Page 13: [1] Formatted	Erkan Istanbulluoglu	09/10/2017 21:04:00

Font: Cambria Math, Highlight

Page 13: [1] Formatted	Erkan Istanbulluoglu	09/10/2017 21:04:00

Font: Cambria Math, Highlight

Page 13: [1] Formatted	Erkan Istanbulluoglu	09/10/2017 21:04:00

Font: Cambria Math, Highlight

Page 13: [1] Formatted	Erkan Istanbulluoglu	09/10/2017 21:04:00

Font: Cambria Math, Highlight

Page 13: [1] Formatted	Erkan Istanbulluoglu	09/10/2017 21:04:00

Font: Cambria Math, Highlight

Page 13: [1] Formatted	Erkan Istanbulluoglu	09/10/2017 21:04:00

Font: Cambria Math, Highlight

Page 13: [1] Formatted	Erkan Istanbulluoglu	09/10/2017 21:04:00

Font: Cambria Math, Highlight

Page 13: [1] Formatted	Erkan Istanbulluoglu	09/10/2017 21:04:00

Font: Cambria Math, Highlight

Page 13: [1] Formatted	Erkan Istanbulluoglu	09/10/2017 21:04:00

Font: Cambria Math, Highlight

Page 13: [2] Formatted	Erkan Istanbulluoglu	09/10/2017 21:04:00

Font: Cambria Math, Highlight

Page 13: [2] Formatted	Erkan Istanbulluoglu	09/10/2017 21:04:00

Font: Cambria Math, Highlight

Page 13: [2] Formatted	Erkan Istanbulluoglu	09/10/2017 21:04:00

Font: Cambria Math, Highlight

Page 13: [2] Formatted	Erkan Istanbulluoglu	09/10/2017 21:04:00

Font: Cambria Math, Highlight

Page 13: [2] Formatted	Erkan Istanbulluoglu	09/10/2017 21:04:00

Font: Cambria Math, Highlight

Page 13: [2] Formatted	Erkan Istanbulluoglu	09/10/2017 21:04:00

Font: Cambria Math, Highlight

Page 13: [2] Formatted	Erkan Istanbulluoglu	09/10/2017 21:04:00

Font: Cambria Math, Highlight

Page 13: [2] Formatted	Erkan Istanbulluoglu	09/10/2017 21:04:00

Font: Cambria Math, Highlight

Page 13: [2] Formatted	Erkan Istanbulluoglu	09/10/2017 21:04:00

Font: Cambria Math, Highlight

Page 13: [3] Formatted	Erkan Istanbulluoglu	09/10/2017 21:04:00

Highlight

Page 13: [3] Formatted	Erkan Istanbulluoglu	09/10/2017 21:04:00

Highlight

Page 13: [3] Formatted	Erkan Istanbulluoglu	09/10/2017 21:04:00

Highlight

Page 13: [3] Formatted	Erkan Istanbulluoglu	09/10/2017 21:04:00

Highlight

Page 13: [3] Formatted	Erkan Istanbulluoglu	09/10/2017 21:04:00

Highlight

Page 13: [3] Formatted	Erkan Istanbulluoglu	09/10/2017 21:04:00

Highlight

Page 13: [4] Formatted	Erkan Istanbulluoglu	09/10/2017 21:04:00

Font: Cambria Math, Highlight

Page 13: [4] Formatted	Erkan Istanbulluoglu	09/10/2017 21:04:00

Font: Cambria Math, Highlight

Page 13: [4] Formatted	Erkan Istanbulluoglu	09/10/2017 21:04:00

Font: Cambria Math, Highlight

Page 13: [4] Formatted	Erkan Istanbulluoglu	09/10/2017 21:04:00

Font: Cambria Math, Highlight

Page 13: [4] Formatted	Erkan Istanbulluoglu	09/10/2017 21:04:00

Font: Cambria Math, Highlight

Page 13: [4] Formatted	Erkan Istanbulluoglu	09/10/2017 21:04:00

Font: Cambria Math, Highlight

Page 13: [4] Formatted	Erkan Istanbulluoglu	09/10/2017 21:04:00

Font: Cambria Math, Highlight

Page 13: [4] Formatted	Erkan Istanbulluoglu	09/10/2017 21:04:00

Font: Cambria Math, Highlight

Page 13: [4] Formatted	Erkan Istanbulluoglu	09/10/2017 21:04:00

Font: Cambria Math, Highlight

Page 13: [4] Formatted	Erkan Istanbulluoglu	09/10/2017 21:04:00

Font: Cambria Math, Highlight

Page 13: [4] Formatted	Erkan Istanbulluoglu	09/10/2017 21:04:00

Font: Cambria Math, Highlight

Page 13: [4] Formatted	Erkan Istanbulluoglu	09/10/2017 21:04:00

Font: Cambria Math, Highlight

Page 13: [4] Formatted	Erkan Istanbulluoglu	09/10/2017 21:04:00

Font: Cambria Math, Highlight

Page 13: [4] Formatted	Erkan Istanbulluoglu	09/10/2017 21:04:00

Font: Cambria Math, Highlight

Page 13: [4] Formatted	Erkan Istanbulluoglu	09/10/2017 21:04:00

Font: Cambria Math, Highlight

Page 13: [4] Formatted	Erkan Istanbulluoglu	09/10/2017 21:04:00

Font: Cambria Math, Highlight

Page 13: [4] Formatted	Erkan Istanbulluoglu	09/10/2017 21:04:00

Font: Cambria Math, Highlight

Page 13: [4] Formatted	Erkan Istanbulluoglu	09/10/2017 21:04:00

Font: Cambria Math, Highlight

Page 13: [4] Formatted	Erkan Istanbulluoglu	09/10/2017 21:04:00

Font: Cambria Math, Highlight

Page 13: [4] Formatted	Erkan Istanbulluoglu	09/10/2017 21:04:00

Font: Cambria Math, Highlight

Page 13: [4] Formatted	Erkan Istanbulluoglu	09/10/2017 21:04:00

Font: Cambria Math, Highlight

Page 13: [4] Formatted	Erkan Istanbulluoglu	09/10/2017 21:04:00

Font: Cambria Math, Highlight

Page 13: [4] Formatted	Erkan Istanbulluoglu	09/10/2017 21:04:00

Font: Cambria Math, Highlight

Page 13: [5] Formatted	Ronda Strauch	29/09/2017 16:10:00

Font: Not Italic

Page 13: [5] Formatted	Ronda Strauch	29/09/2017 16:10:00

Font: Not Italic

Page 13: [5] Formatted	Ronda Strauch	29/09/2017 16:10:00

Font: Not Italic

Page 13: [5] Formatted	Ronda Strauch	29/09/2017 16:10:00

Font: Not Italic